Application of Structural Optimization Techniques to the Design of Specialized Truck Chassis Components

by

Bernardo Johannes Henning

Thesis presented in partial fulfilment of the requirements for the degree of Master of Engineering (Mechanical) in the Faculty of Engineering at Stellenbosch University

Supervisor: Prof. G. Venter

March 2021

Stellenbosch University https://scholar.sun.ac.za

Declaration

By submitting this thesis electronically, I declare that the entirety of the work contained therein is my own, original work, that I am the sole author thereof (save to the extent explicitly otherwise stated), that reproduction and publication thereof by Stellenbosch University will not infringe any third party rights and that I have not previously in its entirety or in part submitted it for obtaining any qualification.

Date: 9 February 2021

Copyright © 2021 Stellenbosch University
All rights reserved.

Stellenbosch University https://scholar.sun.ac.za

Abstract

Application of Structural Optimization Techniques to the Design of Specialized Truck Chassis Components

BJ. Henning

Department of Mechanical and Mechatronic Engineering,
University of Stellenbosch,
Private Bag X1, Matieland 7602, South Africa.

Thesis: MEng (Mech)

March 2021

This thesis focuses on the application of structural optimization techniques to improve the design of specialized truck chassis components with respect to cost-effectiveness, structural performance, and ease of manufacturing. Information regarding optimization and various supporting subjects were gathered from the literature to achieve the project outcome. A component within the chassis, known as the boom, was selected as the first design to receive optimization. Multiple optimization techniques were applied to the boom structure using GENESIS and Design Studio. These optimization techniques included size-, shape-, and topometry optimization. Marginal improvements were found, indicating that the current boom design is at a near-optimal design configuration. This merited a complete redesign of the boom component. Topology optimization was used to guide the redesign procedure of the boom. After doing extensive topology optimization work on the boom, a structure was created that is fundamentally different from the existing boom design. Using the topology optimization results, a step-by-step concept design methodology was developed, which can be used to guide future component redesign procedures. After the methodology development, a second component was identified to be optimized, known as the cross-member. The developed concept design methodology were used to find a new design for the cross-member, which then also served as a test opportunity for the newly developed methodology. Following the prescribed methodology steps, a satisfactory design was found for the cross-member, which proved to be a highly competitive design compared to the original design. Following this result, a detailed conclusion is given regarding the completion of the project objectives, aim, and future recommendations.

Stellenbosch University https://scholar.sun.ac.za

Uittreksel

Toepassing van Struktuur Optimaliseerings Tegnieke op die Ontwerpe van Gespesialiseerde Vragmotor Onderstel Komponente

BJ. Henning

Departement Meganiese en Megatroniese Ingenieurswese,
Universiteit van Stellenbosch,
Privaatsak X1, Matieland 7602, Suid Afrika.

Tesis: MIng (Meg)

Maart 2021

Hierdie tesis fokus op die toepassing van struktuur optimering om gespesialiseerde vragmotor onderstel komponente te verbeter ten opsigte van koste-effektiwiteit, strukturele vermoeë en vervaardiging. Inligting oor optimering en verskeie ander onderwerpe is uit die literatuur versamel soos benodig. 'n Onderdeel in die vragmotor onderstel, bekend as die "boom", is gekies as die eerste ontwerp om te optimeer. Verskeie optimeringstegnieke is op hierdie komponent toegepas met behulp van GENESIS en Design Studio. Hierdie optimeringstegnieke sluit grootte-, vorm- en topometrie-optimering in. Klein verbeterings is gevind, wat daarop dui dat die huidige komponent naby optimaal is. Die resultate ondersteun die herontwerping van die "boom" om 'n verbeterde ontwerp te vind. Topologie-optimering is gebruik vir die herontwerp proses. Nadat die nodige topologie-optimeringswerk op die komponent gedoen is, is 'n ontwerp gevind wat fundamenteel verskil van die bestaande komponent. 'n Stapsgewyse konsepontwerp metodologie is ontwikkel vanaf die topologie resultate, wat as riglyn gebruik kan word om toekomstige herontwerpe te lei. Na die metodologie-ontwikkeling is 'n tweede komponent, bekend as die "cross-member" geïdentifiseer vir optimering. Daar was besluit om slegs die metodologie te gebruik vir die ontwikkeling van 'n nuwe "cross-member" ontwerp, wat terselfdetyd dien as 'n toetsgeleentheid vir die metodologie. Na die uitvoering van die konsepontwerp metodologie is 'n bevredigende ontwerp gevind, wat hoogs mededingend teenoor die oorspronklike ontwerp is. Na hierdie resultaat is 'n gevolgtrekking gemaak oor die voltooiing van die projekdoelstellings, mikpunt en toekomstige aanbevelings.

Stellenbosch University https://scholar.sun.ac.za

Acknowledgements

I would like to express my sincere gratitude to the following people that helped, supported, and guided me in completing this project:

- First and foremost to my supervisor, Prof. Gerhard Venter, for his invaluable support, guidance, and mentorship throughout this project. I was able to learn a great deal and grow as an aspiring engineer, and for that, I thank him.
- To Rudi Jansen van Rensberg, Maurice Grapendaal, and Johann Voster from Triz Engineering, for allowing me the opportunity to work on this project. A special thanks to Rudi for all his assistance and support, without which this project would have faced many hardships.
- To my father Bernard, mother Alet, and brothers Stephan and Lennert, I would like to say thank you for all your unconditional love and support that you gave me throughout it all.
- Last but not least, I would like to thank Lisa McLoud. Thank you for listening to my frustrations, failures, and successes, and motivating me to deliver my best.

Stellenbosch University https://scholar.sun.ac.za

Contents

Stellenbosch University https://scholar.sun.ac.za

Stellenbosch University https://scholar.sun.ac.za

Stellenbosch University https://scholar.sun.ac.za

List of Figures

Stellenbosch University https://scholar.sun.ac.za

Stellenbosch University https://scholar.sun.ac.za

Stellenbosch University https://scholar.sun.ac.za

List of Tables

Stellenbosch University https://scholar.sun.ac.za

Chapter 1

Introduction

1.1 Background

Within the current economic environment, competition between most leading industries is continuously increasing. Engineers and scientists are required to develop technology that is lighter, stronger, faster, more efficient, and environmentally friendly. This requires exceptional design skills, ingenuity, time, and resources. It is however not always possible to find an optimal design with basic analytical approaches and design techniques. Computer-aided design techniques have played a vital role in the advancement of modern technology, where basic modeling techniques and analytical approaches have become commonplace. In the last few decades, design software such as 3D computer-aided design (CAD) and finite element (FE) packages have become popular tools to use for the development of complex designs (Leiva, 2008). When combining these packages with optimization software that uses advanced numerical methods to achieve certain design requirements, it becomes possible to find improvements for complex designs. The growing popularity of optimization amongst the engineering and research industries have led to the application thereof to become vast. Due to the wide range of optimization applications, no universal method exists to solve all optimization problems, therefore, various techniques have been developed over the years, that are tailored to particular types of problems (Snyman, 2005). A sub-branch of the general optimization procedure, known as structural optimization, is specifically used to improve structural designs. Structural optimization is based on linear FE analysis, therefore it is considered a formal and sophisticated optimization procedure. This project will make use of structural optimization, in an attempt to improve a specialized truck design known as a terminal tractor. The results obtained from the structural optimization procedures will consequently be used for the development of a concept design methodology to generate fundamentally new designs.

To effectively apply the structural optimization techniques, a better un-

Stellenbosch University https://scholar.sun.ac.za

derstanding of the terminal tractor's construction, design, and operation is required. The function of a terminal tractor is to move trailers within shipping- and storage yards. The terminal tractor's chassis components experience large forces during operation, which could easily lead to either failures or over-designing. Structural optimization can be used to prevent these events from occurring, by finding improved designs, within required constraints. The terminal tractor design has not yet received any form of formal optimization, such as structural optimization, and therefore, there is a possibility of finding design improvements. There are various types of structural optimization techniques that will subsequently be used to find design improvements. A typical 4x2 terminal tractor is shown in Figure 1.1.

Figure 1.1: Autocar terminal tractor (Autocar, 2019)

1.2 Motivation

In a modern design environment, structural optimization can be a valuable design tool if applied correctly. Competition within the automotive industry is always present, and the use of specialized tools and skills, such as structural optimization, could push design capabilities even further. Structural optimization, in conjunction with current design methods and procedures, will help designers to be effective and efficient during the design process. What makes structural optimization such a valuable design tool is that it can be used to gain insight into structural problems. Consequently, it assists a designer to better understand a problem at hand, which will lead to better design choices, and ultimately, better final designs. When looking at large structures such as trucks that consists of sizeable components, lighter designs could save money, since less material is required for manufacturing. Additionally, safer designs can be found that effectively manage input loading and stress, by reducing the

Stellenbosch University https://scholar.sun.ac.za

probability of structural failure. When optimization is integrated into a design procedure, the required resources such as manpower, material, and time are typically reduced, especially when compared to more traditional design approaches, as shown in Figure 1.2 (Zhang *et al.*, 2020).

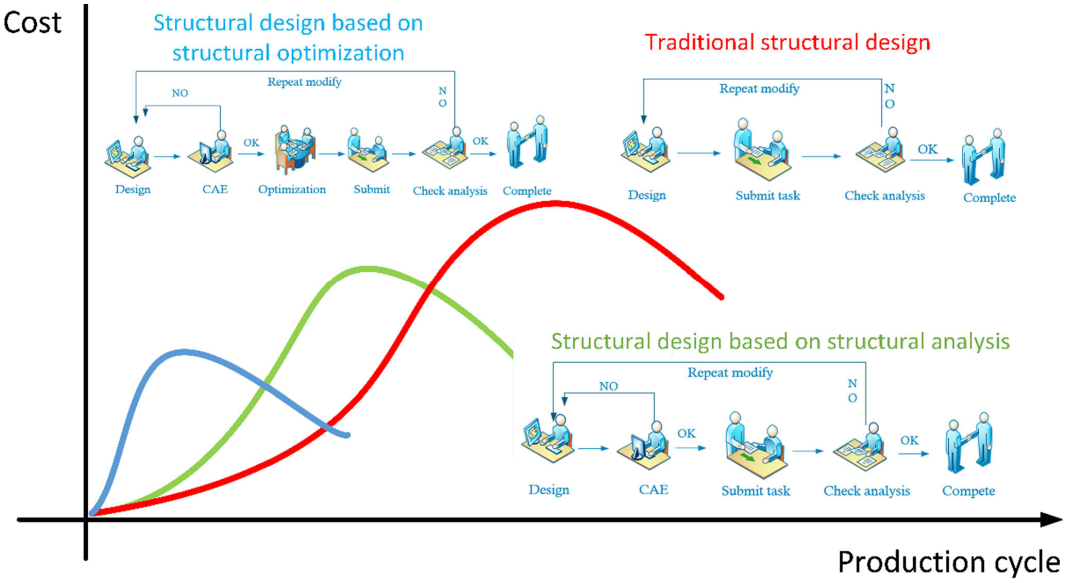

Figure 1.2: Cost vs. production cycle comparison for structural design (Zhang *et al.*, 2020)

The knowledge and experience gained during this project could be used to improve previously developed structures within the automotive industry. This research could also form the foundation for future designs, where the optimization techniques and concept design methodology could serve as an alternative to conventional design methods. This could save both time and resources during the development stage, and assists designers to make better design choices, with increased confidence.

Within the literature, there are countless studies and practical applications that have demonstrated the potential and value of structural optimization. One such example is where Leiva (2008) investigated the effects of the different sub-fields of structural optimization on a car body structure. The objective was to improve the torsional stiffness of the car's structure, allowing its mass to increase up to 2 %. Using the various structural optimization techniques, it was found that the body's torsional stiffness could be improved with a factor of two, by only adding 0.71 kg of material to the existing 288.5 kg body. This is an exceptional result and showcases the potential that structural optimization offers.

Stellenbosch University https://scholar.sun.ac.za

1.3 Aim and Objectives

The aim of this project is to optimize existing components from the terminal tractor chassis, without compromising their structural integrity. The terminal tractor is a large and complex structure, consisting of various components. Two critical components have been identified for optimization, known as the boom and cross-member. The project aims to improve both the boom- and cross-member component designs with respect to cost-effectiveness, structural performance, and ease of manufacturing. This aim will consequently be measured by looking at component mass minimization, which relates to material cost reduction, fatigue life expectancy and the enhancement thereof, as well as smarter, more economical, manufacturing processes such as castings. Using the knowledge gained from the optimization problems, a concept design methodology can be developed and tested. In order to achieve the project aim, the following objectives have been identified:

1. Improvement of a terminal tractor component, using size-, shape-, topometry- and topography optimization
2. The development of new designs, using topology optimization
3. Formulation of a concept design methodology, based on results obtained from Objectives 1 and 2
4. Application and testing of the concept design methodology on a terminal tractor component

Objective 1 will focus on finding design improvements for terminal tractor components that are currently being used. Since all the design changes will be based on the currently used ACTT designs, no conceptual or fundamental design changes will be made, only design improvements. These improvements will be pursued with the use of size-, shape-, topometry- and topography optimization. Objective 2 will focus on finding fundamentally new designs using topology optimization. Topology optimization has more design freedom when searching for new designs within a given design space, as it is not limited to, or based on, the original designs being replaced. The structural optimization techniques are expanded upon in Chapter 2. Objective 3 will attempt to use the knowledge gained from the optimization results, to develop a concept design methodology. The concept design methodology will focus on finding new designs, rather than improving on existing designs. Finally, Objective 4 can be realized by using the concept design methodology to develop a new design for a terminal tractor component. This will also serve as a good opportunity to test and improve the concept design methodology.

Stellenbosch University https://scholar.sun.ac.za

Chapter 2

Literature Study

2.1 Terminal Tractor

A terminal tractor is mainly used to move trailers around shipping- and storage yards, where space is usually limited. These tractors are small and designed specifically to operate in such areas (Autocar, 2019). The terminal tractor comes in two drive-train configurations, namely 4x2 and 6x4. The 4x2 configuration will be the focus of this research project. There exist two variants of the 4x2 drive-train configuration, however, the components of interest have similar designs for both configurations. The components that are considered for optimization are known as the cross-member and boom, depicted in Figures 2.1a and 2.1b, respectively. The partial chassis assembly is shown in Figure 2.1c, illustrating where the boom and cross-member fit within the chassis design.

2.1.1 Boom component

The boom is an important part of the chassis structure, as it is the linkage point between the tractor and the trailer. Past experimental data shows that the boom experiences large torsional forces during operation, more specifically during turning maneuvers. The grey, circular-shaped component, shown towards the rear of Figure 2.1c, is known as the 5th-wheel and it forms the physical connection point between the boom and the trailer. The 5th-wheel is connected to the boom via two bearings as seen in the right-top of Figure 2.1b. The boom is a dynamic part that is allowed movement within the chassis assembly and is actuated by two large hydraulic cylinders. This is used do adjust the height of the 5th-wheel, before connecting to trailers. Furthermore, the boom connects to the cross-member via a pin, which forms a quasi-static connection point relative to the chassis. Due to the complex interface between the chassis, boom, cross-member, and trailer, it was decided to analyze the boom as a separate component to the rest of the chassis. The existing boom has a mass of 389 kg.

Stellenbosch University https://scholar.sun.ac.za

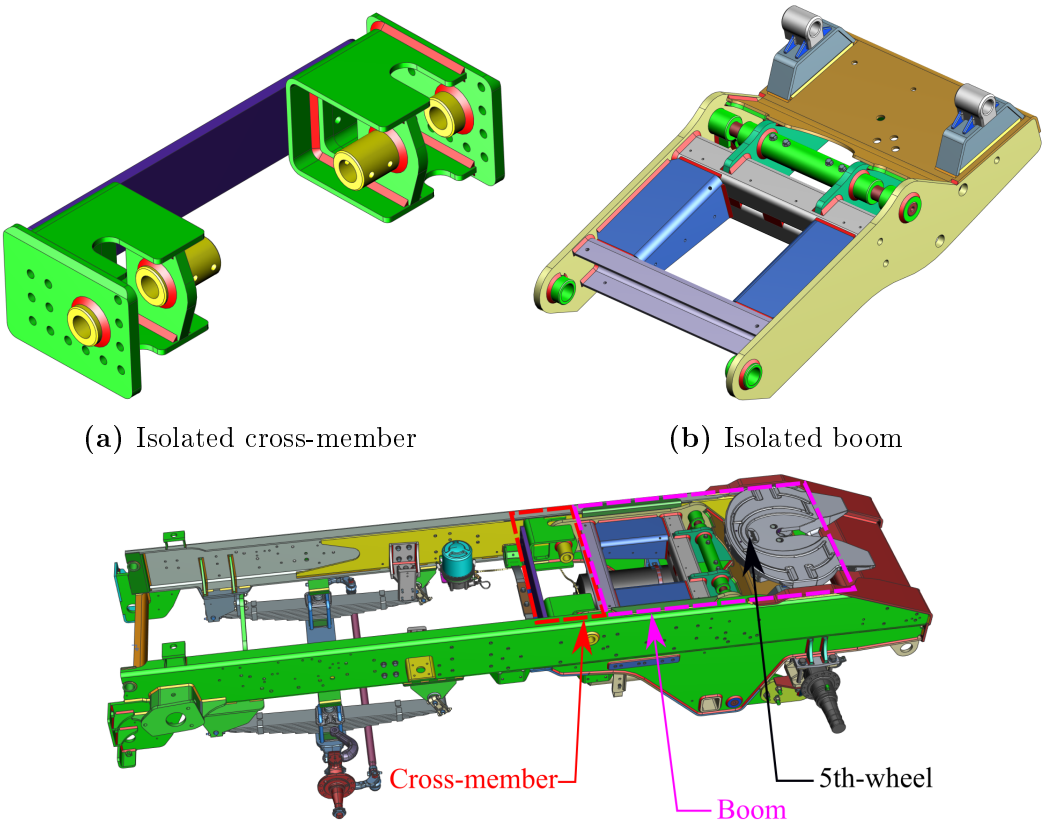

(a) Isolated cross-member (b) Isolated boom

(c) Chassis

Figure 2.1: Depiction of the cross-member and boom, with an illustration of their position within the chassis assembly

2.1.2 Cross-member component

The cross-member is a component positioned within the chassis frame rails, as shown in Figure 2.1. Not only does the cross-member add to the structural rigidity and stiffness of the chassis, but it also has the important function of serving as one of the two interface points between the boom and chassis framework. The mass of the existing cross-member is 117.8 kg.

2.1.3 Component manufacturing procedures

The boom and cross-member are mainly constructed from metal plate-, beam- and tube parts that are connected via bolts and welds. Both the boom and cross-member are constructed from numerous parts, which requires a large number of manufacturing processes for fabrication. In an attempt to ease the manufacturing process, the possibility of casting will be investigated for both of these designs. This will also improve structural performance by removing or minimizing weld- and bolted regions, consequently improving the structure's capability to withstand fatigue.

Stellenbosch University https://scholar.sun.ac.za

2.2 Mathematical Optimization Concepts

Mathematical optimization is the formulation and solution to a constrained or unconstrained problem, where the optimum solution is required. The optimum solution will either be a maximum or minimum, depending on the problem. For the remainder of this thesis, the optimum solution will be assumed to be a minimum. The standard form of an optimization problem is shown by Equation 2.1 (Venter, 2010),

$$\underset{\text{w.r.t. x}}{\text{minimize}}\ f(\boldsymbol{x}),\ \boldsymbol{x} = [x_1, x_2, ..., x_n]^T \in \mathbb{R}^n \tag{2.1}$$

with constraints,

$$g_j(\boldsymbol{x}) \leq 0,\ \ j = 1,\ 2,\ ...,\ m \tag{2.2}$$

$$h_k(\boldsymbol{x}) = 0,\ \ k = 1,\ 2,\ ...,\ p \tag{2.3}$$

$$x_{i_L} \leq x_i \leq x_{i_U},\ \ i = 1,\ 2,\ ...,\ n \tag{2.4}$$

The function, $f(\boldsymbol{x})$, is known as the objective function and the components of the column vector, $\boldsymbol{x}$, are the design variables. The design variables are parameters that may be modified to minimize the objective function. The constraints, $g_j(\boldsymbol{x})$, are known as inequality constraints and $h_k(\boldsymbol{x})$ are known as equality constraints. Lastly, x_{i_U} and x_{i_L} defines the respective upper and lower bounds of the allowed design space (Snyman, 2005; Venter, 2010).

The design variables could typically include, among others, finite element densities, cross-sectional areas, shell element thicknesses, and nodal locations. The design variables differ based on the type of structural optimization technique being used, which will be discussed in Section 2.3. Since the aim is to minimize the mass of the boom and cross-member, structural mass minimization is chosen as the objective function. Constraints such as maximum allowable stress and deformation will ensure that the optimized structure stays within a safe operating range. The upper and lower design bounds will be used similarly as the constraints, to ensure that only the desired design regions are being optimized. All constraints will be defined consistent with the current design practices that are used for the terminal tractor.

This is only the basics of mathematical optimization, but it forms the foundation of all optimization problems. There are various types of optimization algorithms that use different methods to search for optimum solutions. Typically, optimization algorithms are placed into two categories, known as local or global optimization algorithms.

Gradient-based algorithms are categorized under local optimization algorithms. Gradient-based algorithms, as the name implies, uses gradient information to find a solution. These algorithms usually have a single starting point. If a minimum is required, the steepest negative gradient at the starting

Stellenbosch University https://scholar.sun.ac.za

point will be used as the first search direction to progress to a local minimum. A "temporary" minimum within the search direction is determined using line search algorithms such as the Golden Section search (Venter, 2010). Once a minimum has been found within the search direction, a new gradient is determined, consequently, a new search direction is found. This process is repeated until an optimum solution is calculated, which is illustrated in Figure 2.2. Gradient-based algorithms are typically efficient, require little parameter tuning, and can solve problems with many design variables. Flaws of gradient-based algorithms include the possibility of getting stuck in local optima, struggling to solve discrete problems, and their sensitivity to numerical noise (Venter, 2010).

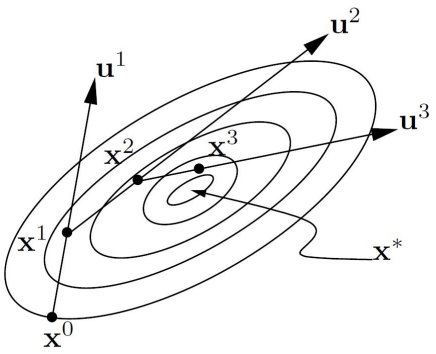

Figure 2.2: Sequence of gradient based algorithm (Snyman, 2005)

Global algorithms are typically non-gradient based algorithms and their way of functioning is very different from their gradient-based counterparts. Local optimization algorithms typically find a single local optimum, even if there are multiple optimum solutions. Global algorithms can find most, if not all of the optimum solutions, and thus have a higher chance of finding the global optimum. These algorithms use a multi-point starting approach to find multiple solutions and they do not need any gradient information (Venter, 2010).

One of the best known, non-gradient based optimization algorithms, is the evolutionary- or genetic algorithm (GA). The GA uses Darwin's concept of natural selection and genetics. In short, the algorithm starts by generating multiple starting points, also referred to as the initial population, where each point is an individual. Each point (individual) contains variable information (genetics) that represents a solution to the given problem. Points with favorable variable information, meaning points with more optimum solutions, are more likely to create new points with shared information. This is similar to mating in the natural selection cycle and the concept of survival of the fittest. This process is repeated, creating new generations with fitter individuals, with

Stellenbosch University https://scholar.sun.ac.za

a resulting set of optimum solutions. It should be noted that a GA is not guaranteed to find the global optimum solution. More information regarding the implementation, advantages, and drawbacks of this algorithm can be found in the article presented by Bajpai and Kumar (2010).

Within the field of structural optimization, gradient-based algorithms are mainly used. This is due to their high level of efficiency, their capability to deal with a large number of design variables and constraints, as well as the availability of cheap analytical gradients.

2.3 Structural Optimization

Structural optimization is a form of optimization that is specifically used to improve and enhance structures, that are modelled using linear FE analyses. Liu *et al.* (2008) describe structural optimization as the idea of gradually changing or removing inefficiently used materials from the design domain, to find an optimal structure design.

These optimization problems are approached numerically. The first step is to discretize the design domain, such as the cross-member or boom, to create a FE model, consisting of many discrete points. These discrete points are known as nodes, and when connected, they form finite elements. The FE model is then used to evaluate each element's contribution to the structure's performance and properties. Depending on the sub-field of structural optimization being used, the element characteristics and properties can be changed accordingly. When solving structural optimization problems using FE- and optimization software, the approximation concepts approach is used. The approximation concepts approach was introduced by Schmit (1960) and is one of the best-known methods to use when solving structural optimization problems. The approximation concepts approach relies on an iterative procedure to gradually improve a structure of interest. Vanderplaats *et al.* (1991) describe the basic program structure of the approximation concepts approach as a process that is based on two iterative loops, more specifically, the outer loop and inner loop. A cycle from the inner loop is defined as an iteration cycle, while an outer loop cycle is known as a design cycle. The process is illustrated in Figure 2.3.

The procedure starts with a full FE analysis of the initial proposed design. Next, the constraints are evaluated and ranked based on their criticality. For the remainder of the design cycle, only the critical and near-critical constraints are considered. This process is known as constraint screening or constraint deletion. Vanderplaats *et al.* (1991) specifies guidelines as to how constraint screening is performed. After the constraint screening is completed, the gradients are calculated. With effective constraint screening, only the critical gradients have to be calculated, which requires less computational power. Furthermore, GENESIS is able to efficiently obtain gradients for both objective- and constraint functions, by doing the calculations as part of the analysis pro-

Stellenbosch University https://scholar.sun.ac.za

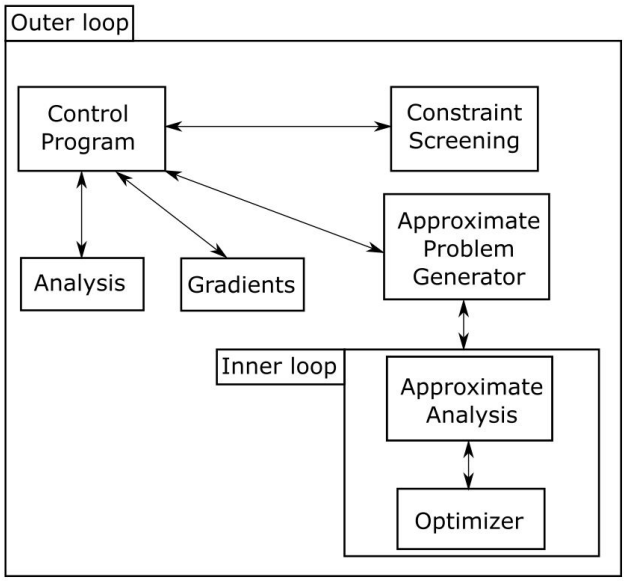

Figure 2.3: Approximation concepts approach procedure (Vanderplaats *et al.*, 1991)

cess. The most commonly used constraints, such as stress limits, have a direct correlation with displacement. The calculations start with Equation 2.5,

$$\boldsymbol{K}\boldsymbol{u} = \boldsymbol{p} \tag{2.5}$$

that undergoes implicit differentiation with respect to the design variables $x_i,\ i = 1, 2, ..., n$, to find Equation 2.6.

$$\frac{\partial \boldsymbol{K}}{\partial x_i}\boldsymbol{u} + \boldsymbol{K}\frac{\partial \boldsymbol{u}}{\partial x_i} = \frac{\partial \boldsymbol{p}}{\partial x_i} \tag{2.6}$$

Equation 2.6 can be rearranged by multiplying with $\boldsymbol{K}^{-1}$ to find Equation 2.7.

$$\frac{\partial \boldsymbol{u}}{\partial x_i} = \boldsymbol{K}^{-1}\left[\frac{\partial \boldsymbol{p}}{\partial x_i} - \frac{\partial \boldsymbol{K}}{\partial x_i}\boldsymbol{u}\right] \tag{2.7}$$

If the $\boldsymbol{K}$ matrix was decomposed during a previous analysis, the calculation of $\frac{\partial \boldsymbol{K}}{\partial x_i}$ should be a simple procedure, since $\boldsymbol{K}^{-1}$ is effectively available. The gradient information is only required to be calculated once for each outer loop during the optimization procedure, which provides significant computational savings. This entire procedure is presented in detail by Vanderplaats (2005). To further ensure the quality of the gradients being calculated, intermediate gradient responses can be determined with the use of intermediate variables, combined with Taylor series expansions (Stewart, 2012). The idea behind the Taylor series expansion and intermediate variables is to convert a non-linear problem into a linear problem, ensuring high-quality approximations for the inner loop, as well as an efficient optimization process. An intermediate

Stellenbosch University https://scholar.sun.ac.za

variable example is where stress, σ, is highly non-linear with respect to cross-sectional area, A, displayed in Equation 2.8,

$$\sigma = \frac{F}{A} \tag{2.8}$$

To linearize the problem, an intermediate variable can be created by inverting the area, better known as a reciprocal variable. Equation 2.9 shows the linearized form of Equation 2.8, using an intermediate variable X.

$$\sigma = FX, \quad \text{where } X = \frac{1}{A} \tag{2.9}$$

Hence, by creating an intermediate variable, the non-linear problem was converted to a linear problem. After solving linearised problems, the original variable(s) can easily be recovered, for example:

$$A = \frac{1}{X} \tag{2.10}$$

To linearise a non-linear function, that contains non-linear variables, a Taylor series expansion can be used, combined with the use of intermediate variables to linearise the entire function and its variables. Using these steps, non-linear problems can be solved explicitly with simplified linear functions, whilst still retaining the original problem's non-linearity. Once the desired gradients are obtained, the program moves to the inner loop. Within the inner loop, approximation models are created using the gradients. The approximation models are solved using a general optimization technique. The solution is then used to update the FE model and analysis data, thus a new design is created. Using the newly obtained data, a FE analysis is conducted to assess the new design. Once the new design converges, an adequate, optimal design is found and the program is terminated, otherwise, the program repeats (Vanderplaats *et al.*, 1991; Leiva, 2008; Leiva and Watson, 2016).

Until now, structural optimization has been discussed in general. Structural optimization does however consist of various techniques or sub-fields, namely size-, shape-, topology-, topography- and topometry optimization. All of these methods prove their worth in different situations, applications, and requirements. To grasp these techniques, an investigation into each will be required.

2.3.1 Size optimization

Size optimization is used to find plate thickness and component cross-sectional areas that are optimal for a given structure (Leiva and Watson, 2016). The design variables represent physical dimensions, such as a truss or bar element cross-sectional area or shell element thickness. Figure 2.4a depicts a simple bracket that consists of two plates, shown in green and red, connected with

Stellenbosch University https://scholar.sun.ac.za

a weld. Size optimization is used to reduce the mass of the bracket, whilst adhering to constraints such as material yield stress. An optimized bracket, shown in Figure 2.4b is found that shows a clear reduction in the element thickness for both the red- and green plates. From Figure 2.4, it can be noted that the overall dimensions, such as length, height, and width of the bracket stay constant.

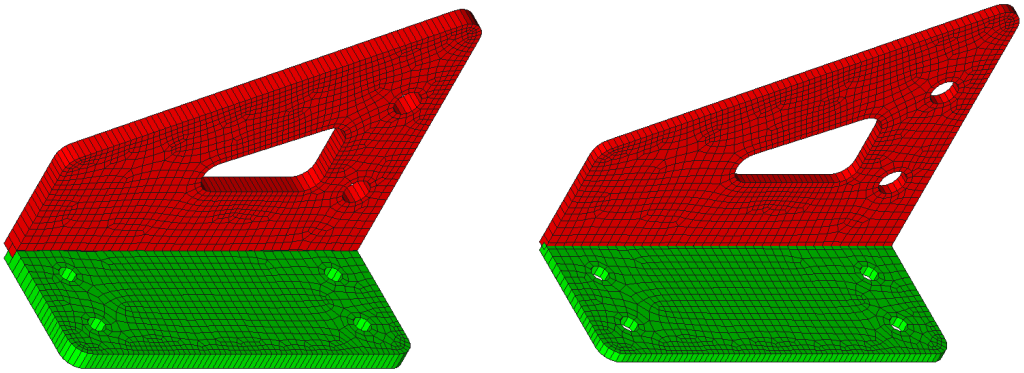

(a) Original bracket **(b)** Optimized bracket

Figure 2.4: Example of size optimization, displaying shell element thickness changes

When dealing with car chassis, size optimization is an ideal structural optimization technique that can be used to find an optimal shell element thickness distribution, considering that conventional automotive bodies are mostly made from plate-like components and members (Leiva, 2008). Similarly, the terminal tractor chassis is mostly constructed from plates, beams, and tubes, which are ideal for the application of size optimization. There is however a limitation to size optimization when considering that vendors have an inventory list with limited plate sizes. Optimization using a discrete set of plate sizes is required to obtain practical results.

2.3.2 Topometry optimization

Topometry optimization is similar to size optimization and is typically referred to as a special case of size optimization. Size optimization is mostly used to apply a single size design variable to a plate, whereas topometry optimization is specialized to assign multiple size design variables to groups of elements within a single plate (Leiva and Watson, 2016). Due to this specialization, topometry optimization gives the user more control over the elements within a plate being changed and optimized. The value of topometry optimization is that it gives insight into a problem as it makes changes to small areas within a design or even single elements. The results are typically unpractical

Stellenbosch University https://scholar.sun.ac.za

and require simplification if a manufacturable solution is required. Figure 2.5 depicts an example of topometry optimization.

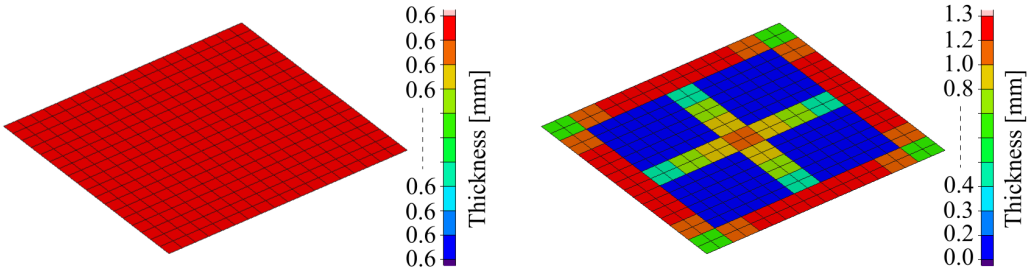

(a) Initial plate **(b)** Optimized plate

Figure 2.5: Example of topometry optimization, displaying the initial shell element mesh and thickness changes that occurred after optimization. The FE plate model is rigidly constrained at all four corners, with a central point load

2.3.3 Shape optimization

Shape optimization is used to change the geometry of a structure, in an attempt to find an optimally shaped structure. FE nodes are selected and assigned shape variables with specifications regarding their allowed nodal position changes that may occur. These shape variables are assigned using perturbation vectors. The shape variables are scale factors of the perturbation vectors that describe the magnitude- and directional change that nodes may experience. The nodes that are allowed to be moved are selected using a shape domain. The domain is a design space constraint, as mentioned in Section 2.2. By adjusting the perturbation scale factors, the relative nodal positions will change, and thus, a resulting shape change will occur (Leiva and Watson, 2016). Figure 2.6 illustrates the capabilities of shape optimization.

As can be seen in Figure 2.6, various nodes within the centre of the bracket have been moved, enlarging the cut-out shape and reducing the component's mass. What should be noted in this example is that nodes are translated and repositioned, which does not require the process of remeshing. GENESIS does this by using shape morphing sets to morph groups of nodes within a mesh to achieve requested shape changes. The Shape optimization is not limited to 2D problems and can be applied to 3D structures, allowing shape changes in all 3 dimensions. Shape optimization can be used to move individual nodes within a FE model, however this function is rarely used as it could cause complications. Typical complications that arise are the creation of jagged surfaces, causing a jagged boundary problem, which negatively affects the optimization procedure and increases computational costs (Shimoda and Liu,

Stellenbosch University https://scholar.sun.ac.za

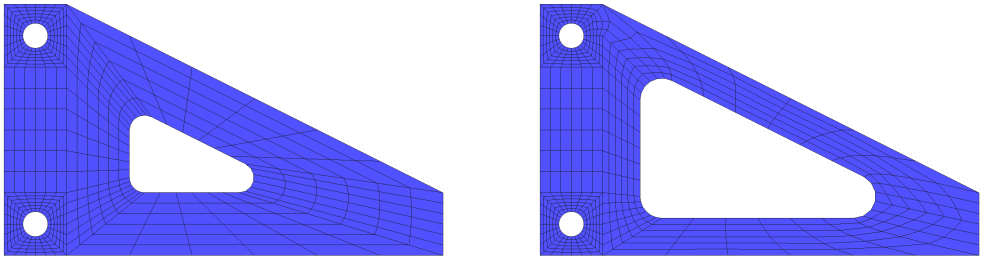

(a) Original plate **(b)** Optimized plate

Figure 2.6: Example of shape optimization on a bracket that is meshed with shell elements

2014). By moving these individual nodes, invalid elements are also typically created, which is detrimental to FE analyses and optimization procedures.

2.3.4 Topography optimization

Topography optimization is a special case of shape optimization that only allows nodes to move perpendicular to the surface. Topography optimization uses pre-defined shape patterns to find an improved structure, for example, stamped beads, grooves, or ribs, to name a few (Pagadala, 2008). Topography optimization is mostly applied to plate-like components, as the resulting geometries are typically ideal for manufacturing processes such as stamping and extrusion. Figure 2.7 shows plates that have been optimized using pre-defined beaded- and rib patters, shown in Figures 2.7a and 2.7b respectively.

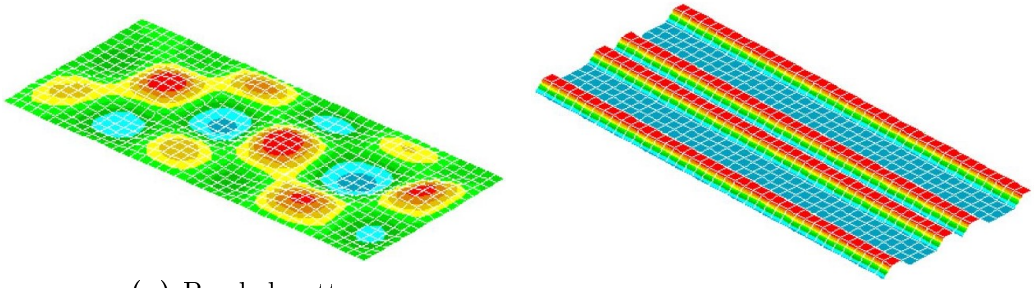

(a) Beaded pattern **(b)** Rib pattern

Figure 2.7: Example of topography optimization, aiming to increase torsional stiffness with the use of surface patterns

Stellenbosch University https://scholar.sun.ac.za

2.3.5 Topology optimization

Topology optimization is a technique that removes ineffective material from a design domain. The topology optimization technique uses element density as a design variable. By reducing an element's density to 0, it is effectively removed from the design domain. During the optimization process, elements are assigned a density fraction between 1 and 0. A well-known method for maximizing topology design stiffness is through strain energy minimization. Elements located in the region of the load path experience high strain, which relates to high strain energy, is assigned a density fraction of 1 or near 1. Elements further away from the load path experience less strain, hence containing less strain energy. These elements offer little to no contribution in dealing with the input loading and, therefore, receive volume fractions of 0 or near 0. Elements that are assigned fractions near 0 are removed from the FE model, whilst the elements with fractions close to 1 are kept (Leiva and Watson, 2016). The result is a new FE model design that can be manufactured using less material, with similar structural capabilities compared to the original design. Figure 2.8 illustrates the process of topology optimization. The figure shows the removal of elements within certain regions of the bracket, indicating that those elements were not effectively contributing to the structure's load carrying capability and deemed removable. The final optimized component design seems quite different when compared to the original design. Designs obtained from topology optimization are usually referred to as organic designs, due to their unconventional or rather "natural" appearances (Femto Engineering). To avoid un-manufacturable designs, manufacturing constraints can be added to the optimization task. Details regarding the manufacturing constraints are presented in Section 2.3.6 and Chapter 4.

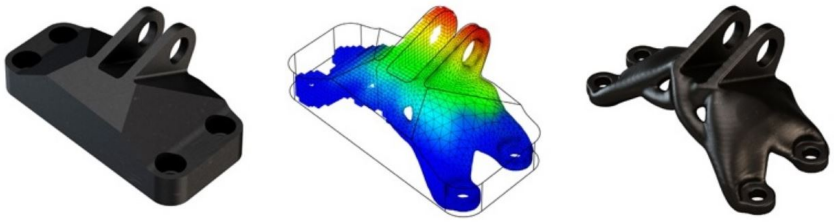

Figure 2.8: Example of topology optimization on a bracket (Metrology and Quality News, 2016)

It is important to note that topology optimization is typically used to optimize structural stiffness, and it does not consider stress- and displacement constraints. This is the reason why topology optimization is often used as a preliminary design tool, as it does not guarantee that the structure will conform to stress- and displacement constraints. After using topology optimization, a

Stellenbosch University https://scholar.sun.ac.za

structure should be evaluated with a FE analysis or refined using other structural optimization techniques, such as size and shape optimization. Topology optimization is know to pose problems such as resulting checkerboard patterns and mesh-dependant results as described by Sigmund and Petersson (1998). With the advancement of commercial software such as GENESIS, checkboard patterns are dealt with efficiently, and should not appear in converged results. Furthermore, mesh-dependant result complications can be dealt with using high quality meshes, as will be discussed in Section 2.3.7.

2.3.6 Manufacturing considerations

Manufacturing is important to consider when doing any type of design. The same principle holds when doing optimization. There are various types of manufacturing processes and it is important to know how the different optimization techniques tie in with these manufacturing processes. Structural optimization and manufacturing types should therefore be considered simultaneously. If these techniques are carelessly applied, it could result in designs that are costly to manufacture or even un-manufacturable. Leiva (2008) suggests guidelines for combining optimization techniques with manufacturing types, but also states that it could change with time. The guidelines are listed in Table 2.1.

Table 2.1: Structural optimization- vs. manufacturing types (Leiva, 2008)

Optimization Types	Stamping	Casting	Extrusion	Tailor Welded
Sizing	Yes	-	-	Yes
Shape	Yes	Yes	-	-
Topology	Yes	Yes	Yes	-
Topometry	-	Yes	-	Yes
Topography	Yes	Yes	-	-

There are various ways in which optimization techniques can be used to improve the design of an automotive chassis. The optimization objective will entirely depend on the requirements. It could be that the optimal design is as light- or as stiff as possible. Leiva (2008) describes the various design requirements that could be achieved using different optimization techniques, as shown in Table 2.2. This table does however describe the objectives that are required for car chassis and not that of a truck. Truck chassis structures are constructed in a similar fashion as car chassis, only with bigger components and different layouts, thus the same rules should apply.

Table 2.2 shows that preliminary designs can always be obtained for any optimization technique. It is important to note that topology, topometry, and topography should only be used to obtained preliminary designs and that all

Stellenbosch University https://scholar.sun.ac.za

Table 2.2: Structural optimization vs. common car chassis optimization task requirements (Leiva, 2008)

Opt. Types	Preliminary	Stiffness	Bonding	Reinforcement	Final Design
Sizing	Yes	Yes	Occasionally	Yes	Yes
Shape	Yes	Yes	-	-	Yes
Topology	Yes	Yes	Yes	Yes	Occasionally
Topometry	Yes	Yes	Yes	Yes	Occasionally
Topography	Yes	Yes	-	Yes	Occasionally

designs should be optimized using size and/or shape optimization when final designs are required. This is to ensure that all constraints are satisfied and to refine the answers obtained from the previously mentioned techniques.

Manufacturing considerations will become very important when using topology optimization. Due to the design freedom that topology optimization tasks typically have, manufacturing constraints can be added to limit the task's design freedom and to find manufacturable designs. These constraints include,

- Mirror or cyclic symmetry
- Extrusion
- Periodic pattern repetition
- Axial and radial filling (Casting)
- Sheet forming (up to 2 combined layers)
- Uniformity

These constraints have significant influences on the topology results and can be used to avoid un-manufacturable designs. In most scenarios, manufacturing constraints reduces the number of design variables. An example of this would be elements that share symmetric positions around a symmetry plane, shares design variables if a symmetric constraint is used (Vanderplaats *et al.*, 1991).

2.3.7 Mesh refinement during the optimization procedure

Mesh refinement is a commonly used practice in FE analyses, as results are typically mesh dependant. In addition to the normal, FE analysis mesh refinement process, so too is mesh refinement a requirement for optimization procedures. This is because FE properties and nodal locations typically serve as variables for optimization procedures, therefore, by changing the mesh size, the optimization task variables will be influenced. If the same optimization task is performed with different mesh sizes, a different result could be expected

Stellenbosch University https://scholar.sun.ac.za

due to the adjusted design variables. For this reason, mesh refinement will be considered when setting up the optimization tasks. A simple example, shown in Figure 2.9, illustrates this phenomenon. A plate, shown in Figure 2.9a, is meshed with CQUAD4, 25 mm elements and subjected to a topometry optimization task. The topometry optimization task assigns element thickness variables to each of the elements within the mesh, which will be optimized during the operation. The results are shown in Figure 2.9b.

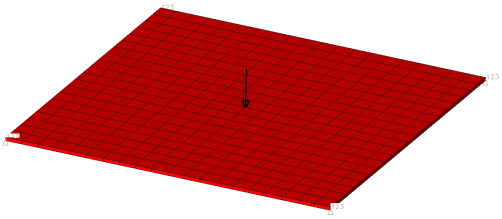

(a) 5 mm thick plate mesh

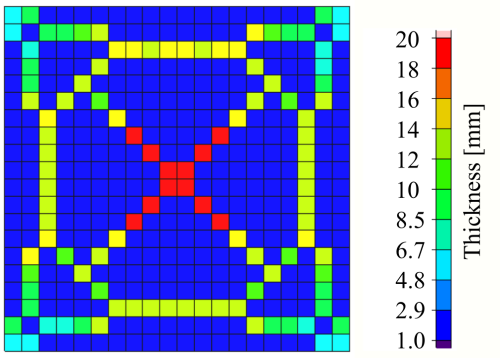

(b) Topometry element thickness results

Figure 2.9: Topometry optimization of a 500x500x5 mm plate using 25 mm CQUAD4 elements. A central point load is applied, with all four corners rigidly constrained

Afterward, the mesh size is reduced to 12.5 mm. Note that linear reductions in mesh sizes typically result in exponential element increases, therefore, mesh refinement should be performed within reasonable bounds. In this example, the quantity of CQUAD4 elements increased from 400 elements to 1600 by halving the mesh size. Considering that the topometry optimization task uses each element as a variable, the number of design variables is increased quite significantly, which should be reflected in the optimization results. The optimization task, aside from the changing design variables, was an exact copy of the first task. After comparing the original optimized plate to the 2nd optimized plate, shown in Figure 2.10, the notion that mesh refinement is important and should be considered during an optimization procedure is confirmed. The effects of mesh refinement for topology optimization tasks are also quite significant, knowing that the density of every element within the design domain serves as a design variable.

Stellenbosch University https://scholar.sun.ac.za

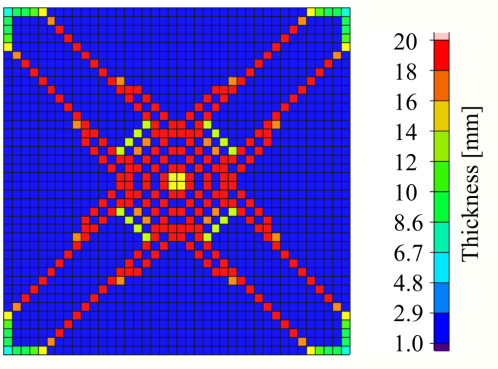

Figure 2.10: Topometry results for a 12.5 mm CQUAD4 element configuration

2.4 Material Considerations

For most of this project, the same material will be used, however it will vary when casting operations are being considered. The current boom is manufactured using high strength ASTM A-572 grade 50 steel plates and tubes (Alro Steel, 2011). This steel is typically used for constructing bridges, buildings, automotive-, and truck parts as it has a good combination of strength, notch toughness, and weldability. The material has a yield strength, σ_{Y}, of 345 MPa and an ultimate tensile strength, σ_{UTS}, of 448 MPa. The Young's modulus, E, and mass density, ρ, are 206 GPa and 7850 $\frac{\mathrm{kg}}{\mathrm{m}^3}$, respectively. The NX steel material will be used for components such as bushes and bearing blocks, having a σ_{UTS}, E, and ρ of 262 MPa, 207 GPa, and 7850 $\frac{\mathrm{kg}}{\mathrm{m}^3}$, respectively. Different materials will be used when casting is being considered as a manufacturing process. Table 2.3 lists several materials that are options for casting operations, ranging from the least- to most expensive. It should be noted that the material becomes considerably more expensive when moving from ductile- to austempered ductile cast iron as it is put through a tempering process. The current, most expensive casting material that is used for chassis component manufacturing is D100-70-03 ductile cast iron. The use of austempered cast iron will be avoided if possible. A Young's modulus and mass density properties of 163 GPa and 7100 $\frac{\mathrm{kg}}{\mathrm{m}^3}$ will be used for the ductile cast irons, respectively, which is based on the current ACTT design practices and recommendations.

2.5 Fatigue Life Design

The gradual degradation and damage of an object or structure are typically referred to as fatigue. Fatigue can become quite severe when introduced to welded regions and geometries that could cause stress concentrations. As mentioned in Section 2.1, both the boom and cross-member are constructed from various plates that are connected using a considerable number of welds. Knowing that welding operations are a big part of the terminal tractor manufacturing

Stellenbosch University https://scholar.sun.ac.za

Table 2.3: Cast iron material options (Monarch Industries, 2014)

Material grade	Tensile strength (MPa)	Yield strength (MPa)	Elongation (%)
Grey cast iron			
G2500	173	n/a	n/a
G3000	207	n/a	n/a
G3500	242	n/a	n/a
G4000	276	n/a	n/a
Ductile cast iron			
D60-40-18	414	276	18
D65-45-12	448	311	12
D80-55-06	552	379	6
D100-70-03	690	483	3
Austempered cast ductile iron			
Grade 750-500-11	750	500	11
Grade 1/900-650-09	900	650	9
Grade 2/1050-750-07	1050	750	7

process, repeated fluctuations of stress, also known as fatigue stress, should be included in the analyses and optimization tasks. This is to prevent or reduce the possibility of fatigue failure.

The standard BS7608 (British Standards Institution, 2014), used to guide the fatigue design and assessment of steel products, lists detailed procedures for approaching fatigue design. The first step in fatigue design is to classify all welded joints. The classification is dependant on a few factors, however focus will be given to the type of stress that is used to assess the joint, as well as the joint geometry. There are two stress types, namely nominal- and hot-spot stress, that can be used in the analysis of fatigue. The classification of a joint will partly depend on the type of stress being used. There are recommendations for selecting the appropriate stress type to use, however both stress approaches can be used, as they should yield similar results. These stress values are then used to assess a component's fatigue life expectancy using the relationship between the experienced stress and fatigue life, represented as S-N curves. Figure 2.11 represents a 97.7 % probability of survival S-N design curve, where Y represents the applied stress range, S_r, which is the difference between the highest and lowest experienced stress during a stress fluctuation cycle. The fatigue life cycles, N, are presented on a log scale, indicated by X. The stress range versus fatigue life relationship curves for each joint class is plotted in Figure 2.11, represented with their own unique joint class symbol for example *B*, *C* or *W1*.
Alternatively, the relationship between the fatigue life cycles, N, and applied stress range, S_r, for constant amplitude loading can be expressed mathematically with Equation 2.11,

$$\log N = \log C_0 - dSD - m \log S_r \tag{2.11}$$

Stellenbosch University https://scholar.sun.ac.za

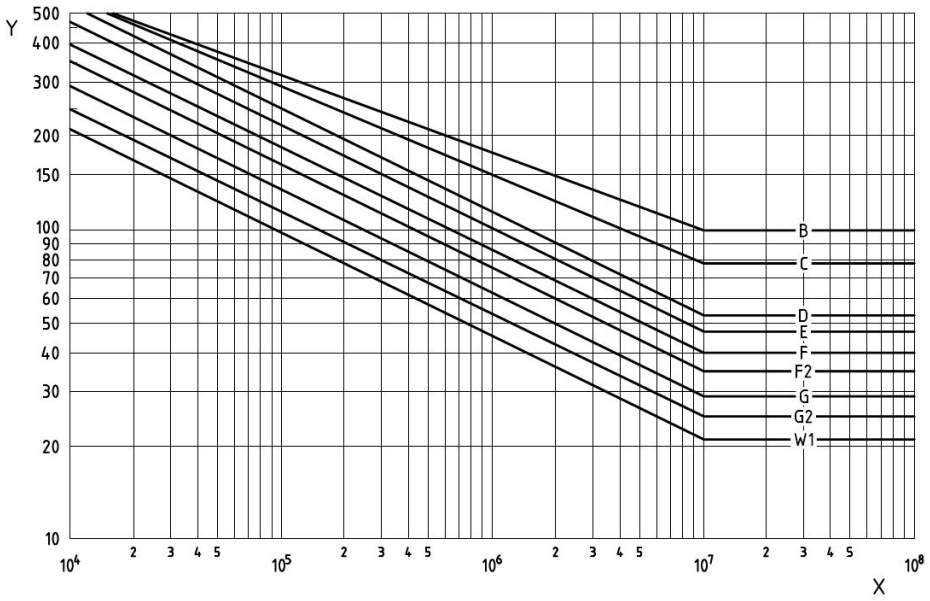

Figure 2.11: Basic S-N, joint class curves with 97.7 % probability of survival (British Standards Institution, 2014)

where C_0 represents the mean line S_r-N relationship, d represents the number of standard deviations from the mean S_r-N curve, and SD, the standard deviation of $\log N$. This equation can be generalized and simplified by introducing a new standard deviation variable term to form Equation 2.12,

$$\log C_d = \log C_0 - dSD \tag{2.12}$$

Equation 2.12 is then substituted into Equation 2.11 and simplified using the log rules, to form Equation 2.13:

$$S_r^m N = C_d \tag{2.13}$$

These equations can be used to calculate the life cycles for both the nominal- and hot-spot stress approach. The parameters required to do the necessary fatigue life calculations for any chosen joint class are listed in Table 2.4.

Another important consideration in the classification of a joint is the correct selection in joint geometry. For both stress approaches, stress concentrations are taken into account in the classifications of the joint detail, therefore it is important that the geometry, simulating a joint being analyzed, is selected correctly. If a joint geometry is misclassified, the joint detail will be incorrect, resulting in a failed analysis. An extensive joint geometry library is presented by BS7608, which should assist in the correct classification of joints.

In the process of calculating fatigue, load cases should be set up for the analysis thereof. These fatigue-focused load cases differ from the ultimate load cases, as the loading is smaller and experienced more frequently. For the analysis of the terminal tractor, load cases, known as fatigue equivalent static

Stellenbosch University https://scholar.sun.ac.za

Table 2.4: Parameter detail for basic S-N curves (British Standards Institution, 2014)

Class	C_o	$\text{Log}_{10}C_o$	m	SD	C_2	S_{oc} [MPa] ($N = 10^7$)
B	2.343×10^{15}	15.3697	4.0	0.1821	1.01×10^{15}	100
C	1.082×10^{14}	14.0342	3.5	0.2041	4.23×10^{13}	78
D	3.988×10^{12}	12.6007	3.0	0.2095	1.52×10^{12}	53
E	3.289×10^{12}	12.5169	3.0	0.2509	1.04×10^{12}	47
F	1.726×10^{12}	12.2370	3.0	0.2183	6.33×10^{11}	40
F2	1.231×10^{12}	12.0900	3.0	0.2279	4.32×10^{11}	35
G	5.656×10^{11}	11.7525	3.0	0.1793	2.50×10^{11}	29
G2	3.907×10^{11}	11.5918	3.0	0.1952	1.48×10^{11}	25
W1	2.500×10^{11}	11.3979	3.0	0.2140	9.33×10^{11}	21

load cases, were used to simulate this frequent loading. The fatigue equivalent static load cases were created by combining and scaling some of the ultimate load cases to simulate the worst-case fatigue loads. The fatigue equivalent static load cases are therefore an estimation of continual and frequent loading that a component experience that could eventually lead to fatigue damage. Further expansion on the fatigue equivalent static loads will be presented in Section 3.1.1.

2.5.1 Hot-spot stress approach

Hot-spot stress, S_H, is the structural stress that is found at the toe of a welded joint. A FE analysis can be used to determine the surface stresses near the welded region, which can then be extrapolated to obtain an estimate for the hot-spot stress at the weld toe. This method is known as surface stress extrapolation (SSE). The principle stress, normal to the weld toe, is used to determine the hot-spot stress. According to BS7608, the most common SSE method is presented by Equation 2.14,

$$S_H = 1.67\sigma_{0.4t} - 0.67\sigma_{1.0t} \tag{2.14}$$

where t is the plate thickness and $\sigma_{0.4t}$ and $\sigma_{1.0t}$ are surface stresses, normal to the weld toe, at distances $0.4t$ and $1.0t$ away from the weld toe, respectively. By rearranging Equation 2.13, fatigue life cycles, N, can be calculated with Equation 2.15,

$$N = \frac{C_d}{S_r^m} \tag{2.15}$$

where S_r is the hot-spot stress, calculated using Equation 2.14. Once the joint class has been selected, parameters C_d and m can be obtained from

Stellenbosch University https://scholar.sun.ac.za

Table 2.4. Additionally, S_{oc} is added to the table, indicating the constant amplitude fatigue limit that should not be exceeded if fatigue failure below 10^7 cycles is to be avoided. A constant amplitude stress value below S_{oc} for a particular joint class should theoretically translate to infinite life, therefore no fatigue failure will occur.

2.5.2 Nominal stress approach

The nominal stress, S_N, is described as the summation of bending and membrane stress at a given location. In order to do fatigue life calculations at a selected joint, the von-Mises stress is selected as the nominal stress in the region near the weld toe, therefore

$$S_r = S_N = \sigma_{VM}, \tag{2.16}$$

where σ_{VM} is the von-Mises stress. Following the same procedure as for the hot-spot stress approach, Equation 2.15 can be solved to obtain the expected fatigue life for the nominal stress approach.

The two methods should predict fatigue lives with the same order of magnitude, however the nominal stress approach is the more conservative approach and lower fatigue life values are expected. Even though both methods should deliver similar results, the nominal stress approach is preferred as the implementation thereof is much easier and generalized, especially when working with complex FE models. This becomes clear when considering that the hot-spot stress approach calculation relies on stresses normal to the weld toe, whilst the nominal stress approach requires the von-Mises stress in the region of the weld toe. Expecting that complex models typically have welding seams in many differing orientations, multiple stresses in different principle directions will be required to calculate the various joints' fatigue lives. It is for this reason that the nominal stress approach is preferred and used for the evaluation of ACTT components, as it is a more generalized approach.

To ensure consistent and accurate nominal stress value measurements, a convention was created, instructing that the stresses are measured two elements away from the welded joint. Elements are selected to be half the size of the weld thickness for consistent weld analyses. These two elements cover the welded area, and they form a region called the weld singularity region. FE stress results within the singularity region are not true representations of the actual stress experienced, and should not be used.

2.5.3 Hot-spot stress- vs. nominal stress approach

A rudimentary weld example problem was created to test the two welding theories and to investigate how these two stress approaches will compare. According to the BS7608 standard, the hot-spot stress for a fillet weld should be

Stellenbosch University https://scholar.sun.ac.za

higher compared to the nominal stress at the weld toe, to validated the stress calculation. Typically, a hot-spot stress value is expected to be around 15 % or higher (British Standards Institution, 2014). To compensate for the higher stress, the standard advises that the nominal stress approach should be used if possible, as the hot-spot stress calculation method does contain deficiencies that are subject to future improvements.

The boom and cross-member are almost exclusively manufactured using fillet welds, therefore a similar example containing a fillet weld will be used. From the joint geometry library, typical T-joint fillet welds are classified as class D and F2 for the hot-spot stress- and nominal stress approach, respectively. The chosen geometry is displayed in Figure A.1 of Appendix A, and available in Table 4 of the fatigue standard BS7608 (British Standards Institution, 2014). The corresponding parameters and constant amplitude fatigue limit for these joints are listed in Table 2.4. Figure 2.12a shows two plates that are joined using 10 mm thick fillet welds, forming a T-joint. The plates are reduced to mid surface planes and meshed using 5 mm CQUAD4 elements, which is half the weld thickness. The FE model is depicted in Figure 2.12b, highlighting the stress singularity region in red. The hot-spot- and nominal stresses can be found using Equations 2.14 and 2.16, respectively. Figures 2.13a and 2.13b show where the stresses are measured in order to calculate the fatigue lives for both approaches. Linear interpolation is used to calculate the stress value for $\sigma_{0.4t}$. The hot-spot- and nominal stress can now be calculated as shown in Equations 2.17 and 2.18,

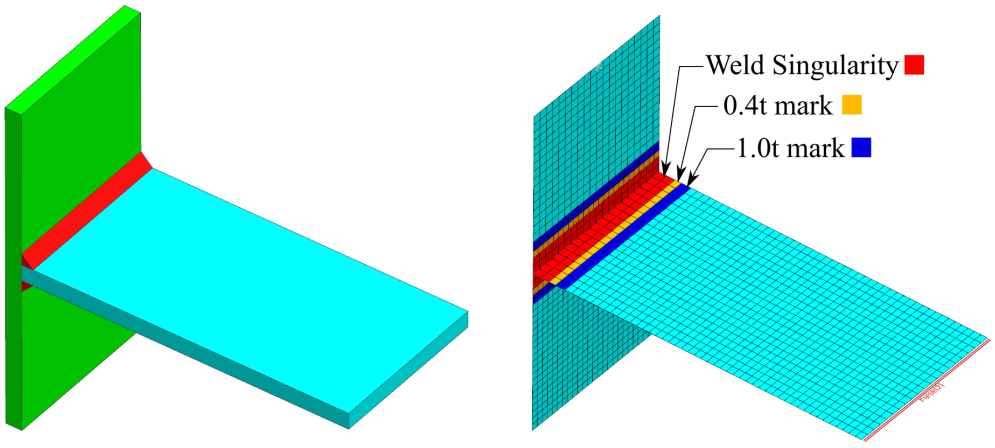

(a) Physical T-joint, with welded detail **(b)** T-joint FE model

Figure 2.12: T-joint FE model, with various mesh region illustrations

$$S_H = 1.67(128.027) - 0.67(121.457) = 132.430 \text{ MPa} \tag{2.17}$$

Stellenbosch University https://scholar.sun.ac.za

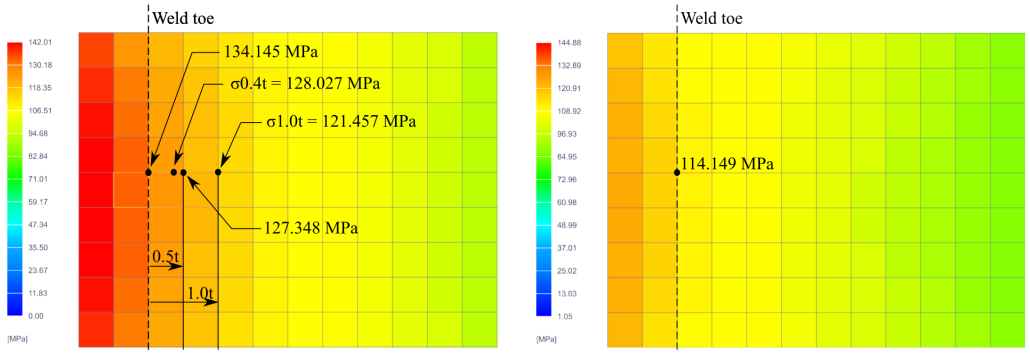

(a) Measurements for hot-spot calculation **(b)** Measured nominal stress

Figure 2.13: Hot-spot and nominal stress measurement example

$$S_r = S_N = \sigma_{VM} = 114.149\,\text{MPa} \tag{2.18}$$

Using these values, the hot-spot stress is calculated to be 16.01% higher than the nominal stress, which is in accordance with what the standard predicts. Using these values and Table 2.4, the fatigue lives can be calculated for both methods.

2.6 Structural Optimization Software

The software packages that will be used during this project include a FE package, NX, and an analysis and optimization package, GENESIS. GENESIS uses Design Studio as a design orientated pre- and post-processor graphical interface. The various software packages can interact, as illustrated in Figure 2.14.

NX is a FE package that is used to create and perform FE analyses (Siemens Product Lifecycle Management Software Inc., 2014). This software package will mainly be used to develop and verify existing FE models. NX also has sophisticated CAD modeling capabilities, if 3D modeling is required.

Design Studio is a pre- and post-processing graphical interface that is coupled with GENESIS. The integration between GENESIS and Design Studio makes it easier for a designer to create and perform optimization tasks. Design studio acts as a link between the FE model developed in NX and the optimization software, GENESIS. Design Studio offers built-in trails that are used to set up or create an optimization problem. These trails include the definition of design objectives, constraints, and design variables, to name a few. Post-processing is possible through contour plots for example stress distribution, deformed shape plots, and animations (Vanderplaats Research & Development, 2018).

As already mentioned, GENESIS will be used for its design analysis and optimization capabilities. GENESIS optimization capabilities include topology-,

Stellenbosch University https://scholar.sun.ac.za

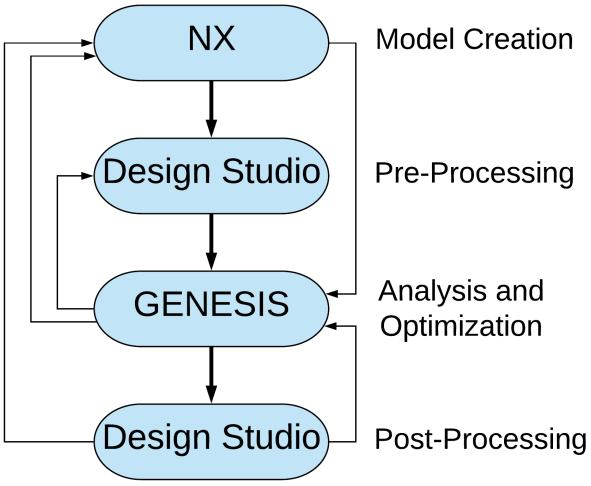

Figure 2.14: Software package interactions

shape-, size-, topography-, topometry- and free-form optimization. GENESIS uses the advanced approximation concepts approach, as discussed in Section 2.3, to find an optimum design. GENESIS has a multitude of functions and features that can be found in the GENESIS brochure (Vanderplaats Research & Development, 2018). Furthermore, GENESIS uses the gradient-based optimization library know as DOT as the default optimizer. A selection of other optimizers are also available within the software package, however DOT will be used for the remainder of this project. No further discussions regarding the mathematics behind the build-in optimization algorithms will take place as the focus is rather to apply the commercial software to solve real-world problems.

Stellenbosch University https://scholar.sun.ac.za

Chapter 3

Boom Design Improvement using Structural Optimization

This chapter focused on achieving the first objective, which is the improvement of the current boom design, using size-, shape-, and topometry optimization. All improvements were made based on the current terminal tractor boom design. The CAD model shown in Figure 2.1b was made available for the project and used to develop a FE model. After the FE model had been developed, the various optimization techniques were used to explore and find design improvements. Due to the high number of weld regions in the boom design, it was decided to disregard topography optimization, as it could introduce numerous discontinuities, and interferences between surfaces and edges that are connected via welds. The possibility of improving the structure using topography does exist, however the application thereof will prove to be a complicated procedure, considering the boom's manufacturing requirements.

3.1 FE Model Development and Comparison

The first step in preparation for the optimization procedure was to develop a FE model that accurately resembles the original CAD model. It is necessary to simplify CAD models as they typically present too much detail, which could negatively affect FE model development and analysis. Once the model was simplified to an acceptable degree, it was discretized into finite elements, forming a FE model. FE model validation was done by simulating known load cases and comparing the FE analysis results with the known load case responses, which were used consistent with the current ACTT practices and simulations. Thereafter, the model was imported into Design Studio, where the optimization tasks were defined and executed. Further preparation was required in Design Studio, such as the isolation of the welded regions within the various meshes, as shown in Figure 2.12. The use of mesh isolation was required to assign different stress constraints and variables to certain mesh areas.

Stellenbosch University https://scholar.sun.ac.za

Section 3.2 will discuss optimization constraints and variable assignment in detail. GENESIS was used to perform FE analyses as part of the optimization procedure, therefore, it was important to ensure that the FE results obtained using NX and GENESIS match to an acceptable degree. Consequently, a comparison was done using both linear static- and eigenvalue analyses.

3.1.1 Boom FE model development

Following the FE model development procedure mentioned in Section 3.1, the CAD model of the boom was simplified by removing all nuts, bolts, small holes, and highly detailed geometries. The boom mostly consists of plates that are ideal for meshing with 2D elements. This required all plates to be reduced to mid-surface planes with the original plate geometries. The 5th-wheel is a very intricate part and will be difficult to simplify, discretize, and analyze, therefore, the decision was made to replace it with a 1D element that has the same moment of inertia around its axis of rotation, as well as its symmetry plane. The detail of the 5th-wheel is also less important in that it is not a designable part and purchased from an external supplier. The hydraulic cylinder rods, required to actuate the boom, were replaced with 1D elements, as well as the connecting pins located in the bushes. The remaining components, which include the bushes and bearing blocks, will be meshed using 3D elements, therefore requiring no further simplification. The simplified boom model is illustrated in Figure 3.1. Figure 2.1b illustrates the original CAD model, whereas Figure 3.1 is the simplified version thereof. Table 3.1 lists the various plate- and tube names, as numbered in Figure 3.1.

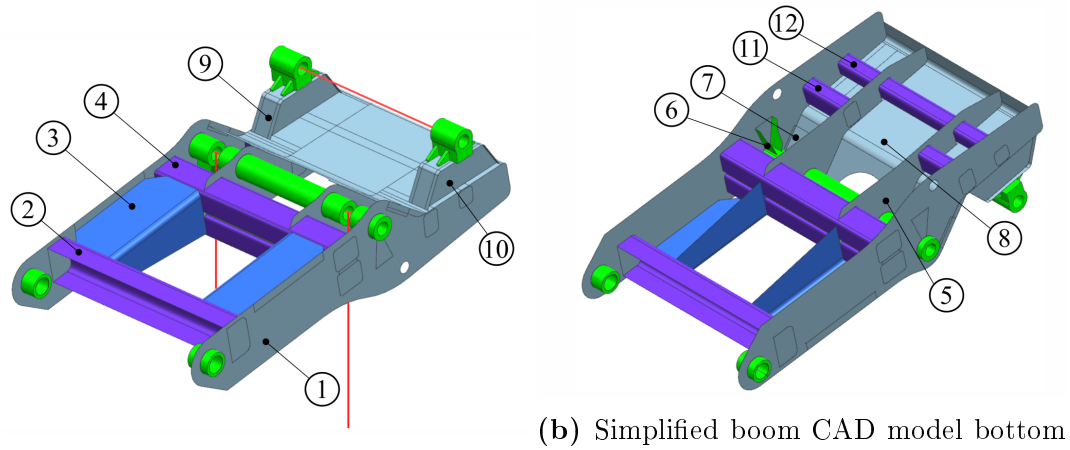

(a) Simplified boom CAD model top view view

(b) Simplified boom CAD model bottom

Figure 3.1: Simplified boom CAD model, derived from the CAD model displayed in Figure 2.1b

Stellenbosch University https://scholar.sun.ac.za

Table 3.1: Plate descriptions as illustrated in Figure 3.1

1	Side plate		5	Centre plates		9	Bearing mount plates
2	U-plate		6	Gussets		10	Bearing contact plates
3	L-plate		7	Stiffener plates		11	Short tubes
4	Centre tubes		8	Backplate		12	Rear tube

A FE model was created by discretizing the simplified boom CAD model. The bushes and bearing blocks, displayed with green in Figures 3.1a and 3.1a, were meshed using solid CTETRA10 elements. The plate components that have been mid-surfaced, were meshed with CQUAD4 elements. The pins, hydraulic cylinder rods, and 5th-wheel were all meshed with CBEAM elements. Figure 3.2a depicts the boom FE model. The CBEAM elements are shown in red, CTERTRA10 elements in green, and the remaining CQUAD4 elements in different colors. Figure 3.2b shows the boom in an upside-down position, without displaying the CBEAM elements. Based on the nominal stress approach recommendations made in Section 2.5.2, mesh sizes were selected to be half the size of the weld thicknesses which are found within plates.

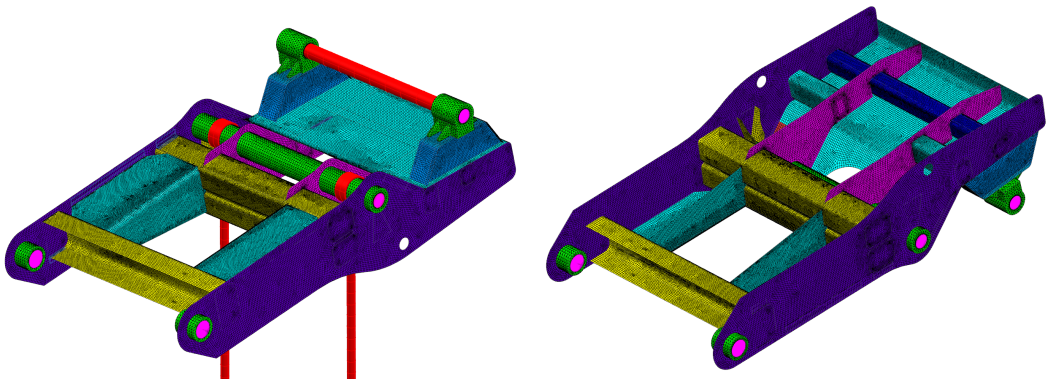

(a) Boom FE model top view **(b)** Boom FE model bottom view

Figure 3.2: Boom FE model

After the FE model creation, load cases, which include physical input loads and boundary conditions, were assigned to the FE model in preparation for the FE analysis. The load cases were based on measured operational data and loads, obtained from a real-life ACTT during operation. The FE analysis includes two ultimate loads and three fatigue equivalent static loads that are required for fatigue design. The ultimate loads were calculated with known input loads that experience gravitational acceleration during operation. Table 3.2 summarizes the input loads of the five load cases with their acceleration scale factors. These load cases include the 1st- and 2nd ultimate load case, ULC 1 and ULC 2, respectively, with the three fatigue equivalent static load

Stellenbosch University https://scholar.sun.ac.za

Table 3.2: Input loading and gravitation acceleration scale-factors for each load case. ULC and FESL represents the ultimate load cases and fatigue equivalent static load cases respectively

Axis	Load	Area	Gravitational acceleration scale factors				
			ULC 1	ULC 2	FESL 1	FESL 2	FESL 3
Z	9.81 m/s^2	Structure	3	1	0.21	-	-
	24 940 kg	Bearings	3	1	0.21	-	-
	43 205 kg	Right bearing	-	-0.4	-	-0.13	-
	43 205 kg	Left bearing	-	0.4	-	0.13	-
	2 935 kg	Bearings	-	-	-	-	0.05
Y	9.81 m/s^2	Structure	-	0.4	-	0.13	-
	24 940 kg	Bearings	-	0.4	-	0.13	-
X	9.81 m/s^2	Structure	-	-	-	-	0.05
	24 94 kg	Bearings	-	-	-	-	0.05

cases, FESL 1, FESL 2 and FESL 3. All loads were applied at the 5th-wheel bearings, with gravity affecting the entire structure.

The FE model boundary conditions are identical for all five load cases. The frontal bushes, as shown in the left-bottom of Figure 3.2a, were constrained to only pivot around their central axes, which would normally be attached to pins located on the chassis. The cylinder rods were connected to both the chassis and boom. Both sides were kept in position using pins that allow rotation around their central axes. The cylinder pins located in the bushes were also allowed to move within the direction of their central axes. The applied boundary conditions and loads of the 2nd fatigue equivalent static load case are shown in Figure 3.3a and Figure 3.3b, respectively.

3.1.2 Boom FE model comparison

After developing the FE model in the NX environment, it was exported to GENESIS and Design Studio where most of the continued FE analyses and optimization tasks were performed. To evaluate the newly developed boom FE model, FE analysis results obtained with GENESIS were compared to a previous, internally validated, ACTT boom model. This comparison can be seen in Figure 3.4, where the stress distributions from the 1st ultimate load cases were compared between the two models. When the FE results are visually inspected, slight discrepancies are found, however, highly stressed regions show similar stress distributions. It should be noted that discrepancies are to be expected knowing that NX and GENESIS have different solvers, and the color-gradient resolution between the user interfaces also differ. Visual comparisons were also done for the 2nd ultimate load case, which showed similar stress distributions. A qualitative comparison approach is insufficient to do a

Stellenbosch University https://scholar.sun.ac.za

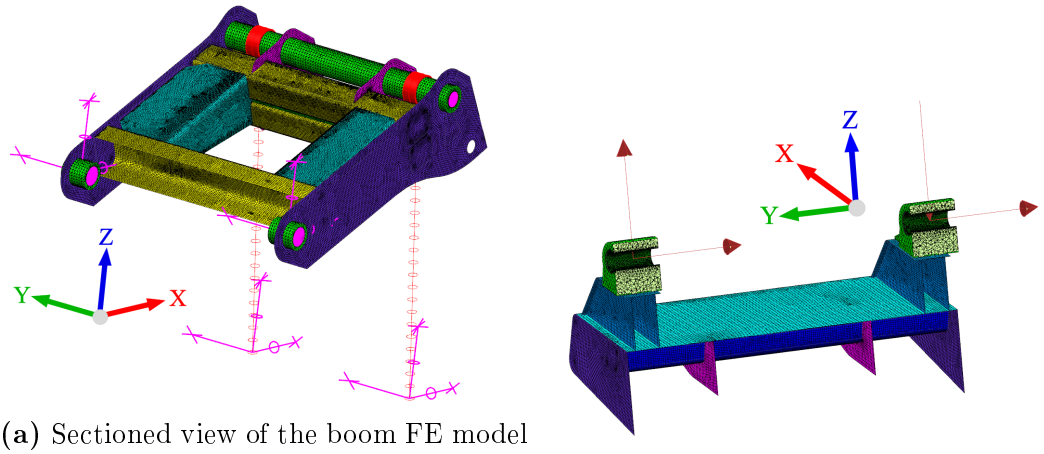

(a) Sectioned view of the boom FE model displaying the applied boundary conditions

(b) Sectioned view of the boom FE model displaying the FESL 2 load case

Figure 3.3: Showcase of the FESL 2 loads and boundary conditions

thorough evaluation of the developed model, therefore, highly stress regions were selected to compare stress results quantitatively. Figure 3.4 pinpoints the regions that were used for the detailed quantitative comparison between the two models. Stress values of individual elements in highly stressed areas were compared, as well as, the average stress of 9-element square clusters within the same region. The quantitative comparison is summarized and listed in Table 3.3. Overall, a highest stress deviation of 9.65 % was found. The most deviation was found at the mid tube stress values, however, these stresses are well below the yield stress of the material and it should have minimal to no effect on the optimization procedure. The measurements made at the mid tube was at a very sensitive region, where multiple weld joints are present. As already mentioned, some deviation is to be expected knowing different solvers were used for the FE analyses. After making a similar qualitative comparison for the 2nd ultimate load case, presented in Appendix B, and knowing the remaining FESL load cases are scaled versions of the two ultimate load cases, no further comparisons were required.

As an additional FE model comparison check, modal analyses were done to verify that the model was properly connected, as originally defined in NX. Table 3.4 lists the first 10 modes obtained from the original model analysis in NX and the newly developed model analysis in GENESIS. From the analyses performed, it was found that the modal responses are near similar, with a largest difference being 4.5 %. By evaluating the listed values in Table 3.3, Table B.1, Table 3.4 and the similarity between the stress distributions depicted in Figure 3.4, the newly developed boom was deemed an acceptable equivalent to the original boom FE model.

Stellenbosch University https://scholar.sun.ac.za

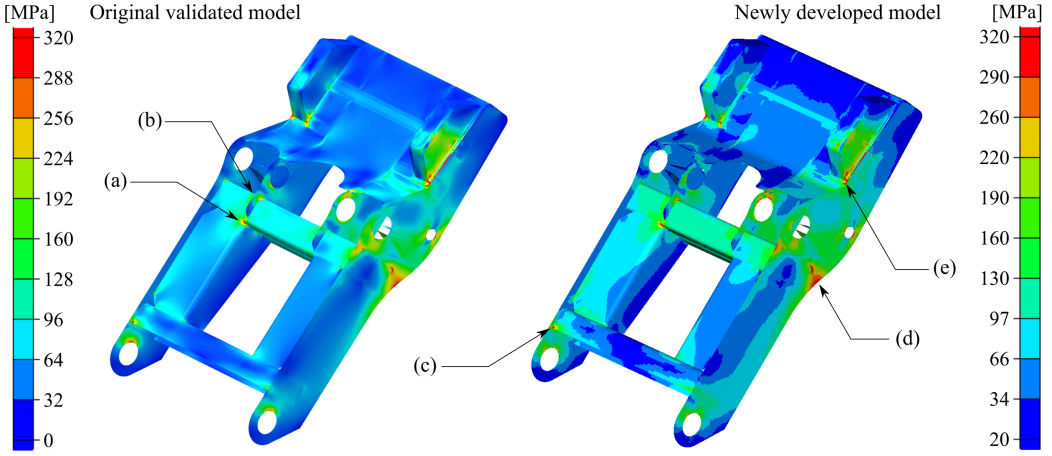

Figure 3.4: Boom stress distribution for the 1st ultimate load case. Shown on the left is the original boom that was designed, validated and provided to the project. Shown on the right is the newly developed boom model that will be used for further optimization procedures. Symbols are used to indicate the measuring areas for the values listed in Table 3.3

Table 3.3: Numerical stress comparison between the original boom FE model developed in NX and the imported model in Design Studio, with percentage difference between measured values. Symbols are used to locate the measuring areas shown in Figure 3.4

Plate description	ULC1: 3g-Z (1 element)			ULC1: 3g-Z (9 elements)		
	Original model	New model	Diff (%)	Original model	New model	Diff (%)
L-Plate (a)	253.87	261.97	3.19	254.3	262.82	3.35
Centre tube (b)	249.23	251.64	0.97	241.85	244.16	0.96
Back plate (c)	313.53	311.62	0.61	306.90	311.62	1.54
Mid plate (d)	223.17	201.64	9.65	242.68	215.95	11.0
Side plate (e)	300.18	305.94	1.92	291.25	297.13	2.02
Bearing mount (f)	214.64	205.09	4.45	213.6	204.15	4.42

3.2 Boom FE Model Optimization

With a completed and validated boom FE model, optimization tasks were created to optimize the model. In preparation to perform optimization tasks, an objective function, design variables, and design constraints were required to be set up. The objective function was selected to minimize the boom's mass. To minimize the objective function, design variables were created to alter the boom design. There exist multiple types of design variables to fit the need for the desired optimization technique being used. Lastly, design constraints were required to control the optimization procedure, to obtain realistic or feasible designs. It is important that the structure does not fail under loading, therefore, stress constraints were applied to the entire structure. These stress constraints were based on material limitations, as discussed in

Stellenbosch University https://scholar.sun.ac.za

Table 3.4: Comparison of the first 10 modes obtained from NX and Design Studio modal analyses

Mode number	NX model [Hz]	DS model [Hz]	Difference [%]
1	55,303	55,300	0,005
2	55,306	55,300	0,011
3	82,640	78,920	4,501
4	93,880	93,700	0,192
5	112,91	112,70	0,186
6	122,79	122,80	0,008
7	123,43	123,40	0,027
8	220,31	220,60	0,131
9	220,63	220,60	0,014
10	267,28	266,70	0,217

Section 2.4. Fatigue also plays an important part in the analysis, thus the necessary weld region detail was added to all meshes for the accurate analysis thereof. Using the meshing convention as described for the nominal stress approach, weld and singularity regions were added to the plate meshes for fatigue-stress constraint assignment. Figures 3.5 and 3.6 both show the boom model with the added weld- and singularity regions, depicted with the colors pink and red, respectively. As mentioned in Section 2.5.2, singularity regions are areas where the FE stress values are elevated and not true representations of the actual experienced stress. The singularity regions will therefore not used for stress measurements. Singularity regions were defined as two elements wide, with a similar thickness as the weld detail. Weld measurement regions were defined next to the singularity regions, which is where the nominal stress measurements are taken.

Due to the number of load cases, weld detail, and individual designable plates, a large number of stress constraints had to be enforced. The stress constraints were based on the current boom acceptance criteria to keep the optimization results consistent with the current design practices used for the boom. For the ultimate load cases, no material should exceed von-Mises stress values of 327.25 MPa. This stress value was calculated based on the material's yield stress, σ_{yield}, of 350 MPa and a safety factor, SF, of 1.07, as shown by Equation 3.1:

$$\sigma_{\text{constraint}} = \frac{\sigma_{\text{yield}}}{SF} \tag{3.1}$$

The weld regions were assigned the same stress constraints as the plates during the analysis of the ultimate load cases. The welded detail does however require specific stress constraint assignment for the FESL load cases as fatigue becomes the main cause of failure. As mentioned in Section 2.5.3, the welded regions should not exceed 35 MPa, since they have been classified as class F2

Stellenbosch University https://scholar.sun.ac.za

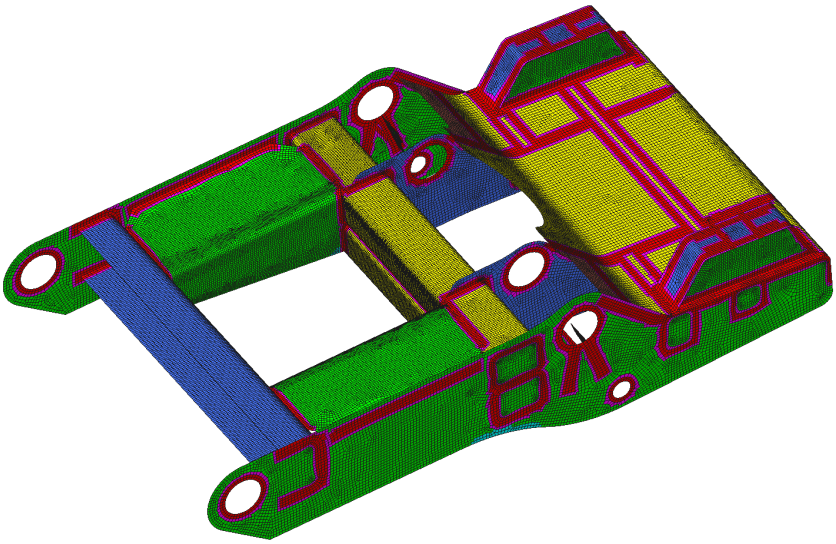

Figure 3.5: Boom FE model after addition of weld-region detail to plate meshes

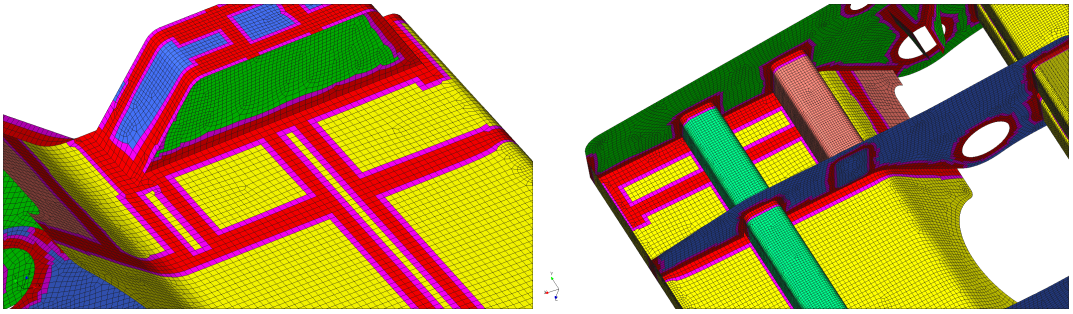

(a) Top view of detailed welded-region **(b)** Bottom view of detailed welded-region

Figure 3.6: Detailed depiction of weld- and singularity regions

geometries. Plate regions, further away from the welded joints, were classified as class B geometries with a constant amplitude fatigue limit of 100 MPa. Consequently, meshes that did not form part of the welded detail were assigned the class B fatigue limit. Due to the large number of stress constraint assignments that were required, a stress constraint table was created. Table C.1, in Appendix C, lists the various plates with their corresponding load case constraints. Table C.1 is an exact description of how the stress constraints were assigned to the various boom sub-components. Some sub-components areas were allowed to exceed the stress constraint limits. These experienced stresses were deemed acceptable in the original boom FE validations, as provided to this project. These altered stress constraint values are highlighted in bold, as presented in Table C.1.

The FE model, depicted in Figure 3.5, was used for all the size-, shape-, and topometry optimization tasks. The objective function and stress constraints were applied similarly for all the optimization techniques, however, the design

Stellenbosch University https://scholar.sun.ac.za

variables varied based on the technique being used.

3.2.1 Boom size optimization

The boom is mostly constructed from plate components, ideal for the application of size optimization. It was, therefore, selected as the first optimization technique to be used. To start the optimization task setup, the objective function and stress constraints were applied to the optimization task as mentioned. In order to use size optimization, various plates were assigned continuous-range size variables that are limited with an upper and lower bound thickness value, with the original thickness as a starting point. The same design variables are assigned to matching plates to ensure that symmetry within the boom design is maintained, for example, the two side plates. All welded-regions within individual plates were also assigned the same plate thickness variable to prevent any varying thickness within those plates. Figure 3.7 displays the final plate thicknesses as fractions of the original thicknesses, with Figure 3.8, summarizing the objective function values and stress constraint violations for the first successful size optimization task, namely Task 1.

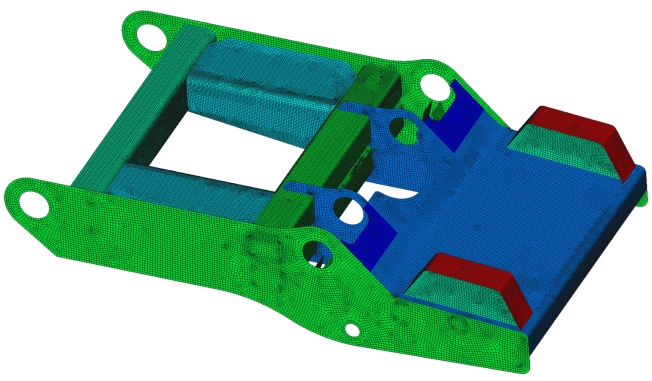

Plate name	Tfrac
Bearing Contact Plates	1.68
Side Plates	1.04
Gussets	1.00
Centre Plates	0.98
Bearing Mount Plates	0.91
U-Plates	0.90
Rear Tubes	0.84
L-Tubes	0.78
Back Plates	0.64
Centre Plates	0.60
Stiffener Plates	0.44
Short Tubes	0.42

Figure 3.7: Size optimization Task 1, displaying final plate thicknesses as fractions of the original plate thicknesses

The objective function starting value is the accumulative mass of all the variable assigned plates, including the weld material mass, totalling at 389.04 kg. The objective function value, as shown in Figure 3.8, was reduced from 389.04 kg to 349.92 kg. Using this formal optimization procedure, a 10.05 % reduction in mass was found when compared to the existing boom design that has received prior in-house non-formal optimization. The new structure also showed no constraint violation, indicating that a feasible design had been found, in terms of material capability. A similar optimization task, Task 2, was executed thereafter, however the design variables of the bearing mount- and bearing contact plates were removed. This was a decision based on the fact that the

Stellenbosch University https://scholar.sun.ac.za

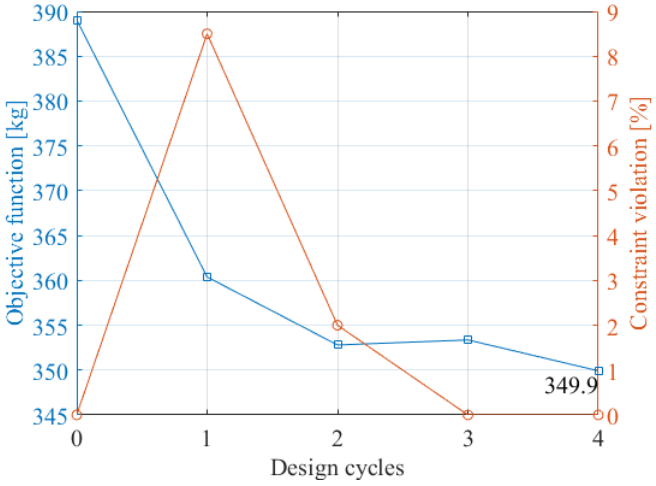

Figure 3.8: Objective function- and constraint summary for Task 1

5th-wheel was modelled differently compared to the physical component, and large changes at its interface points should be avoided. A 9.17 % mass reduction, without any stress constraint violations was achieved. The bearing mount- and contact plates experienced large size changes during Task 1, and therefore, by removing those design variables for Task 2, a smaller mass reduction was expected. Unfortunately, the results obtained from Tasks 1 and 2 are not practical changes that can be implemented, as plate manufacturers only have discrete plate thicknesses available on their catalogs. To find practical results, the continuous-range variables must be replaced with discrete variables using the catalogue plate sizes. The first discrete variable optimization task, namely Task 3, allowed all the plates and tubes to be changed to the available plate- and tube catalog sizes, listed in Table D.1 and Table D.2, respectively. After running the optimization task, it converged with a 3 % increase in mass. This was an unexpected result, as it would mean that the input design is more optimal in terms of mass, compared to the "optimized" structure. Knowing that GENESIS uses gradient-based algorithms, it could be that the algorithm got stuck in a local minimum within the first few design cycles. After some inspection, it was found that the side plates experienced thickness increases at an early optimization task design cycle, never to be reduced again. These are large plates, which could have a significant impact on the entire optimization procedure. Based on this occurrence, it was decided to remove the side plates' design variable, to prevent the adjustment of the side plate thicknesses. Using this approach for the subsequent optimization task, Task 4, a 3.5 % reduction in mass, without any stress constraint violations were found. Unlike the results obtained from Tasks 1 and 2, this mass reduction is tied to practical results that could be implemented. The final plate thickness configuration can be seen in Figure 3.9, with an overall objective function summary of the various optimization runs, depicted in Figure 3.10. Table 3.5 serves as a reference for

Stellenbosch University https://scholar.sun.ac.za

the four optimization tasks definitions.

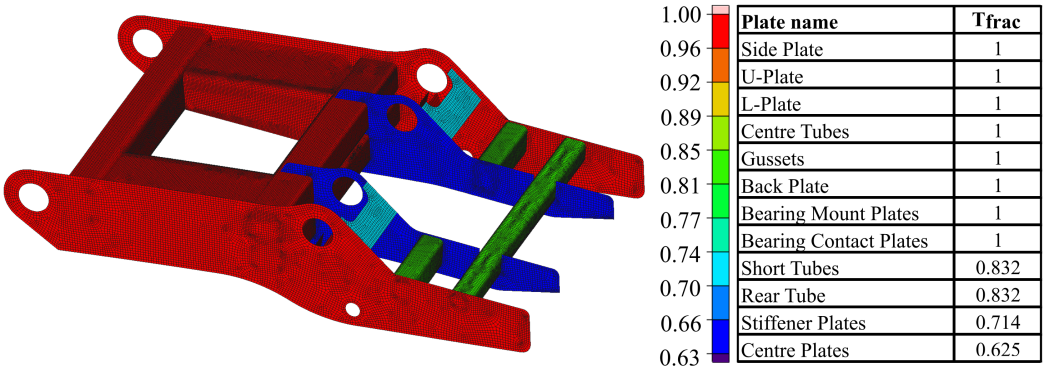

Plate name	Tfrac
Side Plate	1
U-Plate	1
L-Plate	1
Centre Tubes	1
Gussets	1
Back Plate	1
Bearing Mount Plates	1
Bearing Contact Plates	1
Short Tubes	0.832
Rear Tube	0.832
Stiffener Plates	0.714
Centre Plates	0.625

Figure 3.9: Size optimization Task 4, displaying final plate thickness as a fraction of the original thickness. This optimization task used discrete-set optimization, based on the available plate size catalogue

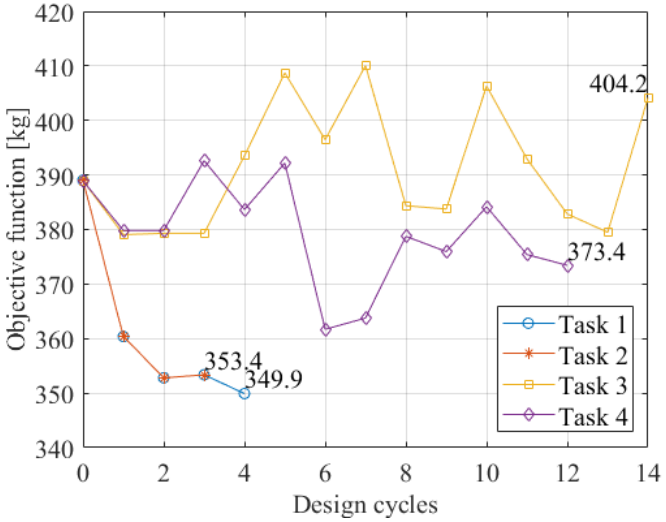

Figure 3.10: Objective function summary for shape optimization Tasks 1 to 4

3.2.2 Boom shape optimization

Now that satisfactory results have been obtained using size optimization, the next step was to use shape optimization to generate design improvements by physically morphing the design. The objective function was selected to minimize the boom's mass. The stress constraints were applied as instructed by the stress constraint table, Table C.1, similar to the size optimization tasks. Lastly, the shape variables were required to be defined. This required the

Stellenbosch University https://scholar.sun.ac.za

Table 3.5: Size optimization task-definition reference summary

Task	Objective function	Optimization method	Size variables omitted
1	Mass minimization	Continuous size	None
2	Mass minimization	Continuous size	Bearing mount plates Bearing contact plates
3	Mass minimization	Discrete size	None
4	Mass minimization	Discrete size	Side plates

creation of shape domains and shape morphing sets, to formulate the design variables for the optimization task. First, the shape domains were created to select all the nodes that were to be moved with the shape variables. The shape variables were created by applying a perturbation vector to the shape domains using shape morphing sets. The shape morphing sets define the mode and direction in which the perturbations should morph the domains. Shape variables are scale factors for the perturbation vectors, defined with an upper and lower scale factor bound. Therefore, shape variables were used to control the magnitude of these perturbations, consequently controlling the intensity of the proposed shape change. Figures 3.11 and 3.12 show shape domains and morphing sets that were used to enforce shape changes within the boom's side plates and L-plate, respectively. Shape domains were also morphed quadratically by applying perturbation vectors between two shape domain nodes.

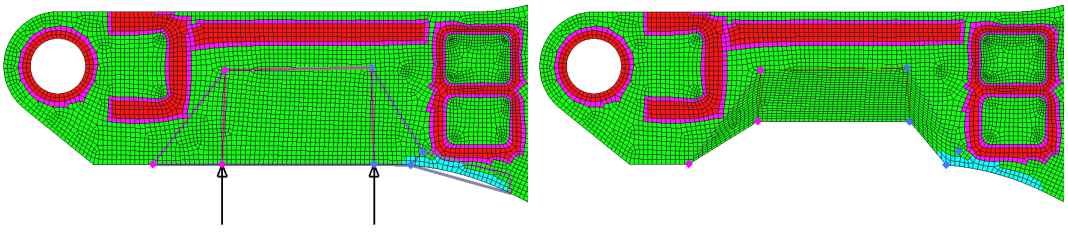

(a) Quad- and Tria-domains **(b)** Morphed plate shape

Figure 3.11: Shape morphing set, enforcing a shape change to the side plate

Overall, 21 shape domains and 10 shape morphing sets were created for the shape optimization tasks. Figures E.1 and E.2 illustrates the various shape changes as defined by the shape morphing sets. The first shape optimization task, Task 1, showed nearly no shape changes. Knowing that the lateral FESL load case stress measurements are close to the design stress constraint limits, it was decided to create an optimization task, with the lateral FESL load case excluded. The second shape optimization task, Task 2, showed a 5 % reduction in mass. This result is a strong indication that the lateral FESL

Stellenbosch University https://scholar.sun.ac.za

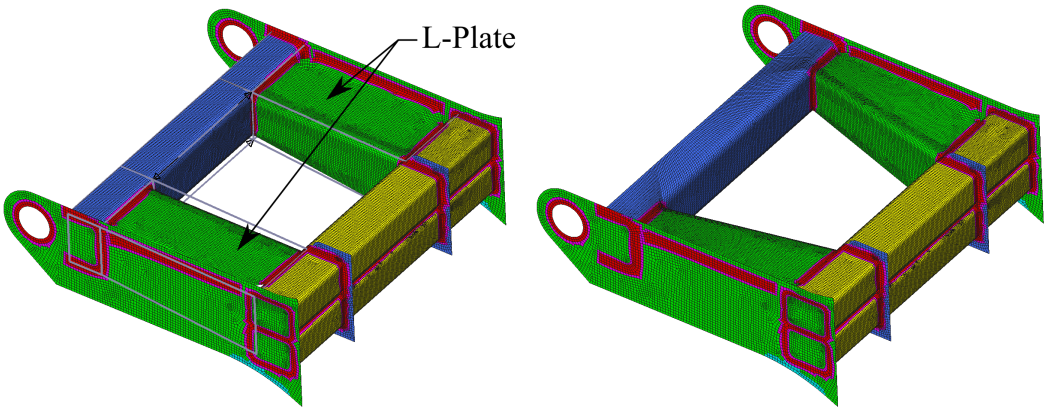

(a) L-plates, with Hexa-domains **(b)** Morphed L-plates

Figure 3.12: Shape morphing set, enforcing shape changes to the L-plates

load case was the cause of the negligible mass reduction in Task 1. It was decided to create another shape optimization task, Task 3, with the lateral FESL load case as the only active load case. The idea was to inspect how the shape changes compare to the second optimization task results. It was found that some of the shape changes were conflicting to a degree where they are almost opposite to each other. Even though there were similar shape changes, the combination of load cases created a stalemate between the conflicting and similar shape changes, resulting in no shape change at all. The conflicting shape changes and objective function value summaries for the 3 tasks are illustrated in Figures 3.13 and 3.14, respectively. The three optimization task definitions are listed in Table 3.6 for reference.

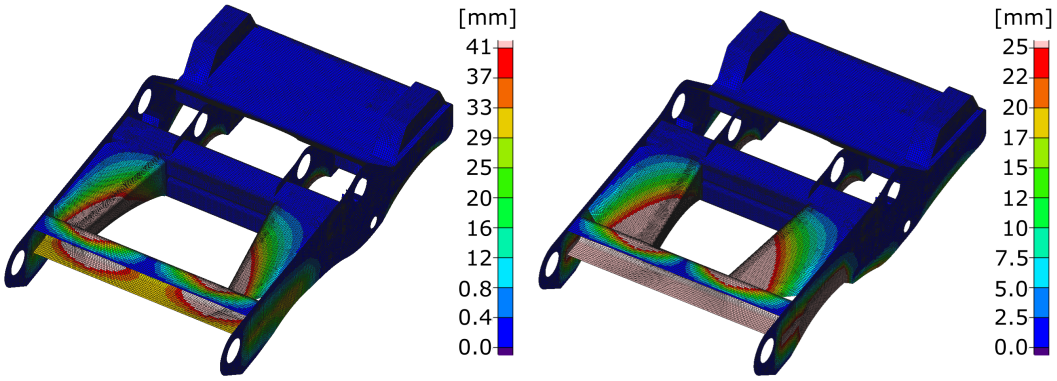

(a) Outward morphing of the L-plates **(b)** Inwards morphing of the L-plates

Figure 3.13: Conflicting shape changes, found at the L-plates

After discovering the conflicting shape changes for the different load cases, a few more shape changes were tested, but no significant improvements were found. As a last attempt, initial shape changes were forced by shifting the

Stellenbosch University https://scholar.sun.ac.za

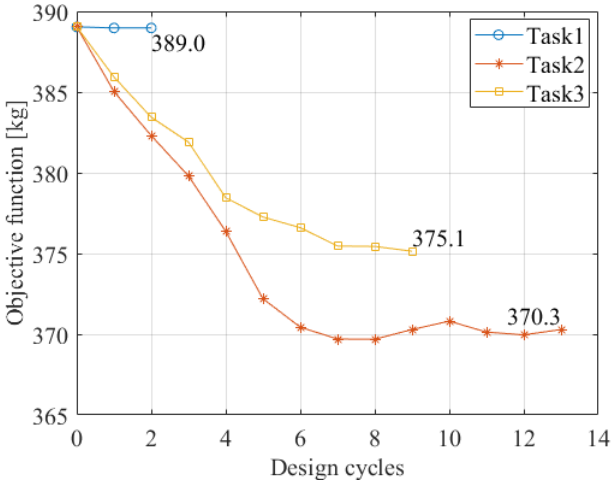

Figure 3.14: Objective function summary for Tasks 1 to 3

Table 3.6: Shape optimization task-definition reference summary

Task	Objective function	Optimization method	Load cases used
1	Mass minimization	Shape	All load cases
2	Mass minimization	Shape	All, except lateral FESL
3	Mass minimization	Shape	Only lateral FESL

initial starting point of the shape variables, but no improvements were found. The results were not surprising, due to the conflicting shape changes that have been identified.

3.2.3 Boom topometry optimization

Thus far, plate thickness and component geometry was optimized using size and shape optimization. Topometry offers a different outcome than the previously mentioned techniques as it gives a designer additional insight into the structure being investigated. Generally, the stress distribution within plates is non-uniform and topometry optimization can be used to highlight these distributions, by adjusting element thickness at specific regions within a single mesh. The results are however expected to be unpractical. The entire topometry procedure and results are mentioned and discussed in Appendix F, as the results were found to be lacking in value.

3.2.4 Combination of size and shape optimization

Now that most of the optimization techniques have been considered, a combination of size and shape optimization was tested. By making small changes to

Stellenbosch University https://scholar.sun.ac.za

some of the plate shapes, it may be possible that some of those plates undergo thickness reductions, and in turn, reduce the structure's mass. For the first few combined optimization tasks, continuous-range size variables were used. The shape and size variables were applied similar to previous optimization tasks, however initial shape-shifts were made based on the knowledge gained from Section 3.2.2. Figure G.1 shows the areas where shape changes were enforced, with Table G.1 and Figure G.2, summarizing the first five optimization tasks. The results showed that mass reductions had been achieved, however, the values are close to that found for the size optimization tasks, again reinforcing the idea that the current boom shape configuration is near-optimal. This is considering that only the discrete plate sizes are to be used for a final design. Consequently, optimization tasks with discrete plate sizes were created. The results showed no improvements as expected. A multi-stage, independent optimization procedure using size and shape optimization was considered. Based on the shape optimization results, similar modifications were expected as mentioned above, regardless of the technique order, therefore it was not attempted.

3.3 Design-based Optimization Summary

Now that the current design has undergone numerous optimization processes, it becomes notable that the current boom design is at a near-optimal design configuration. This is however only true for the current design concept, and it highlights some of the limitations that a designer could face when using size and shape optimization, as it can only improve on a given input design. Considering the boom has already gone through countless design iterations, and non-formal optimization processes during its lifetime, it was interesting to see that GENESIS could still find practical design improvements using size optimization. The results obtained from the optimization processes also support the idea that GENESIS should be used in future design processes, as it will reduce the required development time and resources to progress from a design concept to a finished and optimized design. Until now, the focus was to find improvements based on the current boom design. This limits the design capabilities of GENESIS, hence the previously used optimization techniques are referred to as having limited design freedom. Even though the current boom design has shown to have a near-optimal design, it is only true for the current design concept. The next step was to find a design concept that is fundamentally different compared to the current boom design. GENESIS is able to find such designs using topology optimization, as it controls the material placed within a design space. This means that topology generated designs are not bound by previous design configurations, therefore, the optimizer has unlimited design freedom when searching for a new design in a given design space.

Stellenbosch University https://scholar.sun.ac.za

Chapter 4

Concept Design using Topology Optimization

The results obtained in Chapter 3 indicated that the current boom design configuration is near-optimal and that only small design improvements are possible. In an attempt to find significant boom design changes and improvements, fundamentally new designs should be explored that could potentially replace the currently used boom design. In the pursuit to find new designs, topology optimization should serve as a useful optimization technique to use. Topology optimization follows a sophisticated procedure to find and create designs within a given design space. Topology optimization increases the potential to find fundamentally new designs, that have not yet been considered using conventional design approaches. This Chapter will therefore focus on redesigning the boom structure with the use of topology optimization, to ultimately replace the currently used boom design.

4.1 Initial Topology Model Development

The starting point in a topology optimization procedure is to identify a component or structure that requires a redesign. This identified component's design is then replaced with a new model that is designable using topology optimization. To start the boom redesign procedure, an initial, designable topology model needs to be created based on the available design space. The available design space for the initial model includes the unused space within the chassis, where the boom is normally located. When creating an initial topology model, it is advantageous to use as much of the available design space as possible, allowing GENESIS maximum freedom when finding new designs. Functional components are also included in the initial topology model, such as the frontal- and central bushes that connect the boom to the chassis and hydraulic cylinders, as well as the bearings that connect the boom and 5th-wheel. The functional components will not be used as designable regions, however they

Stellenbosch University https://scholar.sun.ac.za

are required for the FE model development and analysis. The FE simulation, boundary conditions, and input loads will remain consistent with the original boom model simulation. The allowable design space, after the functional components have been added, is filled with material that will serve as the designable region for the topology optimization procedure. Figure 4.1 depicts the initial boom topology model that will be used for the topology optimization tasks. The functional components that will be kept unchanged are highlighted in red, whilst the designable region is highlighted in green. The FE simulation was created and analyzed in NX, after which it was exported to Design Studio and validated. The initial boom topology model has a mass of 1771.6 kg, using G4000 grey cast iron as the designable material.

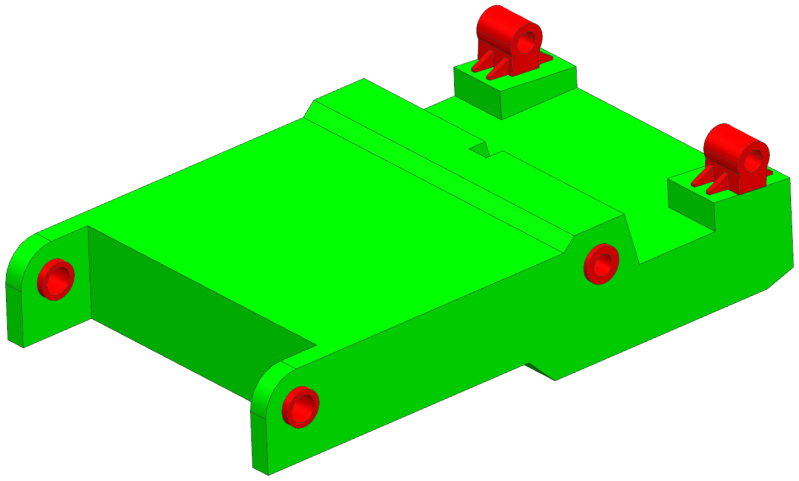

Figure 4.1: Initial boom topology model, highlighting the designable and non-designable regions in green and red, respectively

4.2 Topology Optimization Setup and Manufacturing Constraint Testing

Similar to the previously used optimization techniques, topology optimization tasks required the definition of an objective function, variables, and design constraints. The typical approach in finding lighter structures, when using topology optimization, is to minimize the strain energy of the design, in an attempt to find the stiffest structure for a given mass fraction. By minimizing the strain energy, material is retained in the region of the load path to maximize structural stiffness. Strain energy minimization was consequently selected as the topology objective function. The topology variables are defined using regions of material. The density of all the elements that are located within a design region will serve as variables to be modified during the topology optimization procedures. Ineffective material will be removed by changing

Stellenbosch University https://scholar.sun.ac.za

the corresponding element densities to zero. The green body representing the design space, as shown in Figure 4.1, was selected as a topology design region. Finally, design constraints were required to guide the optimization procedure. Mass fraction constraints were used to reduce the model to a desirable mass. The ideal was to find lighter structures than the current design, however, heavier structures were also considered. Topology optimization is known to find organic designs that are difficult to manufacture using traditional approaches. Considering that manufacturing is an important aspect of the project objectives, various manufacturing constraints were considered for the optimization tasks. The manufacturing constraints that were identified for the development of the new boom model included symmetry, casting, extrusion, and paired sheet stamping. The remaining manufacturing constraints were not found applicable to this design.

Optimization tasks with various combinations of the manufacturing- and mass fraction constraints were tested. A symmetry constraint was added to all the optimization tasks, as symmetrical designs were required. This was quite important knowing that some of the FE load cases are asymmetrically defined. Optimization tasks that used extrusion and sheet stamping as manufacturing constraint did not deliver any feasible or manufacturable structures. This could have been due to the complexity of the boom, exceeding the capabilities of the manufacturing constraints being used. Casting and symmetry delivered the most usable and realistic results, therefore, showing the most potential. It should be mentioned that the casting procedure conforms to the requirements of a typical sand casting, therefore a parting plane for the mould halves, as well as a filling direction needs to be defined. The results merited further investigation into the combination of casting and symmetry constraints. The first plausible design for a castable boom, with a mass fraction of 0.4, is shown in Figure 4.2, which equates to 708.6 kg.

Even though this design is manufacturable, it is considerably heavier than the current boom design, therefore, further refinement was be required. Minimum and maximum member size design parameters were added to avoid the formation of large clumps of material and to spread the material distribution. The mass fraction constraint was also lowered in an attempt to find a structure with a mass similar to the current design's mass. Figure 4.3 depicts the improved boom casting, retaining 30 % of the initial topology design mass, which is 531.5 kg. This structure is lighter than the previous optimization task result, however, when comparing the 531.5 kg with the original boom mass of 389 kg, a mass increase of 36.6 % is calculated. A 36.6 % mass increase is unacceptably high and needed to be reduced. The next step was to do a formal refinement process in an attempt to reach a more desirable or acceptable structure in terms of mass and structural performance.

Stellenbosch University https://scholar.sun.ac.za

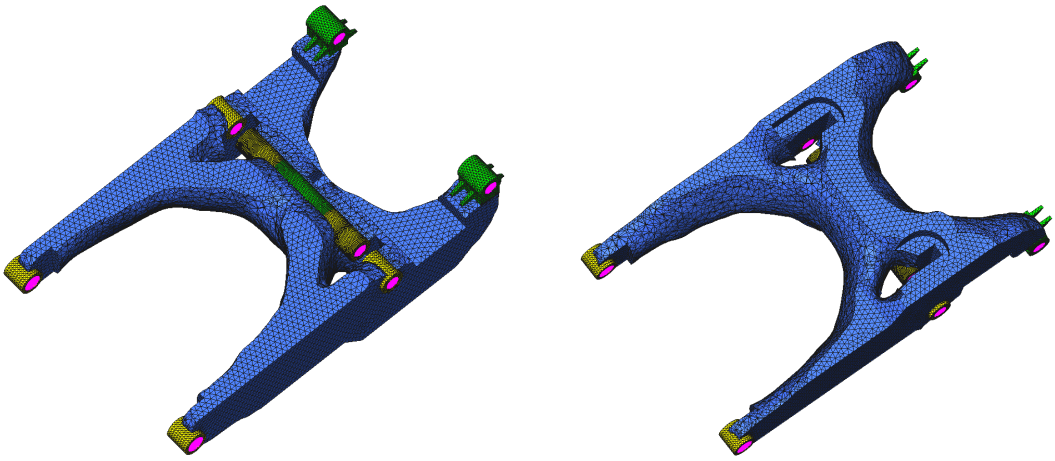

(a) Top view of castable design (b) Bottom view of castable design

Figure 4.2: Test result of a topology optimization test-run that used casting and symmetry as manufacturing constraint, with a resulting castable design

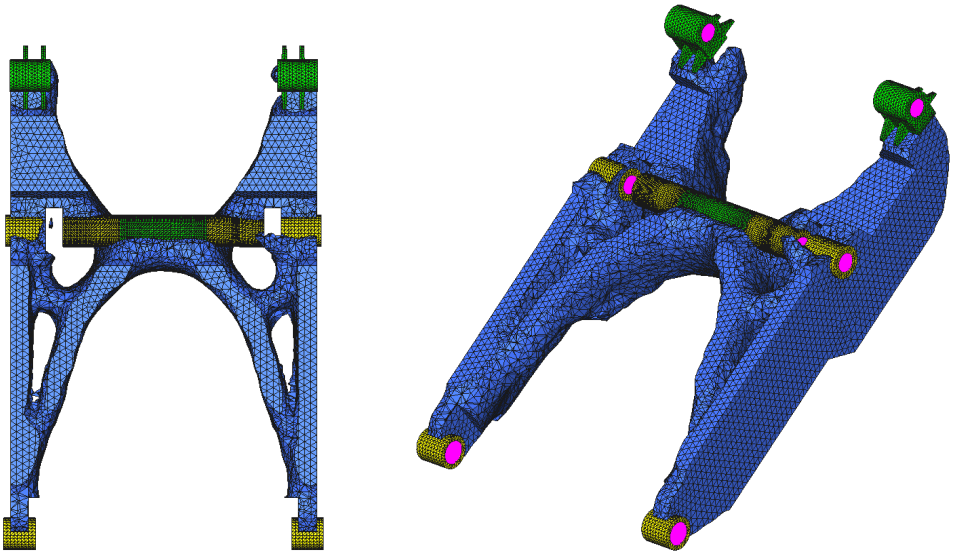

(a) Improved casting top view (b) Improved boom casting isometric view

Figure 4.3: Improved boom casting

Stellenbosch University https://scholar.sun.ac.za

4.3 Topology Optimization Process Refinement

The structure found in Figure 4.3 showed potential, however a considerable mass reduction was still required to find a feasible design. In an attempt to achieve the desired mass reduction, attention was directed to the allowable mass fractions and element sizes, as it could have a big influence on the topology result. To avoid using a drawn-out iterative approach of tuning these parameters, a few mass fraction design points were selected, based around the current boom design's mass. In addition to the mass fraction refinement, mesh refinement was required at each mass fraction design point, to increase the likelihood of finding different, more-optimal designs, and to avoid mesh dependant results as shown in Section 2.3.7. By lowering the mesh size, the topology resolution was increased, and more smoothed-out and detailed designs could be found. To explore the design possibilities as thoroughly as possible, one design point was selected to be heavier than the current boom, one design point with the same mass, and two design points that were lighter than the current boom. Even though a lighter structure would be preferred, the possibility of a heavier structure being more-optimal compared to the original design does exist, as the changed manufacturing process and material could be an economically viable option. The spread of design points is also an important contribution to the development of the concept design methodology. The design points were selected to be 115 %, 100 %, 85 %, and 75 % of the 389 kg structure's mass. The mass fraction, MF, for each design point was calculated based on the 1771.6 kg of the initial topology design, shown in Equation 4.1.

$$MF = \left(\frac{389}{1771.6}\right) \times \left(\frac{\text{Design point } \%}{100}\right) \tag{4.1}$$

Resulting mass fractions of 0.25, 0.22, 0.19 and 0.165 were found. A total of 12 planned optimization tasks were executed, as shown in Table 4.1. It should be noted that the stated refinement tasks were performed independently, therefore no optimal mesh solution detail was transferred between the tasks.

Table 4.1: Boom topology optimization task schedule

MF / Mass [kg]	Mesh size [mm]		
	25	20	15
0.250 / 442.9	Task 1	Task 2	Task 3
0.220 / 389.0	Task 4	Task 5	Task 6
0.190 / 336.6	Task 7	Task 8	Task 9
0.165 / 292.3	Task 10	Task 11	Task 12

The selection of mesh sizes, listed in Table 4.1, was based on two criteria. Meshes were tested for their discretization accuracy and solving time. Tested

Stellenbosch University https://scholar.sun.ac.za

mesh sizes include 35 mm, 25 mm, 20 mm, 15 mm, and 10 mm. The 35 mm mesh size was found to be a usable mesh size for analysis purposes, however, it was too coarse when compared to the other mesh sizes. Low-resolution meshes are not ideal when using topology optimization. A low-resolution mesh will limit GENESIS's ability to find effective designs and it could also cause jagged surfaces and geometries. A FE analysis of the 35 mm mesh size model was performed, and it solved within 2 minutes and 30 seconds. Next, the 25 mm and 20 mm meshes were used. Both mesh sizes already showed smoother, more accurate discretization of the model and the simulations solved within 4- and 6 minutes, respectively. The 15 mm mesh did not show considerable improvement in the discretization of the model, however, the simulation time experienced a relatively large increase, solving within 14 minutes and 30 seconds. This is a substantial increase in solution time when compared to the coarser, 25 mm, and 20 mm meshes. Finally, the 10 mm mesh was attempted. The meshing operation itself became an intensive process, and the simulation analysis was aborted after 45 minutes. Knowing that a FE analysis is performed for each optimization design cycle, it was decided to disregard the 10 mm mesh, to avoid unreasonably high, computationally-expensive optimization tasks. All meshes, previous to the 10 mm mesh, showed reasonable solving times, however it was decided that the 35 mm mesh is overly coarse, and not fit for the topology optimization refinement process. Table 4.2 summarizes the mesh size solving time and discretization quality.

Table 4.2: Mesh size solving time and visual quality

Mesh size [mm]	FEA solution time [minutes]	Mesh quality
35	2.5	Overly coarse
25	4	coarse
20	6	Fine
15	14.5	Fine
10	45+	Overly fine

Figures 4.4 and 4.5 show a selection of the results obtained from the optimization tasks defined in Table 4.1. The results are displayed using a top view of the initial topology model, as this is where the most deviation is found when comparing the optimization results. Since the side of the initial topology model has a much smaller cross-section than the top, very small- to no differences can be found from this view when comparing results. The resulting structures from the 25 mm mesh size tasks were more or less similar to the structure found for Task 1 as shown in Figure 4.4. Overall, the 25 mm mesh produced bad results when compared to the other mesh sizes. For this reason, only Task 1 will be shown for the collection of 25 mm optimization tasks. The resulting structures for Tasks 3, 5, and 6 are also quite similar to one another,

Stellenbosch University https://scholar.sun.ac.za

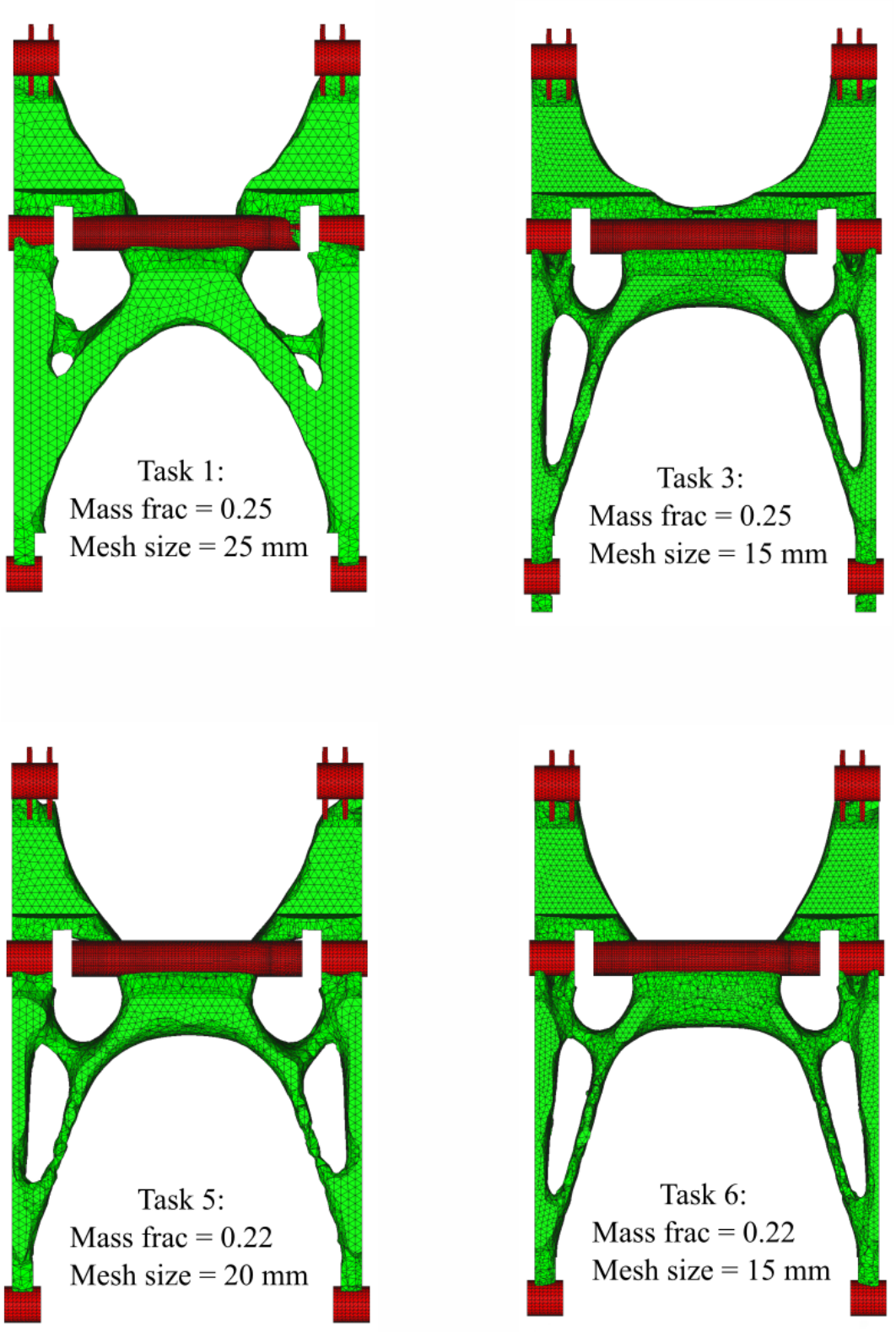

Figure 4.4: Top view of topology results found for Tasks 1, 3, 5, and 6

Stellenbosch University https://scholar.sun.ac.za

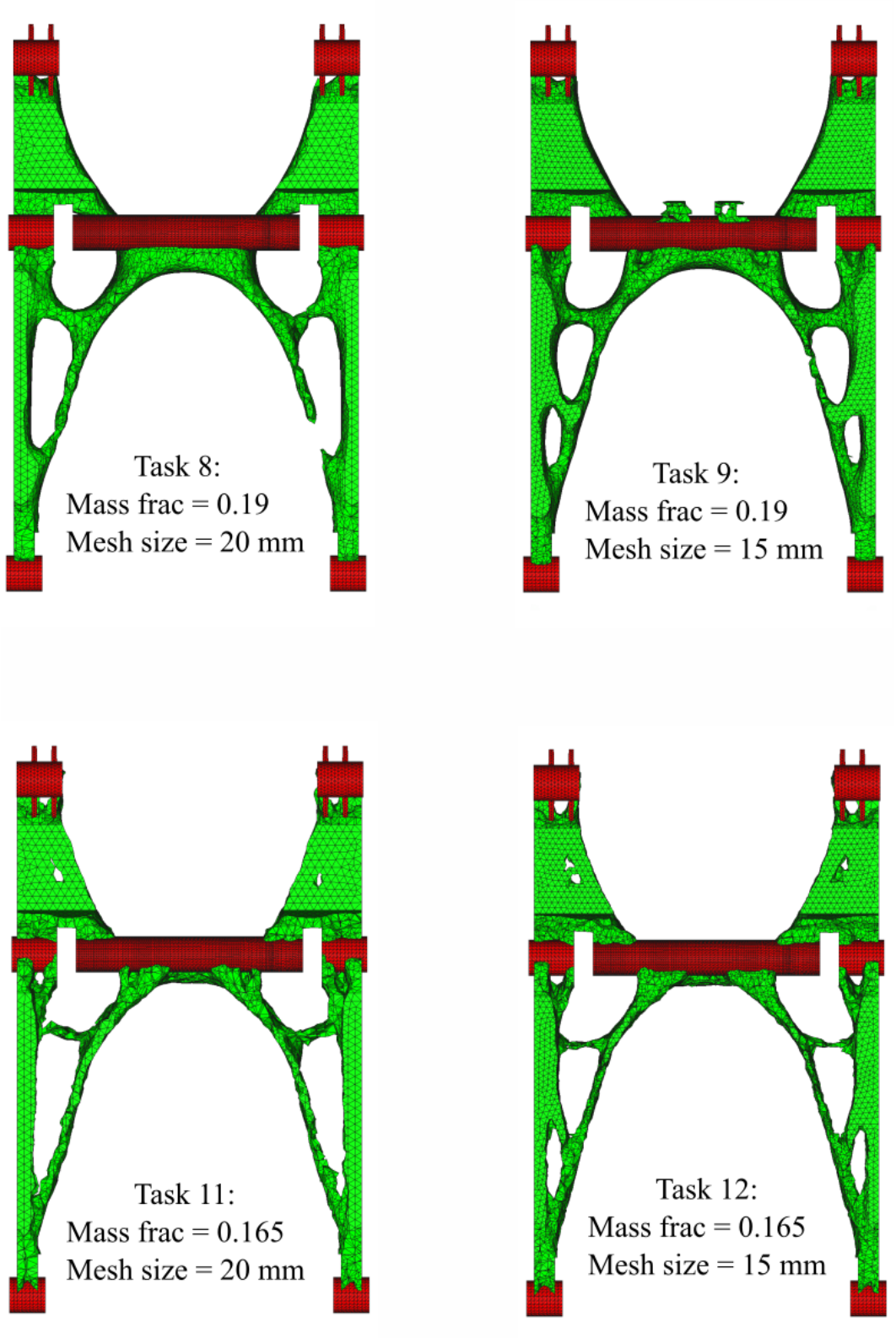

Figure 4.5: Top view of topology results found for Tasks 8, 9, 11, and 12

Stellenbosch University https://scholar.sun.ac.za

and a big improvement can already be seen when they are compared to the structures found in Figure 4.3. Moving to even lower mass fractions, discontinuities were found. Task 8 had a similar design to that of the higher mass fractions, however, material discontinuities started to appear. Structurally, the design was found to be valid, as it was obtained from a converged optimization problem. Furthermore it should be noted that material does exist within the discontinuity region, however the elements were assigned low density values. The most sensible way to avoid material discontinuities is to use higher mass fraction constraint, indicating that the 0.19- and 0.165 mass fractions are at the lower end of usable fractions for this design. Nevertheless, the discontinuities can be fixed when new models are developed. A new and interesting result was found for Task 9. The topology structure is fundamentally similar to that of the previous tasks, however extra cross-members have been added in the frontal area of the boom. This result is a good illustration of the value that mesh refinement offers during the optimization procedure and why it should be used. Finally, the lowest mass fraction tasks were performed and more material discontinuities were found. The material discontinuities are better shown in Figure 4.6. Even though material discontinuities existed within the resulting designs, it gave a good indication to where the material should be placed, which is a good starting point for a new design. The optimization tasks results that were not shown in Figures 4.4 and 4.5, namely Tasks 2, 4, 7, and 10, can be found in Appendix H.

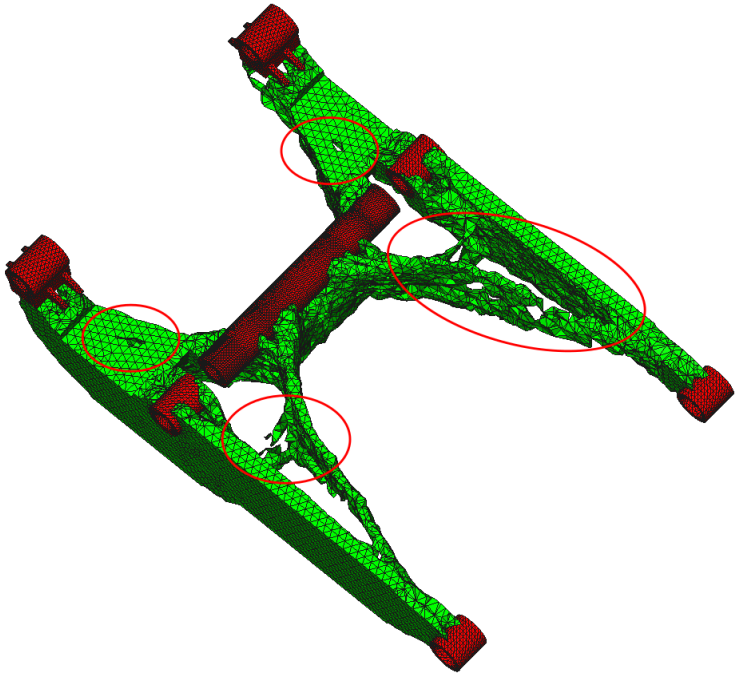

Figure 4.6: Material discontinuities visible at multiple regions in the design

Stellenbosch University https://scholar.sun.ac.za

Overall, the fundamental design concept stayed constant throughout the optimization tasks. Some of the tasks showed a large number of discontinuities, however, this can be fixed when developing new models. The modification found by Tasks 9 and 12 is interesting, but it also adds complexity to the design. Concern about the validity of these two designs is also raised, due to the number of discontinuities. It was therefore decided, not to use the results from Tasks 9 and 12. Now that the necessary topology results have been obtained, the resulting structures can be interpreted and refined to final designs.

4.4 Topology Results Interpretation and Refinement

With the scheduled topology tasks being completed, further interpretation, development, and refinement, based on the topology results, are required. The topology designs will be used as starting points in the development of new models. The newly developed boom models will be reproduced to accurately represent the topology results. The necessary changes for improved manufacturability will be made during the model development, if it is required. Knowing that the topology optimization procedure did not include any stress constraints, it will be important to conduct FE analyses of the models. This is to ensure that the designs only experience stresses within the chosen material's stress limits and capabilities. Further improvement can be made by applying shape optimization to the models, to remove some of the excess- and ineffective material from the designs. The two design points that will be used for further model development include Tasks 5 and 11, as shown in Figures 4.4 and 4.5, respectively.

4.4.1 Task 5 result interpretation

Starting with the result interpretation of Task 5, the topology structure was exported to the NX modelling environment. Using the top and side view of the topology structure, a traced design was created. Knowing that the design will be manufactured using a casting procedure, the necessary modifications such as edge blends were added. The interpretation of the topology model is shown in Figure 4.7. The entire structure, disregarding the functional components, can be manufactured with a single casting. If this structure were to be cast using G4000 gray cast iron, the structure would weigh 714 kg. This is a much heavier structure compared to the current boom mass of 389 kg, and further refinement was required to create a feasible design. The developed model's mass is an indication of the difficulty to reproduce the topology results accurately, however, the fundamental design concept was captured within the

Stellenbosch University https://scholar.sun.ac.za

interpreted design. The next step was to do a FE analysis to assess the performance of the structure. Consequently, a FE simulation similar to that of the initial topology model simulation was created. G4000 gray cast iron was used as meshing material. Welding will not be required in the manufacturing of the new design, therefore, the FESL load cases were removed from the FE analysis. Consequently, the design was only evaluated on the ultimate load cases. From the FE analysis, maximum stresses of 265 MPa and 180 MPa were found for the 1st- and 2nd ultimate load cases, respectively. Figure 4.8 depicts the FE analysis results.

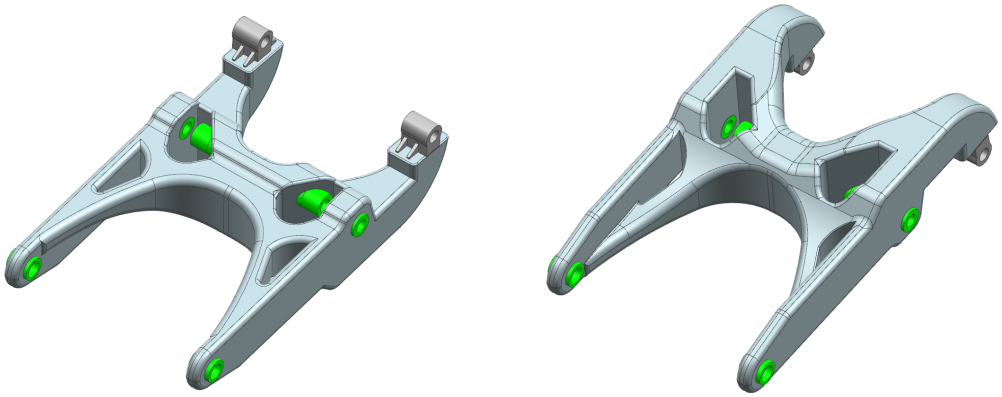

(a) Top view **(b)** Bottom view

Figure 4.7: Task 5, topology result interpretation

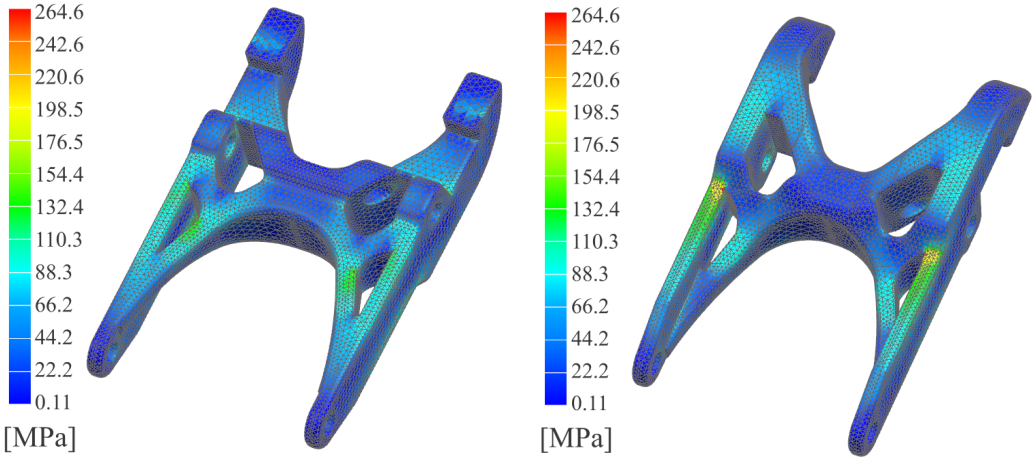

(a) Top view **(b)** Bottom view

Figure 4.8: Task 5, FE analysis result, displaying a maximum stress of 265 MPa

From the FE analysis, it was found that the overall structure is experiencing low stresses. This is easily notable in Figure 4.8a and Figure 4.8b. This

Stellenbosch University https://scholar.sun.ac.za

is likely caused by the excessive amount of material that the design contains. The maximum experienced stress of 265 MPa is due to a small stress concentration region, caused by a geometry transition at the sides of the model, as shown in Figure 4.8b. Shape optimization can be used to reduce both structural mass and improve the geometry of the stress concentration region, in an attempt to find a lighter, more optimal design. Using Design Studio, 38 shape domains and 14 morphing sets were created to enforce the desired shape alterations. The goal was to target areas of low stress, enforcing shape changes that should reduce the material mass significantly, as well as, improving stress concentration regions. Figure 4.9 shows the model with the various shape domains and a single morphing set on the side-rear of the structure. The shape morphing sets are made available in Appendix I. Stress constraints of 275 MPa, which is the tensile strength of G4000 gray cast iron, were used for the shape optimization tasks. Three of these shape optimization tasks were performed, namely Tasks A, B, and C, with modified shape perturbation magnitudes after each task. These modifications were based on previously obtained task results. A fourth optimization task, Task D, with an inflated stress constraint of 327.25 MPa was also performed, to test if a further mass reduction is possible when stronger materials are used. The four optimization tasks are listed in Table 4.3 for reference. Depicted in Figure 4.10a are the boom's mass reduction summaries obtained from the optimization tasks. Upon inspecting Figure 4.10b, it becomes notable that the design shape changes are reaching their limits, due to the material's stress limitations, and not the perturbations. Overall, the same dominating shape changes occurred for every optimization task, depicted in Figure 4.11. These shape changes include the size reduction of the bearing block supports at the back, as well as the cross-member thicknesses in the frontal part of the boom. Most of the material was removed from the bottom of the boom, as can be seen by the flattening of the structure in Figure 4.11. From the shape optimization results, it was found that the model's mass can be reduced from 714 kg to 522 kg, which is a 27 % reduction. The combination of various shape changes can lead to crude shape formations, therefore, the structure required manual shape alterations. Similar to the initial model development, a new model was created, followed by a FE analysis of this new model. The developed model is depicted in Figure 4.12. The model adheres to the material's stress limit, however, large portions of the structure are still experiencing low stresses, which is likely an indication of excess material. The final boom structure consists of a mass of 536 kg.

The possibility to delve deeper into the refinement of Task 5's design exist, however it becomes a more difficult process, which can become time-consuming. Considering that a second design point was still to be explored, time-consuming operations were avoided at this stage. A decision was made to continue with the second chosen design point, which is Task 11.

Stellenbosch University https://scholar.sun.ac.za

Table 4.3: Shape optimization task-definition reference summary for Task 5 topology result refinement

Task	Obj. function	Opt. method	Perturbation magnitudes	σ constraints
A	Mass minimization	Shape	Unique to Task A	270 MPa
B	Mass minimization	Shape	Unique to Task B	270 MPa
C	Mass minimization	Shape	Unique to Task C	270 MPa
D	Mass minimization	Shape	Replication of Task C	327.25 MPa

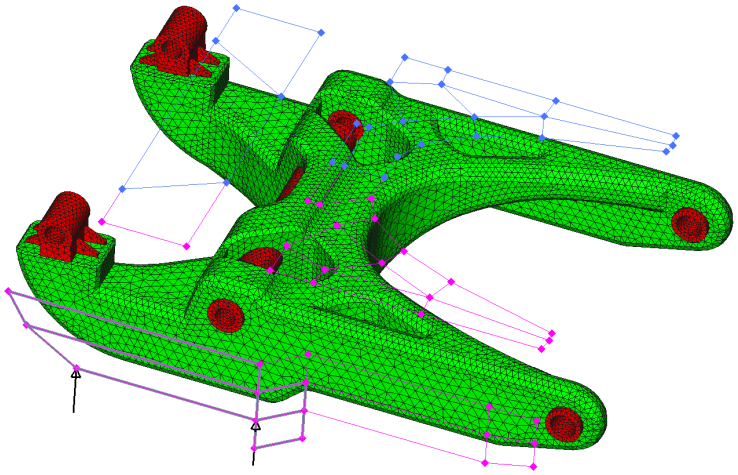

Figure 4.9: Boom shape domains, with a visible shape morphing set

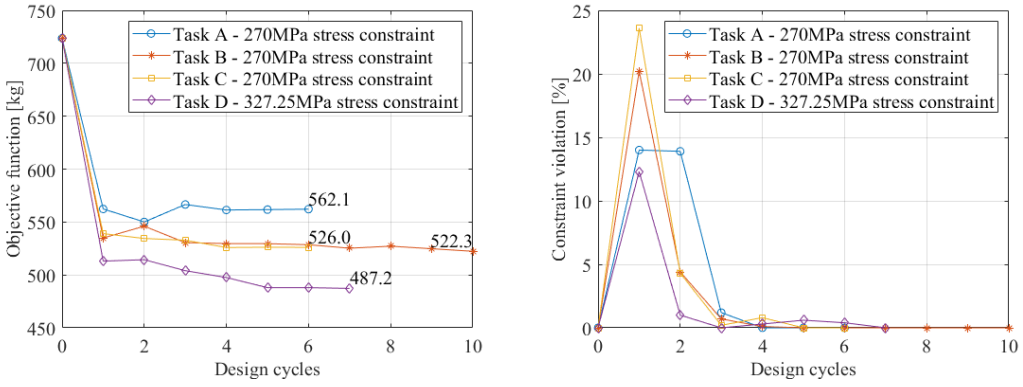

(a) Objective function summary **(b)** Stress constrain violation summary

Figure 4.10: Objective function- and stress constraint violation summary graphs, for Task 5's shape optimization sub-tasks

4.4.2 Task 11 result interpretation

The model interpretation, development, and refinement for Task 11 followed the same procedures that were used for the development of Task 5's model.

Stellenbosch University https://scholar.sun.ac.za

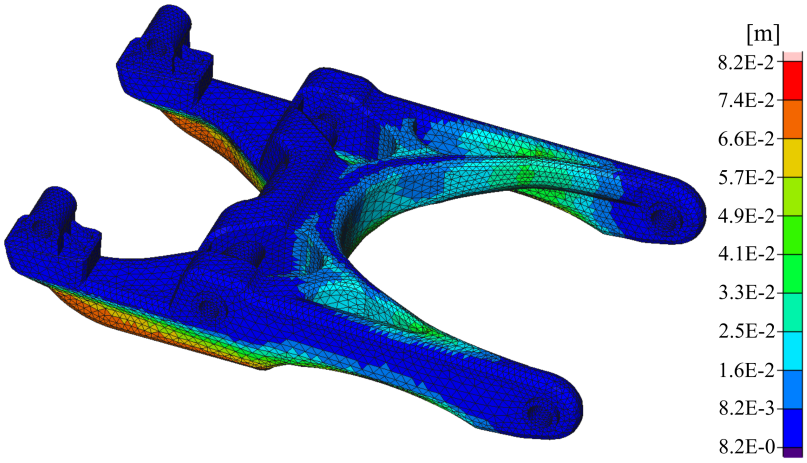

Figure 4.11: Boom shape changes, displaying nodal displacement

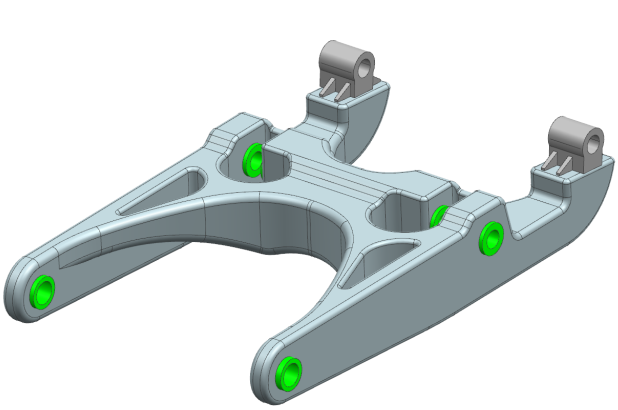

(a) Task 5 refined boom - side view

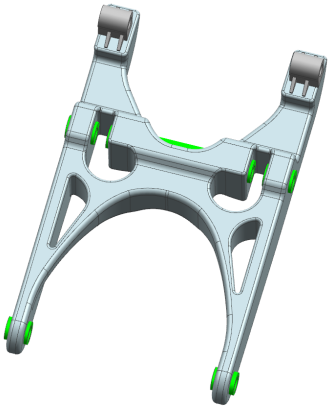

(b) Task 5 refined boom - top view

Figure 4.12: Task 5, refined boom structure

The model developed from Task 5 topology results, contained a large amount of excess material due to a combination of mass fraction and inaccurate result interpretation. The removal of large amounts of excess material, with the use of shape optimization, can become a difficult and time-consuming process. By starting with a topology structure that was designed with a lower mass fraction constraint, the possibility of avoiding the addition of large amounts of excess material during the interpretation procedure becomes valuable. During the model development process, all material discontinuities were fixed by adding the missing material. The developed model is depicted in Figure 4.13. This structure, if manufactured from G4000 gray cast iron, weighs 588 kg. This is double the mass of the predicted mass fraction of Task 11, however, taking into account the number of material discontinuities that were fixed and the precise topology structure detail that could not be captured, it is not an unreasonable

Stellenbosch University https://scholar.sun.ac.za

result. The starting point for this design is already much closer to the original mass, as well as the predicted mass fraction mass when compared to Task 5's interpreted results. It becomes notable that developing a model directly from topology results is a difficult process and the addition of excess material is difficult to avoid.

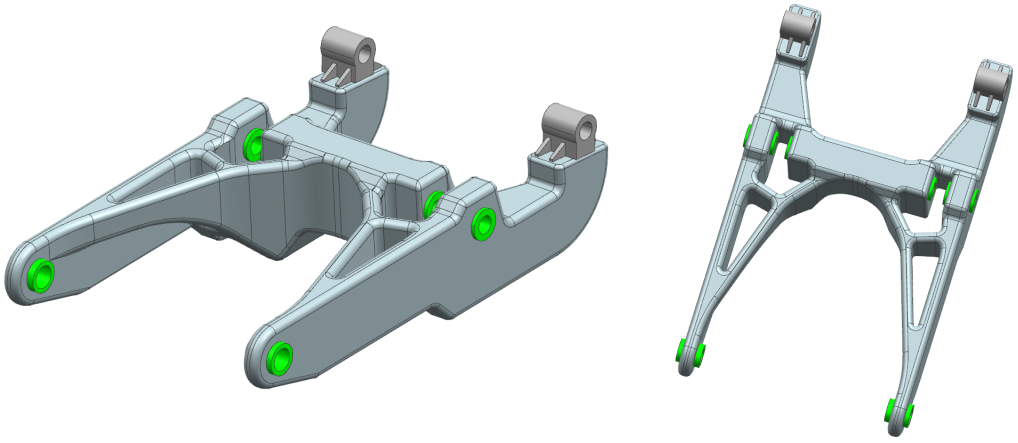

(a) Topology results interpretation - side view **(b)** Interpretation - top view

Figure 4.13: Task 11, topology results interpretation

The design was still quite heavy, and a significant amount of unnecessary material was found within the vertical direction of the boom. After conducting a FE analysis, maximum stresses of 349.6 MPa and 188.9 MPa were found for the 1st and 2nd ultimate load cases, respectively. The structure is therefore already experiencing stresses that exceed the material stress limitations of G4000 grey cast iron. These high stresses are found in the same region as in Task 5's model. With the use of shape optimization, the geometry in this region could be improved, in an attempt to lower the stress. After transferring the model to Design Studio, similar shape changes were applied as for Task 5. These shape changes are presented in Appendix J. A stress constraint of 275 MPa was used for the optimization tasks. Figure 4.14 depicts a summary of three optimization tasks, Task A, B, and C that had varying perturbation magnitudes, with Figure 4.14a showing the objective function summary and Figure 4.14b, the constraint violations summary. The three task definitions are listed in Table 4.4. The shape changes that were found are similar to that shown in Figure 4.11, with the dominating shape change occurring at the rear of the structure. It should be noted that the stress was reduced from roughly 350 MPa to 270 MPa, conforming to the stress constraint, while still reducing the mass of the structure as required from the optimization objective. This showcases the value of shape optimization during this procedure.

Stellenbosch University https://scholar.sun.ac.za

Table 4.4: Shape optimization task-definition reference table for Task 11 topology result refinement

Task	Obj. function	Opt. method	Perturbation magnitudes	σ constraints
A	Mass minimization	Shape	Unique to Task A	270 MPa
B	Mass minimization	Shape	Unique to Task B	270 MPa
C	Mass minimization	Shape	Unique to Task C	270 MPa

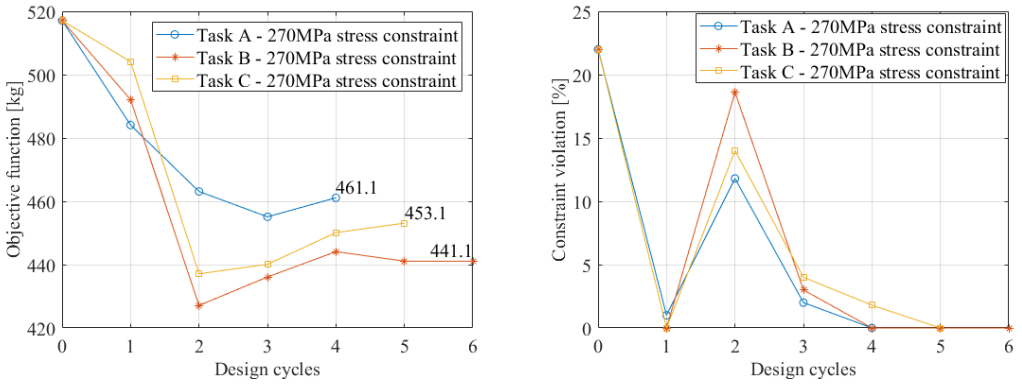

(a) Objective function summary **(b)** Stress constrain violation summary

Figure 4.14: Objective function- and stress constraint violation summary graphs, for Task 11's shape optimization sub-tasks

In an attempt to push the design's mass closer to that of the original boom, it was decided to consider one of the stronger casting materials currently being used for terminal tractor component manufacturing. D80-55-06- and D100-70-03 cast iron have yield strengths of 380 MPa and 480 MPa, and tensile strengths of 550 MPa and 690 MPa, respectively. By only using the material yield strengths, a substantial increase in the material stress limitations is seen compared to G4000. A shape optimization run with a stress constraint of 350 MPa was performed to achieve an improved mass reduction. Based on the new stress constraint, D80-55-06 and D100-70-03 will each have safety factors of 1.085 and 1.37, respectively. This is already an increase compared to the current boom model safety factor, which is 1.07. Furthermore, a 389 kg to 386.1 kg mass reduction was found. The summary of the optimization run is displayed in Figure 4.15a, with the resulting shape changes, shown in Figure 4.15b.

After modifying the boom design based on the shape optimization results that were found, a FE analysis was performed. It was found that larger portions of the structure now experiences larger stresses, however, there are still areas that experience small stress increases. Using the information obtained for the shape optimized structure, FE analysis, and the general topology results that could not be captured in the initial interpretation, a final design,

Stellenbosch University https://scholar.sun.ac.za

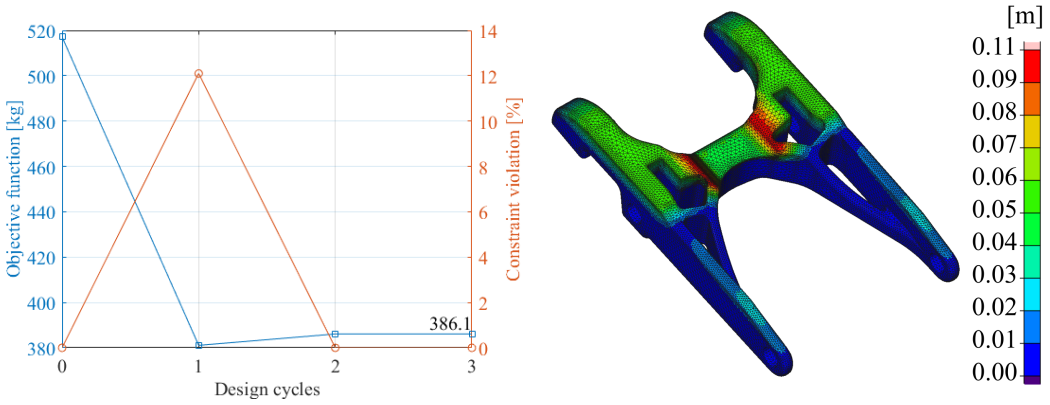

(a) 350 MPa stress constraint shape optimization run

(b) Resulting shape changes, with nodal displacement results

Figure 4.15: Shape optimization on the interpreted boom, with an elevated stress constraint limit of 350 MPa

depicted in Figure 4.16, was developed. Additional material was removed in lower stressed regions that were identified from FE analysis, with the topology results supporting the decision. A structure with a mass of 394 kg was created, weighing 1.29 % more than the current boom. This structure is able to stay within the material yield stress limitation of D100-70-03 cast iron. A maximum stress of 416 MPa was measured, resulting in a safety factor of roughly 1.15. This is an improvement compared to the current boom design's safety factor of 1.07. The FE results of both the 1st- and 2nd ultimate load cases are displayed in Figures 4.17a and 4.17b, respectively. As can be seen, the bulk of the model is still experiencing far lower stresses than the material yield limitations, with a few small areas experiencing larger stresses.

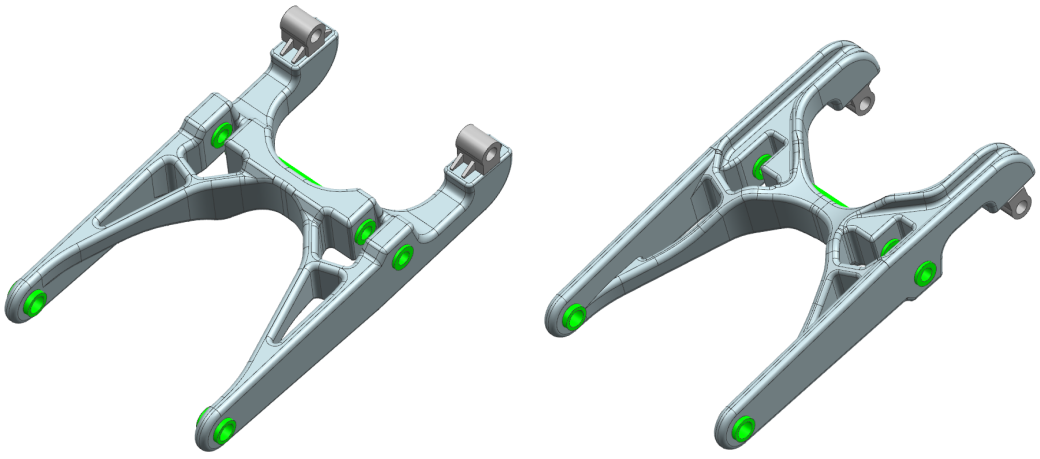

(a) Task 11, refined boom - side view

(b) Task 11, refined boom - top view

Figure 4.16: Task 11, refined boom structure

Stellenbosch University https://scholar.sun.ac.za

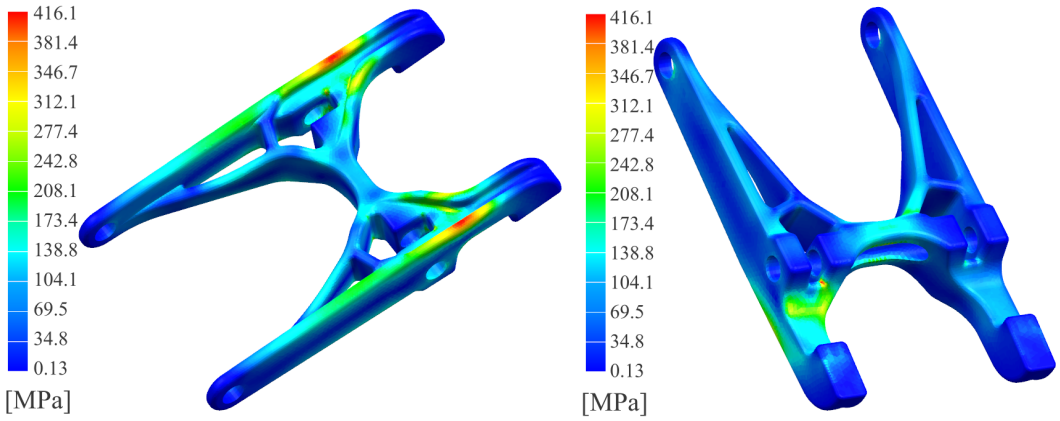

(a) ULC 1 - FE results **(b)** ULC 2 - FE results

Figure 4.17: FE results of Task 11's refined boom model

4.5 Topology Concept Design Summary

Both design points, which include Tasks 5 and 11, show potential for further refinement, however, a satisfactory design has been found from Task 11. Task 5 results showed a heavy and sturdy design that could potentially be refined to a lower mass, however this could become an iterative process that is difficult and time-consuming. It was realized that the first topology design interpretations contained a lot more material mass than the stated topology mass fraction constraint when compared to the second interpretation. Based on the model development findings, lower mass fractions should typically serve as better starting points in the development of new models. From the design process, it can be seen that using the lighter mass fraction, such as for Task 11, desired results can be obtained much quicker, avoiding a drawn-out iterative process. Shape optimization also showed its usefulness in refining the structure by cutting away material that was unintentionally introduced during the design interpretation step. Shape optimization is also a useful method of eliminating or improving stress constraint geometries. Overall, Task 11 is an interesting and structurally valid design that could potentially replace the original boom design that is currently being used in the ACTT. Table 4.5 compares the original boom to Task 11's refined boom, with Figure 4.18, to visually illustrate how these two designs compare.

Using the results that have been obtained from the extensive optimization work done on the boom, a concept design methodology can be developed. The methodology will focus on redesigning automotive structures, such as the boom and similar components. The development of the design methodology will be based on the knowledge and results gained from the various optimization tasks thus far. This methodology will attempt to simplify the entire topology

Stellenbosch University https://scholar.sun.ac.za

Table 4.5: Design comparison between Task 11's refined boom and the original boom design

Topic of comparison	Original boom	Task 11, refined boom
Mass [kg]	389	394
Material	ASTM A-573 Grade 50 steel	D100-70-03 cast iron
Safety factor	1.07	1.15
Component [#]	30	8
Manufacturing	Welding	Casting
requirements	Laser / Water jet cutting	Machining (additional)
	Sheet forming	

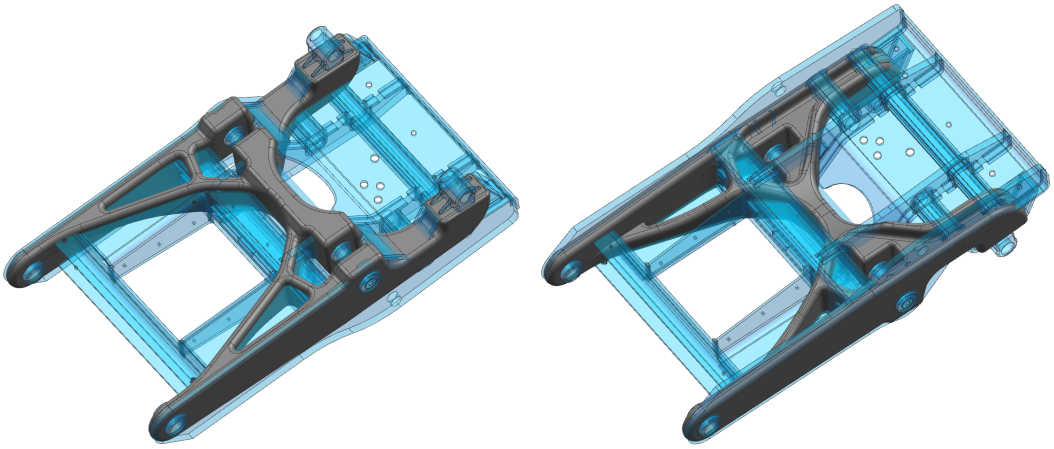

(a) Boom top view overlay **(b)** Boom bottom view overlay

Figure 4.18: Overlay comparison between Task 11's refined boom and the original boom

optimization process and assist designers with using structural optimization when designing or replacing components in future work.

4.6 Concept Design Methodology

This methodology will focus on finding new designs that aren't based on previous structures or components, but only on their functioning. These designs should be able to integrate into an existing system, therefore, functional dimensions and design constraints will be required to develop the initial topology model(s). The methodology will specifically focus on designing structures that are light with high stiffness. This is achieved through specific topology objective function- and design constraint definitions. The methodology will be developed based on the optimization- and design results obtained from Sections 4.1 to 4.4. The methodology outcome is not limited to finding light and

Stellenbosch University https://scholar.sun.ac.za

stiff structures, as different objective functions and design constraint combinations can be defined, if required. An assumption is made that users, new to the methodology, do not have access to previously obtained results for example the work that has been done on the boom. It is however required that users have a fair amount of experience with using topology optimization within Design Studio. The basic functioning and operation of Design Studio will therefore not be included in the methodology procedure steps. The concept design methodology has four phases, with detailed sub-tasks to guide a designer from the initial starting phase to a final product or design concept.

4.6.1 Phase 1: Initial topology model development

The first phase requires the development of an initial topology model. The model should include as much material (volume) as possible, allowing GENESIS more design freedom during the optimization procedure.

1.1. Identify the available design space within the system.

1.1.1. If moving parts are being replaced, ensure that the necessary design space is identified to avoid component interference

1.2. Identify and add functional components within the available design space

1.3. Add material around and within the functional components and design space, respectively

1.4. Create a FE model and simulation. The model and simulation should resemble the functioning of the model being replaced, therefore, use the same load cases, which include input loading and boundary conditions

1.4.1. Be sure to assign appropriate material / material properties to all meshes. Material density has a significant influence on the topology optimization task and the results thereof

1.4.2. Use a mesh size with a reasonable resolution to accurately capture the geometry of the structure. Mesh size effects the number of topology variables, therefore avoid too high- and low mesh resolutions

1.5. Import the model into Design Studio and check that the simulation solves correctly. Small alterations or modifications to the model might be required

Once the initial topology model development is satisfactory, move to Phase 2.

Stellenbosch University https://scholar.sun.ac.za

4.6.2 Phase 2: Optimization task definition and manufacturing constraints testing

Phase 2 will focus on setting up the general optimization task and exploring design possibilities with different manufacturing processes and design constraints. Manufacturing constraint parameter turning will also be considered. A final design is not the aim in this phase, but rather the exploration of design concept possibilities.

2.1. Define an objective function(s). There exist various types of objective functions. This methodology will focus on maximizing structural stiffness with the use of strain energy minimization. An option is given to select specific load cases for the optimization task.

2.2. Define a topology region(s). A starting mass fraction definition is required for the first design cycle. Begin with a starting mass fraction equal to the planned topology constraint upper limit. If unsatisfactory results are obtained, consider lowering the mass fraction starting point.

* NOTE: Decide on mass fraction constraints (Step 2.3.), whilst setting up the topology region(s). A starting mass fraction, equal to, or lower than the upper limit of the mass fraction constraint needs to be defined. Avoid increasing the mass fraction starting point past the upper limit constraint, as it will immediately cause topology constraint violations for the first design cycle.

2.2.1. Within the topology region definition, a window requesting manufacturing constraints will be presented to the user. A user-defined axis-system should be set up for the correct application of manufacturing constraints

2.2.2. Minimum and maximum size constraints parameters can also be defined to avoid overly thin or thick material sections. Leave the spread fraction at the default 0.5 value (Spread fraction controls the smoothing of 3D elements for post-processing evaluation).

2.3. Define a topology constraint(s). There exist various types of constraints. This methodology will aim to minimize the structural mass, using a mass fraction parameter. Define a maximum upper mass fraction limit / bound (a lower bound can also be defined. Multiple mass fractions could be used if more than one topology region has been defined.

2.4. Based on the preliminary results, any necessary changes should be made before moving to Phase 3

Phase 2 should be repeated multiple times to test the various manufacturing constraints and parameter effects. Finding unrefined structures is expected

Stellenbosch University https://scholar.sun.ac.za

and should not cause any concern. Attention should be given to the tuning of steps 2.2. and 2.3. This will be an iterative process, however it is necessary as the main details of the design concept are captured in Phase 2. Once a satisfactory output structure has been obtained, an optimization refinement procedure can be performed, as listed in Phase 3.

4.6.3 Phase 3: Topology optimization process refinement

Phase 3 is a refinement process for the results obtained in Phase 2. The goal is to further reduce structural mass and refine the topology results. This could be achieved by simply removing material with lower mass fraction constraints or finding small design changes by altering the mesh resolution. Therefore, the process will rely on mesh refinement and mass fraction refinement to achieve improved and refined structures. The idea of Phase 3 is not to change the fundamental design concept, but only to refine the topology results for the final design phase.

3.1. Select multiple mesh sizes for the required mesh refinement process. The default number of mesh sizes is 3.

  3.1.1. Avoid using overly coarse meshes, as low resolution meshes could negatively effect topology optimization procedures. Similarly avoid using overly fine meshes with impractical solving times.

3.2. Select multiple mass fraction constraints for the desired structural mass outcomes. The default number of mass fraction constraints is 3.

  3.2.1. Use mass fractions equal to, or less than the desired outcome mass. Higher mass fractions should typically be avoided.

* NOTE: If material properties are to be changed, it is advised to restart with Phase 2, as certain properties, such as material density, has a significant effect on the topology results

If unsatisfactory results have been obtained, it is recommended to restart at Phase 2. If satisfactory results have been obtained, continue to Phase 4.

4.6.4 Phase 4: Result interpretation and design refinement

Phase 4 revolves around the final refinement steps to achieve a manufacturable or refined design concept. The topology results will be interpreted to create a new model(s). Not all of the results will necessarily be used. This is a decision based on the user and the desired outcome.

Stellenbosch University https://scholar.sun.ac.za

4.1. Import the topology results into NX or any CAD environment. Use the topology results as a blueprint to develop a new model.

  4.1.1. Changes, that will increase manufacturability, should be added if possible.

4.2. Create a FE model and simulation similar to Phase 1.

4.3. Identify low-stress areas and stress concentration regions.

4.4. Import the new model to Design Studio and create a shape optimization task, targeting the low stress- and stress concentration regions.

  4.4.1. Create shape morphing sets to remove material in low stress regions.

  4.4.2. Create shape morphing sets to add material in high stress regions, or to change the geometry of stress concentration regions.

  4.4.3. Define an objective function. The most general objective function would be to minimize mass.

  4.4.4. Define design constraints. Material stress constraints are typically used.

    4.4.4.1 Consider the use of safety factors for the shape optimization tasks

4.5. The model that was developed in step 4.1. can be adjusted and refined, using the shape optimization results, to achieve a final design.

4.6. Conduct a final FE analysis check. Final adjustments to the model can be made manually, based on the FE results, if required.

* Repeat steps 4.1. to 4.6. for an unsatisfactory design.

The concept design methodology is concluded once an acceptable design has been found throughout Phase 4.

Stellenbosch University https://scholar.sun.ac.za

Chapter 5

Cross-member Redesign using the Concept Design Methodology

After doing extensive design optimization work on the boom, using the various optimization techniques, it was found that the currently used design is at a near-optimal configuration. The same is expected for the cross-member, as it is a critical component within the ACTT chassis, which has undergone numerous design improvements. If improvements were to be found using size- or shape optimization, it would likely be small changes or support the idea that the cross-member is near-optimal, in terms of its design configuration. With the use of topology optimization, a new cross-member design concept could potentially be generated. This Chapter will therefore focus on finding a new conceptual design using the concept design methodology, which is based on topology optimization. The cross-member redesign procedure will follow the concept design methodology, as presented in Section 4.6, to assess and validate the proposed methodology, whilst finding a new design concept. One of the aims when redesigning the cross-member is to find a castable design, consequently avoiding the use of welded connections. This will improve the component's structural performance, by limiting fatigue damage that is often found at welded detail. Furthermore, the use of casting constraints conforms to the aims set out for this project, which is to ease the manufacturing process by designing castable components.

5.1 Execution of Phase 1: Initial Topology Model Development

Phase 1 lists the steps that need to be taken to develop a FE model, which will be used for the topology optimization procedure. This model will be called the initial topology model, as mentioned in the methodology.

Stellenbosch University https://scholar.sun.ac.za

5.1.1 Identification of design space, functional components, and interfering parts

The cross-member is located between and around multiple components, some of which are moving, such as the boom. When creating the initial topology model, the surrounding components need to be taken into consideration to avoid any possible interference. Functional, non-designable components should also be added to the model as required. In order to visualize the available design space for the initial cross-member topology model, Figure 5.1 is presented, followed by a detailed description of how the initial topology model was created.

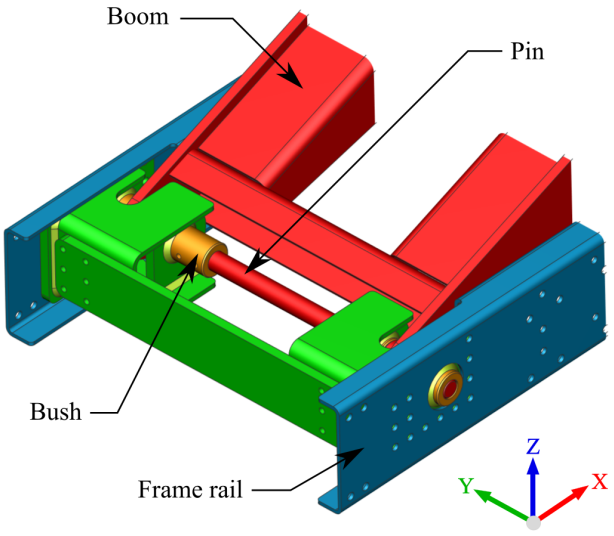

Figure 5.1: Cross-member location within the sectioned chassis frame-rails

The first step in finding the available design space for the initial topology model is to identify a design space volume or "box", that could fit all the components of interest. At this stage, no distinctions are made between design space, functional components, or interfering parts. As a starting point, the box needs to exist between the two frame-rails, within the Y-axis direction. The design space box is also limited to fit within the U-channel of the frame-rail, which is used as the vertical, Z-axis limits. Finally, the design space is boxed in with the boom, which is found in the positive X-axis direction away from the cross-member, and various other components in the negative X-axis direction. Using the design space limits, a preliminary design space volume was identified. Within this preliminary design space box, space is reserved for functional components such as the bushes and cross-member pin, around which the boom connects. Furthermore, functional material for the connection interface between the cross-member and frame-rails need to be identified and isolated from the design space. This is to prevent the removal of functional

Stellenbosch University https://scholar.sun.ac.za

material during the topology optimization procedure. Noting that the cross-member is connected to the chassis frame-rails via bolts, necessary material is required for the bolted connection to exist in the topology results. Finally, space needs to be created for interfering parts, such as the boom. It should be noted that the boom is a dynamic part within the chassis assembly, and space needs to be created for all the various positions where the boom can exist. A resulting design space volume was found, with a developed input model, as shown in Figure 5.2. Red regions are functional components, purple regions are functional material that should not be removed or modified, and green is the topology design region.

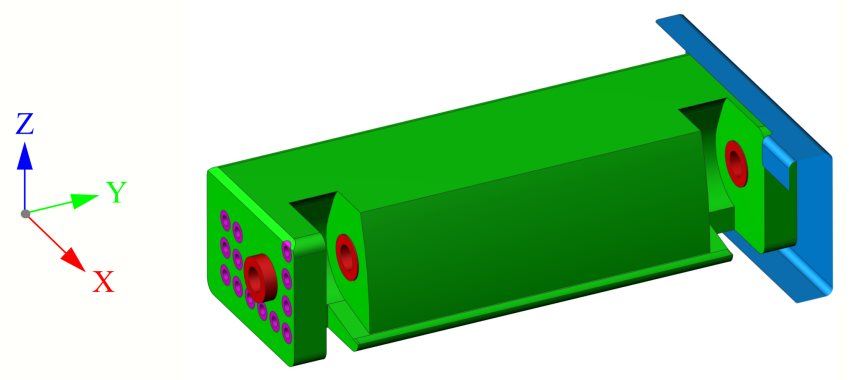

Figure 5.2: Initial cross-member topology model, with the designable space highlighted in green

5.1.2 Cross-member initial topology FE model development

For the FE model development, it was decided to add the initial cross-member topology model into the chassis structure, to create one large FE model. This is to ensure that boundary conditions for the cross-member FE analysis are accurately defined, knowing that it connects to the chassis frame-rails via bolts. If the chassis is omitted in the FE model, the bolted connections would have to be used as direct boundary conditions to the environment. Typically, these boundary conditions are defined as rigid connections, which will result in an over-constrained cross-member, and an inadequate representation of the actual boundary conditions. During the ACTT's operation, the chassis experiences deformation, which is then translated, and partly resisted by the cross-member. During this time, the cross-member also moves, twists, and deforms. Knowing this, the complexity and nature of the cross-member's boundary condition can only be captured by including the chassis into the FE model. Furthermore, the boom connects to both the cross-member and chassis. Input loads are directly

Stellenbosch University https://scholar.sun.ac.za

translated from the boom to both the cross-member and chassis, simultaneously. If the cross-member were to be analyzed separately from the chassis, the true loading condition would not be met, resulting in flawed or inaccurate results. For these reasons, the chassis and cross-member are found to be reliant on each other, if accurate boundary- and loading conditions are to be achieved. A FE model was created, as shown in Figure 5.3. A more detailed FE model of the cross-member is shown in Appendix K with visible finite elements and bolted detail. The boom structure has been omitted from the FE model, however, the relevant reaction forces and moments are supplied to the chassis and cross-member to simulate the transferral of input loading that the boom experience. It should be mentioned that the chassis FE model was provided for this project, which contained the original cross-member model.

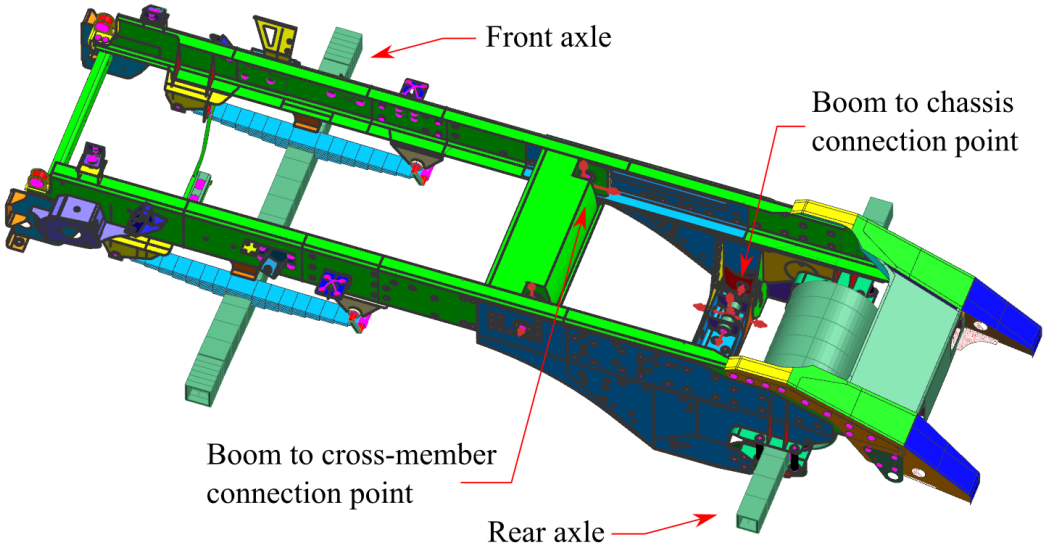

Figure 5.3: Combined cross-member- and chassis FE model, with the finite elements currently hidden

A decision was made to use material within the ductile cast iron range, listed in Table 2.3, for the development of the initial cross-member topology FE model, as one of the aims is to find a castable cross-member design. This decision is based on the fact that the cross-member will experience significant strain during operation, therefore, the ductility of ductile cast iron range is preferred over the ordinarily brittle grey cast irons. The remaining components such as the bushings and pin were assigned the ASTM grade 50 steel material. Furthermore, the FE simulation contains the two ultimate load cases as used in Chapter 3 and 4, however, the boundary conditions have been modified to exist at the truck axle endpoints, where the wheels are located. After creating the FE model and simulation, a FE analysis was performed. The FE model and simulation was exported to GENESIS, solved, and compared to the NX results, exhibiting similar results. The initial topology model development

Stellenbosch University https://scholar.sun.ac.za

was, consequently, deemed satisfactory, and ready to undergo optimization in Phase 2.

5.2 Execution of Phase 2: Optimization Task Definition and Manufacturing Constraint Testing

In Phase 2, manufacturing process constraints and parameter tuning will be used to explore plausible designs for continued refinement. It was decided to focus on using casting constraints, as this is an aim set for the cross-member design. By making this decision, Phase 2 becomes simplified by reducing the number of design parameters to be used. Designers need to make this decision when using the methodology, as there exist various manufacturing constraints, some of which, are not applicable for a required design outcome.

5.2.1 Defining the topology objective, regions, and design constraints

The topology tasks require the set up of a topology objective function(s), topology regions, manufacturing-, and topology constraints. The first step in setting up the topology task is to select a topology design objective. For the outcome that is currently required, an objective function is defined to minimize strain energy. By minimizing strain energy, the optimizer removes ineffective material from the design domain, hence minimizing the material, whilst retaining material within the load path regions to ensure high structural stiffness. The areas colored in green, as shown in Figure 5.2, will be used as the topology design region. With the definition of a topology region, manufacturing constraints are selected for that chosen region. As already mentioned, casting is an important consideration for the task definition and concept design outcome. It was decided to consider casting in both the X- and Z-axis directions. The parting plane is selected to be on the centreline of the bushings, simplifying the envisioned mold design and addition of cores during the physical casting operation. Casting within the Y-axis seems unpractical, and a decision was made not to use it as a potential casting direction. As for most components found in the ACTT chassis design, symmetry is a requirement. The same is true for the cross-member, therefore, a symmetry constraint will be present in all the cross-member topology tasks. A ZX-symmetry constraint, at the centre of the design region, is used to ensure symmetrical results. Upper mass fraction topology constraint limits are defined to control the retained material within the design region. This is to drive material removal during the design and to ensure that a competitively weighted design is found, compared to the original cross-member.

Stellenbosch University https://scholar.sun.ac.za

Using the above-mentioned topology task definitions, and combinations of tuned parameters, preliminary designs can be found for the continued refinement in Phase 3. The initial topology model can be updated based on the results that are obtained from the optimization tasks if required.

5.2.2 Preliminary cross-member topology results

To start the design procedure, an optimization task was created with the single symmetry constraint. The resulting structure formed a box, removing most material within the centre of the design region. This result could be refined to something that is manufacturable out of plates, however the idea is to move towards a castable design. To achieve this, casting constraints were added to the topology tasks. These manufacturing constraints include Z- and X-axis direction casting constraints. Starting topology mass fraction- and mass fraction constraint values of 0.3 were selected, which is the default value for both parameters. By applying this mass fraction constraint to the topology region, an estimated upper limit of 173.8 kg of mass will be retained, which includes the functional material. This mass does not compare well to the current cross-member mass of 117.8 kg, however it is an acceptable starting point. Limitations to the task design freedom are to be avoided at this stage, consequently, no member size limits were used. The topology results for the Z- and X-axis casting tasks are shown in Figure 5.4a and Figure 5.4b, respectively.

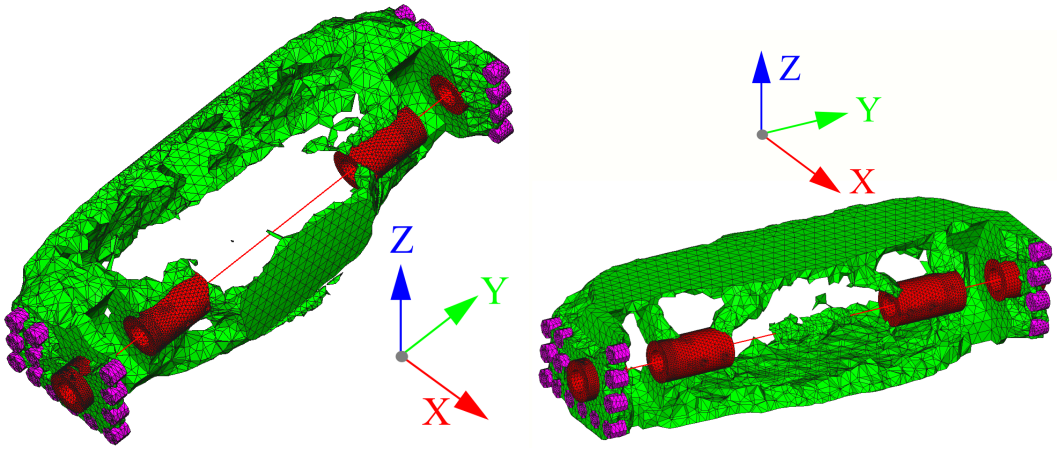

(a) Z-axis casting constraint **(b)** X-axis casting constraint

Figure 5.4: Preliminary, castable cross-member structures

The Z-axis casting result was found to be lacking in refinement potential and a less practical result in terms of casting and manufacturing. The opposite was found to be true for the X-axis casting direction result, which showed ample potential for further improvement. For this reason, the X-axis casting

Stellenbosch University https://scholar.sun.ac.za

result was selected for continued refinement. It was also noted that the functional material is isolated without any supporting material. This is due to the material being removed during the optimization task. It was decided to update the initial topology model, by adding supporting functional material around the area where bolted connections are found. Figure 5.5 shows the updated initial topology model, with the added material highlighted in yellow.

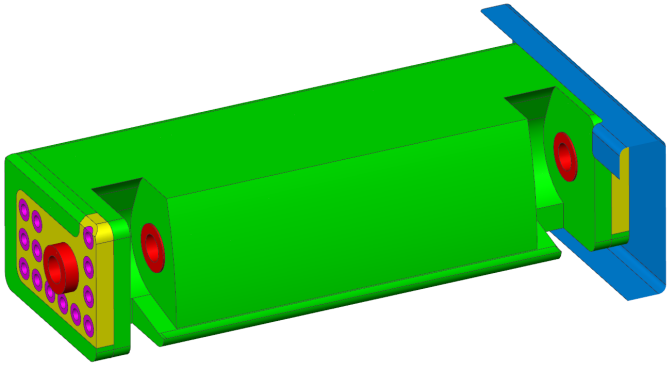

Figure 5.5: Updated initial cross-member topology model, with added functional material, highlighted in yellow

To obtain a resulting structure that can compete with the current cross-member design, a lower final mass is required, therefore, a lower mass fraction needs to be selected for the optimization task. A new topology task was created with a mass fraction, resembling the mass of the currently used cross-member, which includes the mass of the functional material. Additionally, member size limits were defined, preventing the formation of material clumps, or overly thin areas. The result from the new topology task, which includes the new model, new mass fraction, and added parameters, is shown in Figure 5.6.

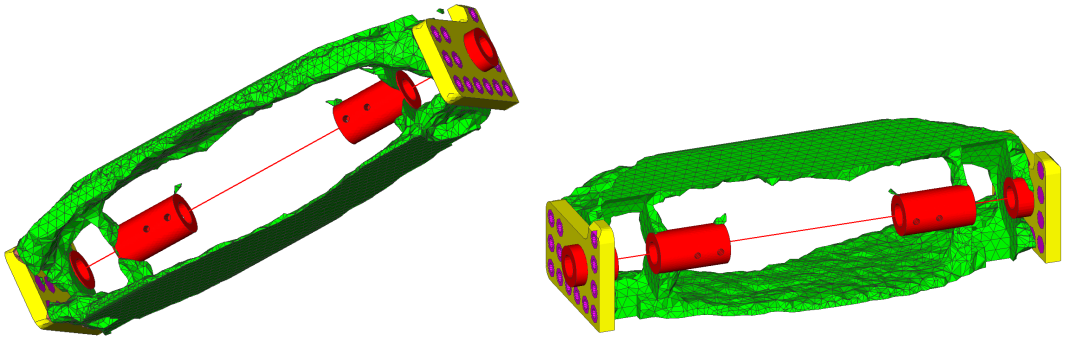

(a) Rear view of the topology result **(b)** Front view of the topology result

Figure 5.6: Improved X-axis, cross-member casting design

Stellenbosch University https://scholar.sun.ac.za

Table 5.1: Cross-member topology optimization task schedule

MF / Mass [kg]	Mesh size [mm]		
	24	16	12
0.173 / 117.8	Task 1	Task 2	Task 3
0.146 / 103.1	Task 4	Task 5	Task 6
0.119 / 88.36	Task 7	Task 8	Task 9

By reducing the mass fraction constraint to a realistic value and modifying the initial topology model, a design was found that shows ample potential for further refinement and development. Not only is this newfound design castable, but also a fundamentally new design compared to the currently used cross-member design. The next step in the concept design methodology will be to refine the optimization task by doing a mesh size- and mass fraction refinement, as described in Phase 3 of the concept design methodology.

5.3 Execution of Phase 3: Topology Optimization Process Refinement

Now that an acceptable preliminary design has been found, further topology task refinement can be used to improve on the design in preparation for Phase 4.

5.3.1 Mesh size and mass fraction selection

To start the refinement process, a selection of mesh size and mash fractions were identified. Using combinations of the mesh size and mass fraction constraints, an optimization task schedule was created. This schedule consists of a combination of three mesh sizes and three mass fraction constraints. The mesh sizes were selected based on discretization accuracy and the avoidance of overly small elements that could result in unrealistic solving- and optimization time.

When interpreting and developing a new model based on topology results, it is very difficult to capture the precise geometry of the topology results, and the unintentional outcome is typically to add more material, rather than less. This effect adds up, with a resulting developed structure that is much heavier than the upper mass fraction limit used for the optimization procedure. For this reason, the mass fractions constraints were selected to generate structures with equal- or less mass compared to the currently used cross-member design. Table 5.1 lists the various selected mesh size and mass fraction constraints, with the corresponding optimization tasks.

Stellenbosch University https://scholar.sun.ac.za

5.3.2 Refined cross-member topology results

After performing the various scheduled optimization tasks, satisfactory results were obtained. The result for Task 9 is displayed in Figure 5.7. The remaining optimization task results can be seen in Appendix L.

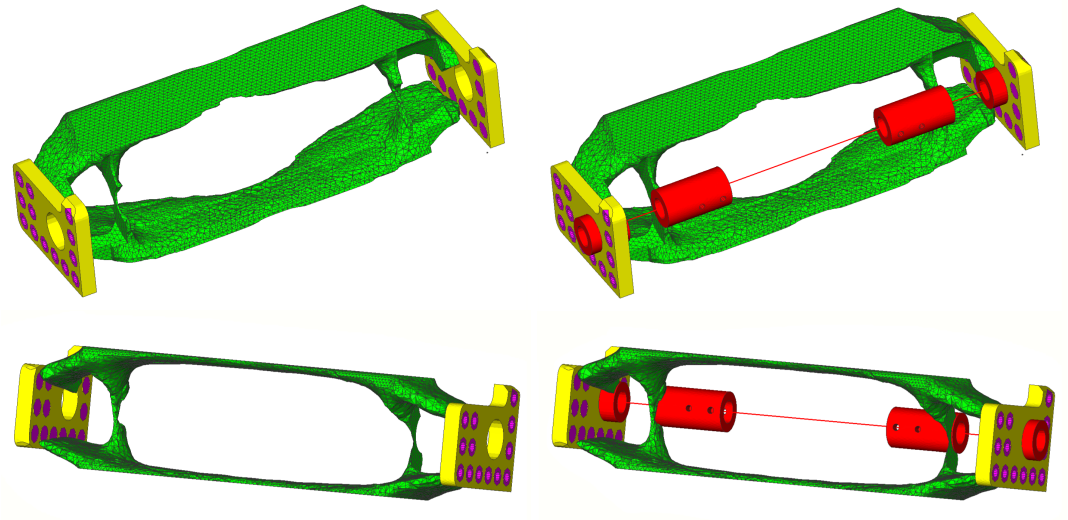

(a) Cross-member topology result, illustrating the castable design

(b) Cross-member topology results, with added functional components

Figure 5.7: Task 9, cross-member topology results

Overall, the optimization task results converged to one design. Naturally, the tasks with the higher mass fractions showed thicker and wider member sizes, however the design concept stayed constant. The resulting structures are also similar to those found at the end of Phase 2. The repetitive design results can be seen as an indication that an optimal design for the loading condition has been found. The next and final phase will be to do a final refinement step to ensure that a structure is found that complies with stress constraints, aimed mass, and manufacturing constraints.

5.4 Execution of Phase 4: Result Interpretation and Design Refinement

Phase 4 requires the interpretation and refinement of the topology optimization results found in Phase 3, to develop a final concept design. It was decided to use the results found from Task 9 for continued work.

Stellenbosch University https://scholar.sun.ac.za

5.4.1 Task 9 topology result interpretation

To start the design procedure, a new cross-member model was created, based on the topology results found from Task 9. To avoid complications during the shape optimization refinement procedure, the necessary changes were made to increase the manufacturability of the design and to eliminate stress concentration regions. Previously, it was found difficult to fix stress concentration regions using shape morphings sets, and this could have a negative impact on the shape optimization results. Consequently, stress concentration regions were removed manually. The developed cross-member model is displayed in Figure 5.8. The newly developed cross-member model was used to replace the initial topology model within the chassis. After developing the FE model and simulation, a FE analysis was performed, with the highest resulting stress of 250 MPa, found from the 2nd ultimate load case. The FE results are presented in Appendix M. Based on the FE stress results, both D60-40-18 and D65-45-12 should suffice as a chosen material from the ductile range, having yield strengths of 276 MPa and 311 MPa, respectively. When considering safety factors, the use of D60-40-18 becomes questionable, since a small safety factor (SF) will place the current design at the stress constraint limit. The expectation is that no or little improvement will be made using shape optimization, as the design is already at the stress constraint limit, which will consequently hinder the removal of material. Based on this expectation, it was decided to use D65-45-12 with a safety factor of 1.07, which is similar to that used for the boom. A resulting stress constraint of 291 MPa is calculated using Equation 3.1.

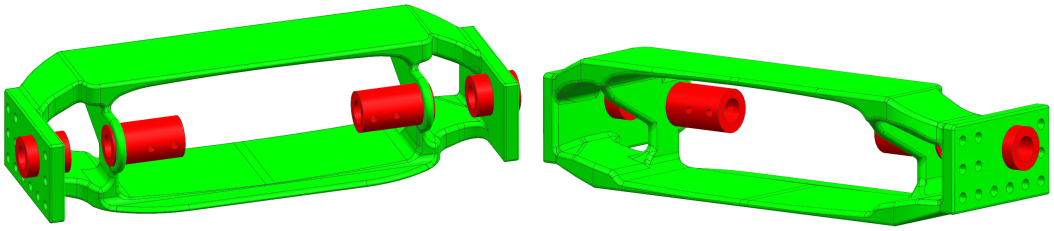

(a) Front view of interpreted design **(b)** Rear view of interpreted design

Figure 5.8: Task 9, cross-member topology result interpretation

5.4.2 Shape optimization refinement

Now that a satisfactory FE model has been created, shape optimization can be performed to further improve and refine the current design. The focus will mainly be to remove material in low-stress areas. The likelihood of developing zero stress concentration regions during the interpretation process is very low, therefore, existing stress concentrations should be dealt with using

Stellenbosch University https://scholar.sun.ac.za

shape optimization. A shape optimization task, containing 35 shape domains and 16 shape morphing sets was created. Shape morphing sets that presented noteworthy results are shown in Appendix M, Figure M.3. An objective to minimize mass was defined, as well as a stress constraint of 291 MPa. A shape optimization task was performed with the result presented in Figure 5.9.

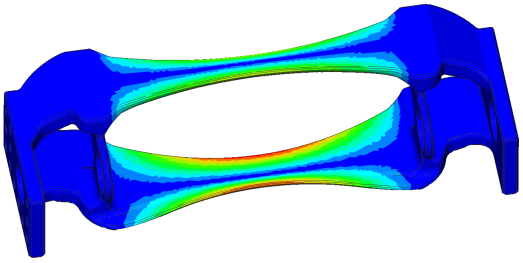

Figure 5.9: Interpreted cross-member, shape optimization result

Upon inspecting the shape optimization result, it was found that a large amount of material is removed within the centre of the cross-member. Knowing that the cross-member experiences torsional loads that are partly resisted by the material that has now been removed, the resulting shape changes could not be accepted. It was decided to add two additional load cases, simulating the worst-case torsional situations that the cross-member could experience. The first load case was defined to experience a large upwards vertical force at the left-rear wheel, causing the left-front wheel to slightly lift off the ground. This causes the chassis framework to experience a large torsional load. This load case is known as the chassis twist load case. The second load case simulates a slipping event of the right wheels, while the left wheels have sufficient traction, creating a torsional load within the chassis framework. This load case is known as the split mu load case. These two load cases were added to the shape optimization task that was previously defined. Simplified illustrations of the two added load cases are presented in Appendix N, Figure N.1. To ensure that a resulting cross-member structure is found with an equal or higher stiffness than the current cross-member design, displacement constraints were added to the axle endpoints to be equal or lower than the current displacements experienced. This included a vertical displacement limit of 60.1 mm at the left-rear wheel for the chassis twist load case, as well as, 31.4 mm and 28.7 mm longitudinal displacement limits at the right-front and right-rear wheel for the split mu load case, respectively. After running the improved shape optimization task, it was found that the optimizer stayed consistent with the shape changes that were previously found. The resulting shape changes are shown in Figure 5.10, with the highest experienced stress of 278.2 MPa. Furthermore, the optimization task summary showed that all displacement constraints were adhered to, therefore, indicating that the structural stiffness of the chassis assembly is improved, or matched at the very least using any of the two proposed

Stellenbosch University https://scholar.sun.ac.za

structures. Upon a closer inspection of the structure shown in Figure 5.10, it was found that the left-rear wheel displaced 53.6 mm for the chassis twist load case. The right-front and right-rear each displaced with 25.8 mm and 23.1 mm for the split mu load case, respectively. These displacements are all below the required limit, indicating that the shape-optimized cross-member design increases the structural stiffness of the chassis assembly.

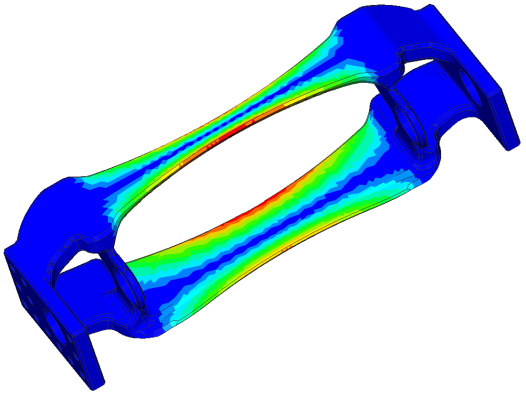

Figure 5.10: Cross-member shape result after the addition of the new load cases, displaying the highest measured stress of 278.2 MPa

5.4.3 Concept design finalization

After evaluating the shape optimization results, it was decided to create three concepts. The first concept, Concept 1, would be a design that is simply based, or inspired, by the shape optimization results as shown in Figure 5.9. Another interpretation of the shape optimization results is that the material in the central region of the cross-member is not required, which is based on the extreme shape changes that occurred. It was decided to create a second concept, Concept 2, by removing the top-central part of the cross-member, leaving the pin and the bottom-central part to form a four-bar structure, which should provide adequate structural stiffness. Lastly, a third concept, Concept 3, was created by removing the entire central part of the cross-member, consequently, splitting the cross-member into two parts, with only the pin existing between the two cross-member pieces. The three concepts are presented in Figure 5.11.

Three new FE models were created, similar to the FE model in the 1st interpreted cross-member evaluation, using each of the three new concepts. The two extra load cases, as defined in Section 5.4.2 were also added to the FE simulation. FE analyses of each concept were performed, with a summary of the results as shown in Table 5.2. The FE results are shown in Appendix N, Figures N.2 and N.3. As can be noted from the FE analyses summary, only Concept 1's design was close to satisfying all the design constraints. Concept 1

Stellenbosch University https://scholar.sun.ac.za

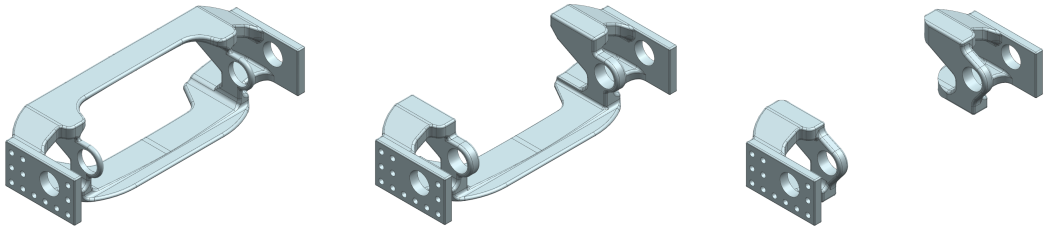

(a) Concept 1 (b) Concept 2 (c) Concept 3

Figure 5.11: Cross-member concepts, developed for Phase 4 evaluation

showed a stress limit violation for the 2nd ultimate load case, however, the violation is roughly 2.5 % over the stated limit. The violated area was also found to be quite small. Based on the area size, a reasonable expectation would be that the material in this region will experience local plastic deformation before distributing the stress within the region, without concern of failure or material degradation. Stronger materials such as D80-55-05 could also be considered, which will result in a SF of roughly 1.27. Further refinement of Concept 1 was performed, however no significant improvements were found. Looking at the results of Concept 2, the design could potentially be developed into a usable design, however it was outperformed by Concept 1 in terms of structural performance, and outperformed by Concept 3 in terms of mass. When comparing Concept 2 with Concept 1, no mass reduction is found. This is due to the bushing mount being thickened. For this reason, it was decided not to continue the refinement of Concept 2. Due to Concept 3 pushing the boundary of being a unique- and different concept, it was decided to refine and improve the design in an attempt to conform to the design constraints. After some refinement, it was possible to achieve a highest stress of 389.5 MPa, which is much lower than the previous stress of 468.2 MPa. This stress is still exceeding the capabilities of D65-45-12, however a material such as D100-70-03 could be considered for this design, which will have an SF of roughly 1.24.

Table 5.2: Model- and FE result summary for Concepts 1, 2, and 3

Load case	Measurements	Original design	Concept 1	Concept 2	Concept 3
1st ULC	σ_{max} [MPa]	223.4	243.5	263.5	235.6
2nd ULC	σ_{max} [MPa]	374.7	298.5	395.8	468.2
Chassis Twist	σ_{max} [MPa]	200.3	136.5	125.1	115.3
Split Mu	σ_{max} [MPa]	209.6	214.6	286.9	223.1
Chassis Twist	$disp_{LR}$ [mm]	60.1	56.9	59.6	60.2
Split Mu	$disp_{RF}$ [mm]	31.4	26.8	26.9	29.5
Split Mu	$disp_{RR}$ [mm]	28.7	24.3	24.5	26.9
-	mass [kg]	117.8	92.97	93.24	76.87

Stellenbosch University https://scholar.sun.ac.za

With the completion of the final step in Phase 4, which includes FE analyses and final refinement steps, the end of the concept design methodology was reached. The next step will be to evaluate the design(s) to determine if a satisfactory outcome has been reached.

5.5 Cross-member Redesign and Methodology Evaluation Summary

With Phase 4 reaching completion, a decision was made that acceptable designs were found. With the concept design methodology now being completed, both the cross-member concept designs and methodology can be evaluated based on the outcomes that were reached.

5.5.1 Cross-member redesign evaluation

With the concept design methodology concluded, two plausible concepts were found, which are Concepts 1 and 3. Based on the material choice originally made, only Concept 1 was deemed as a realistic and acceptable design, however, with the necessary design- and material choice adjustments, Concept 3 could also prove to become a competitive design. It should be noted that the designs that are intended to be created using the concept design methodology, are not completed, ready to be manufactured designs, but rather concepts as the methodology's name imply. The design could still be put through multiple iterations of optimization or manual refinement to suit the needs and desired outcome of the designer. Due to Concept 3's lack to conform with the current desired outcome, it was decided to select Concept 1 as the final design. A comparison was made between Concept 1 and the original cross-member model that is currently being used. A summary of this comparison is shown in Table 5.3.

Table 5.3: Design comparison between Concept 1 and the original cross-member

Topic of comparison	Original cross-member	Concept 1
Mass [kg]	117.8	92.97
Material	ASTM A-573 Grade 50 steel	D65-45-12 cast iron
Safety factor (aim)	1.070	1.070
Safety factor (achieved)	0.934	1.042
Component [#]	11	5
Manufacturing requirements	Welding Laser / Water jet cutting Sheet forming	Casting Machining (additional)

Stellenbosch University https://scholar.sun.ac.za

Based on the design comparison, Concept 1 has a much lower mass than the original cross-member design, as can be seen from the comparison summary, which equates to a 21.1 %, or 24.8 kg, reduction in mass. This is a satisfactory result, considering that Concept 1 also proved to provide additional stiffness to the chassis structure, whilst staying below the yield stress limit of the material. Concept 1 also poses various other benefits such as the easing of the manufacturing process, as it consists of fewer components and requires fewer fabrication steps. Overall, Concept 1 proved to be a competitive design, that should be considered as a potential replacement for the currently used cross-member design. Figure 5.12 gives an insightful look as to how the design of Concept 1 compares to the original cross-member design.

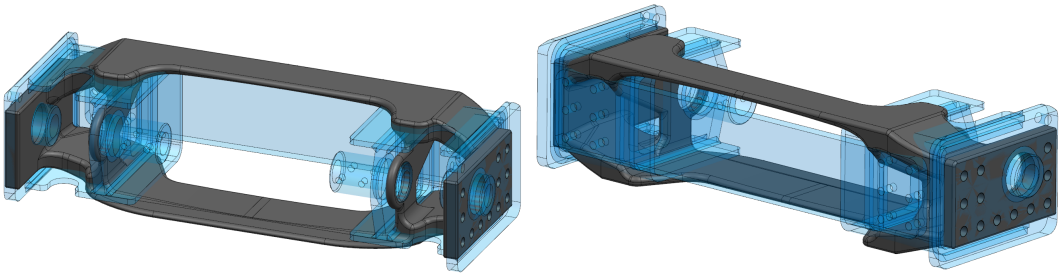

(a) Cross-member overlay front view **(b)** Cross-member overlay rear view

Figure 5.12: Overlay comparison between Concept 1 and the original cross-member

5.5.2 Concept design methodology evaluation

During the process of redesigning the cross-member design, the concept design methodology was followed with the utmost care and strictness to ensure a valid and meaningful evaluation thereof. For the desired outcome of designing a component to conform with certain manufacturing constraints, mass minimization, high stiffness, and uniqueness, the methodology was able to deliver satisfactory results to these requests. Knowing that the methodology was developed based on a previous component's optimization processes and results, and that the two components, namely the boom and cross-member, are very different from each other, it was proven to be a well-thought-out methodology that is universally applicable within the automotive design realm.

Stellenbosch University https://scholar.sun.ac.za

Chapter 6

Conclusion and Recommendations

Presented in Chapter 1, is a thorough motivation as to why the application of structural optimization techniques could prove useful for improving the designs of truck chassis components. Based on the proposal of using structural optimization for such an application, a project aim and objectives were formulated in an attempt to successfully improve truck chassis components that were deemed appropriate for such a venture. The first part of this chapter focuses on evaluating the completion of the various objectives. Supported by the outcome of the objectives, a discussion on the fulfilment of the project aim takes place, after which a conclusion is drawn regarding the entirety of the project. To finish off, recommendations for future work are made.

6.1 Project Objective Completion

The project aimed to improve both the boom- and cross-member component designs with respect to cost-effectiveness, structural performance, and ease of manufacturing. The development of a concept design methodology, based on the optimization results, was also required, after which it was tested. In order to achieve the project aim, four objectives were defined to guide the attainment thereof. Following is a detailed discussion on the manner and extent to which the project objectives have been completed. The outcome summaries of Objectives 1, 2, 3, and 4 are also presented at the end of Chapters 3, 4, and 5.

6.1.1 Objective 1

Objective 1 required the improvement of a terminal tractor component, specifically using size-, shape-, topometry-, and topography optimization. The boom was selected as the first component to be optimized. A FE boom model was developed, after which it underwent extensive optimization procedures, using size-, shape-, topometry-, and a combination of size- and shape optimization. Topography optimization was found to be an unsuitable technique for this

Stellenbosch University https://scholar.sun.ac.za

design as it is fabricated with extensive welding operations, which will conflict with the optimization technique. Evaluating the results obtained from the optimization tasks, it was found that the currently used boom design is at a near-optimal design configuration. The best practical optimization result showed a 3.5 % reduction in mass, which is a marginal improvement. Nevertheless, an improved structure in term of mass was found, which satisfied the Objective 1 requirements. Knowing that the boom component previously received numerous design iterations and non-formal optimization, it was a satisfactory result.

6.1.2 Objective 2

Objective 2 focused on diverging from the current boom design in an attempt to find a design that is conceptually new and different, which could be achieved using topology optimization. To start the optimization process, a new model was created to fill the space that the current boom is occupying within the chassis. Once the model was completed, topology optimization was used to find new designs within the design space. The optimization procedure was guided using strain energy minimization and mass fraction constraints, in order to achieve stiff- and light structures. An optimization task schedule was created with four chosen design mass outcomes. Additionally, mesh refinements were performed to avoid any mesh dependant optimization complications from occurring. The optimization schedule listed 12 topology tasks to be performed, which delivered satisfactory results. Based on the topology results, a new boom model was developed, after which it was improved using shape optimization. A final boom design was consequently found that is fundamentally different from the current boom design. Furthermore, the design proved to be competitive in terms of structural performance and manufacturing requirements, compared to the current boom. Easing of the manufacturing process was achieved by reducing the manufacturing requirements to a single casting, with some minor machining work potentially being required. The casting also indirectly improved the structural performance of the design by eliminating the requirement of welded connections. Finally, the overarching structural performance of the boom was improved, with a safety factor increase from 1.07 to 1.15. The final boom design was found to be slightly heavier than the currently used design, with a marginal increase of 5 kg, or 1.3 %.

6.1.3 Objective 3

Objective 3 was formulated specifically to contribute towards achieving a part of the project aim, which was to develop a concept design methodology. The concept design methodology development was based on the results found during the execution of Objective 2, therefore the boom topology results. Using the results, failures, and knowledge gained from the topology work performed

Stellenbosch University https://scholar.sun.ac.za

on the boom, a detailed, but concise step-by-step procedure was created. The procedure was divided into four main phases; Phase 1, initial topology model development, Phase 2, optimization task definition and manufacturing constraint testing, Phase 3, topology optimization process refinement, and finally, Phase 4, result interpretation and design refinement. These steps were developed in a manner to guide a user using the methodology from the point of initial identification of a component being replaced, up until a final satisfactory concept design. This concluded Objective 3.

6.1.4 Objective 4

After the development of the concept design methodology, Objective 4 was pursued. Objective 4 required the application and testing of the methodology on a new component. It was consequently decided to use the concept design methodology to improve the cross-member design. The idea was to redesign the cross-member and evaluate the methodology simultaneously. Following the methodology procedure, an initial topology model was created, after which optimization task definition and manufacturing constraint testing was performed. Using the results obtained, the topology optimization process was refined, producing topology results that were primed for the final phase, Phase 4. A new design was developed by interpreting the topology results. As a final refinement step, shape optimization and the interpretation thereof was used to push the design to a point of maximum structural stiffness, while using the minimum amount of structural mass. The concept design methodology was concluded with a resulting concept design that proved to be competitive in terms of cost-effectiveness, structural performance, and ease of manufacturing. Furthermore, it was possible to confirm the validity and effectiveness of the methodology, due to the satisfactory concept design that was obtained.

6.2 Fulfilment of Project Aim

Each objective played a significant- and unique role towards the fulfilment of the project aim. It became notable that trade-offs will be required when doing optimization as it is difficult to achieve designs that are both lighter, stronger and easier to manufacture. This is especially true if a component has already passed through a number of design iterations since its conception. However, by redesigning components with the use of topology optimization, boundaries can be pushed in terms of the desired outcome. This was found to be true during the execution of Objectives 2 and 4. The final cross-member showed to be competitive in terms of cost-effectiveness, structural performance and ease of manufacturing. Furthermore, the concept design methodology was used to drive this design, which confirmed the successful development- and effectiveness of the methodology.

Stellenbosch University https://scholar.sun.ac.za

6.3 Conclusion

This project succeeded in using the field of structural optimization to propose realistic and relevant design improvements on components that are currently being used in practice. Due to the manner and extent to which these structural designs are analyzed and scrutinized, the optimization procedure had to be integrated into these evaluation processes in a very specific way and it was found to work exceptionally well. The extent to which optimization was used during the course of the project showcased the high level of applicability that structural optimization has on practical, real world problems and the value that it could generate. With optimization it is possible to evaluate existing designs based on their optimality and make the necessary changes to further enhance designs. When moving to the realm of component redesign and design conceptualization, optimization serves as an invaluable tool to assist and guide a designer during the design procedure, as substantiated by this project. Optimization therefore offers a designer a variety of options to achieve superior designs. For these reasons, the contributions made by this project could serve as a starting point for future structural optimization work and design problems, as well as a continuation point in the development and use of optimization methodologies within the automotive industry.

6.4 Recommendations for Future Work

With the project concluded, multiple recommendations can be made for continued work within the field of structural optimization. The following list of recommendations was selected as most relevant for continued work:

- Development of a complementary algorithm, or script, that can be combined with GENESIS to do parameter optimization and tuning after each completed optimization task. The parameters could include, amongst others, mass fractions and initial shape changes
- The use of superelements during optimization procedures, to reduce the computational requirements for each design cycle that succeeds the initial FE analysis cycle. This will reduce the time required to perform an optimization task, or allow designers to attempt optimizing large models
- An optimization procedure that attempts to minimize the maximum stress by using structural mass as a budget. By increasing the allowable mass, a lower maximum stress can be achieved and vice versa. Using this procedure, a stress vs. mass design trade-off curve can be developed and used to find desirable design points
- The expansion of the concept design methodology to consider different objective functions and design outcomes

Stellenbosch University https://scholar.sun.ac.za

Appendices

Stellenbosch University https://scholar.sun.ac.za

Appendix A

Fatigue Geometry

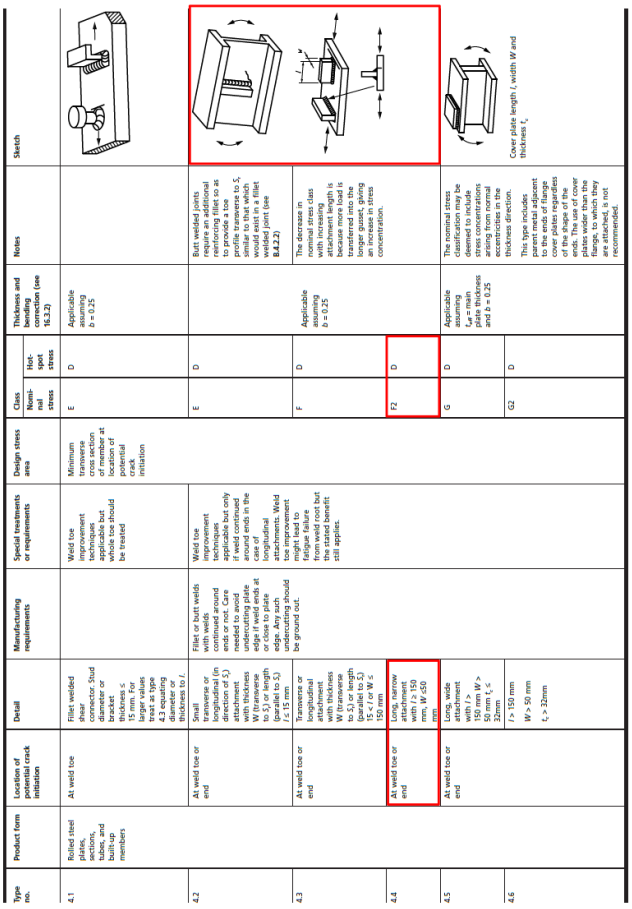

Type no.	Product form	Location of potential crack initiation	Detail	Manufacturing requirements	Special treatments or requirements	Design stress area	Class		Thickness and material correction (see 16.3.2)	Notes	Sketch
							Non-fillet stress	Hot-spot stress			
4.1	Rolled steel plates, sections, tubes, and welds in such members	At weld toe	Fillet welded stiffener, stud connector, stud diameter or longitudinal thickness ≤ 15 mm. For larger values treat as edge 4.3 equating diameter or thickness to t.		Weld toe improvement techniques applicable but welded stud should be treated	Minimum transverse cross section of member at location of potential crack initiation	E	D	Applicable assuming $b = 0.25$		
4.2		At weld toe or end	Small transverse or longitudinal (in direction of S_r) attachment with thickness W (transverse to S_r) or length (parallel to S_r) $l < 15$ mm.	Fillet or butt welds with welds continued around ends or not. Care needed to avoid undercutting plate edge if weld ends at or close to plate edge. Any such undercutting should be ground out.	Weld toe improvement techniques applicable but only if welds continued around ends in the case of transverse attachments. Weld toe improvement might lead to failure data from weld root but the stated benefit still applies.		E	D		But welded joints require an additional reinforcing fillet so as to provide a toe profile transverse to S_r similar to that which would exist in a fillet welded joint (see 8.4.2.2)	
4.3		At weld toe or end	Transverse or longitudinal attachment with thickness W (transverse to S_r) or length (parallel to S_r) $15 < l$ or $W \leq 50$ mm				F	D	Applicable assuming $b = 0.25$	The decrease in nominal stress class with increasing attachment length is because more load is transferred into the longer gusset, giving an increase in stress concentration.	
4.4		At weld toe or end	Long, narrow attachment with $l \geq 150$ mm, $W \leq 50$				F2	D			
4.5		At weld toe or end	Long, wide attachment with $l > 150$ mm $W > 50$ mm $t < 32$mm				G	D	Applicable assuming L_M = main plate thickness and $t < 0.25$	The nominal stress classification may be deemed to include stress concentrations arising from normal eccentricities in the thickness direction. This type includes parent metal adjacent to the welds of flange cover plates regardless of the shape of the cover plate and of cover plates wider than the flange, to which they are attached, is not recommended.	
4.6			$l > 150$ mm $W > 50$ mm $t_f > 32$mm				G2	D			Cover plate length l, width W and thickness t_f

Figure A.1: Weld geometry selection, displayed in red (British Standards Institution, 2014)

Stellenbosch University https://scholar.sun.ac.za

Appendix B

Boom Model Validation

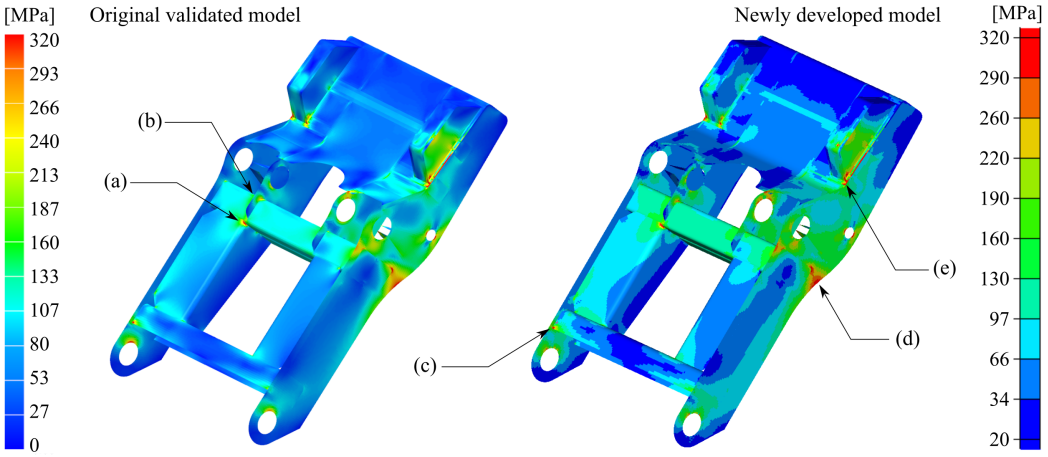

Figure B.1: Boom stress distribution for the 2nd ultimate load case. Shown on the left is the original boom that was designed, validated and provided to the project. Shown on the right is the newly developed boom model that will be used for further optimization procedures

Table B.1: Numerical stress comparison between the original boom FE model developed in NX and the imported model in Design Studio, with percentage difference between measured values, for the 2nd ultimate load case

Description	ULC2: 1g-Z / 0.4g-Y (1 element)			ULC2: 1g-Z / 0.4g-Y (9 elements)		
	Original model	New model	Diff (%)	Original model	New model	Diff (%)
L-Plate	230.95	231.37	0.18	186.26	187.08	0.44
Centre tube	247.30	244.07	1.31	249.43	247.28	0.86
U-plate	150.53	153.51	1.98	154.27	160.41	3.98
Side plate	316.87	313.14	1.18	295.57	291.60	1.34
Back plate	284.01	269.66	5.05	211.27	208.42	1.35

Stellenbosch University https://scholar.sun.ac.za

Appendix C

Stress Constraint Table

Table C.1: Stress constraint table, indicating the general stress constraints that are used for the boom evaluation. A few areas within the boom are allowed to exceed the general stress constraint limits and are highlighted in bold

Optimization Stress Constraints [MPa]						
Element group	Region	Load case				
		Ultimate		FESL		
		ULC1	ULC2	FESL1	FESL2	FESL3
Pshell 2: L-Plate	Plate / Edge	327,3	327,3	100,0	100,0	100,0
Pshell 5: Back Plate	Plate / Edge	327,3	327,3	100,0	100,0	100,0
Pshell 11: Stiffner Plates	Plate / Edge	327,3	327,3	100,0	100,0	100,0
Pshell 13: Side Plates	Plate / Edge	327,3	327,3	100,0	100,0	100,0
Pshell 14: Mid Plates	Plate / Edge	327,3	327,3	100,0	100,0	100,0
Pshell 15: Mid Tubes	Plate / Edge	327,3	327,3	100,0	100,0	100,0
Pshell 16: Short Tubes	Plate / Edge	327,3	327,3	100,0	100,0	100,0
Pshell 17: Back Tube	Plate / Edge	327,3	327,3	100,0	100,0	100,0
Pshell 18: U-beam	Plate / Edge	327,3	327,3	100,0	100,0	100,0
Pshell 19: Bearing Contact Plates	Plate / Edge	327,3	327,3	100,0	100,0	100,0
Pshell 20: Bearing Mount Plates	Plate / Edge	327,3	327,3	100,0	100,0	100,0
Pshell 21: Gussets	Plate / Edge	327,3	327,3	100,0	100,0	100,0
Pshell 36: Side Plates	Plate / Edge	**384,0**	327,3	100,0	100,0	100,0
Pshell 37: L-Plate	Plate / Edge	**440,0**	327,3	100,0	100,0	100,0
Pshell 38: Mid Tubes	Plate / Edge	**384,0**	327,3	100,0	100,0	100,0
Pshell 44: Side Plate	Weld	No constraint	No constraint	35,0	**82,0**	35,0
Pshell 45: L-Plate	Weld	No constraint	No constraint	35,0	**82,0**	35,0
Pshell 46: Back Plate	Weld	No constraint	No constraint	35,0	**82,0**	35,0
Pshell 47: Stiffner Plates	Weld	No constraint	No constraint	35,0	**82,0**	35,0
Pshell 49: Mid Plates	Weld	No constraint	No constraint	35,0	**82,0**	35,0
Pshell 50: Mid Tubes	Weld	No constraint	No constraint	35,0	**82,0**	35,0
Pshell 51: Short Tubes	Weld	No constraint	No constraint	35,0	**82,0**	35,0
Pshell 52: Back Tube	Weld	No constraint	No constraint	35,0	**82,0**	35,0
Pshell 53: U-beam	Weld	No constraint	No constraint	35,0	**82,0**	35,0
Pshell 54: Bearing Contact Plates	Weld	No constraint	No constraint	35,0	**105,0**	35,0
Pshell 55: Bearing Mount Plates	Weld	No constraint	No constraint	35,0	**75,0**	35,0
Pshell 56: Gussets	Weld	No constraint	No constraint	35,0	**82,0**	35,0

Stellenbosch University https://scholar.sun.ac.za

Appendix D

Plate and Tube Catalogue

Table D.1: Available plate thicknesses to be used for discrete optimization tasks

Available plate thicknesses [mm]	
4.763	25.40
7.938	31.75
9.525	34.93
12.70	38.10
15.88	44.45
19.05	50.80
22.23	-

Table D.2: Available tube dimensions to be used for discrete optimization tasks

Available tube dimension combinations [mm]			
Member thickness	Squares 127x101.6	Squares 76.2x76.2	Squares 76.5x101.9
2.1082	-	x	-
3.1750	x	x	x
3.4036	x	x	x
4.1910	x	x	x
4.7752	x	x	x
6.3500	x	x	x
7.9502	x	x	x
9.5250	x	x	x
12.700	x	-	-

Stellenbosch University https://scholar.sun.ac.za

Appendix E

Shape Changes to Boom Shell Meshes

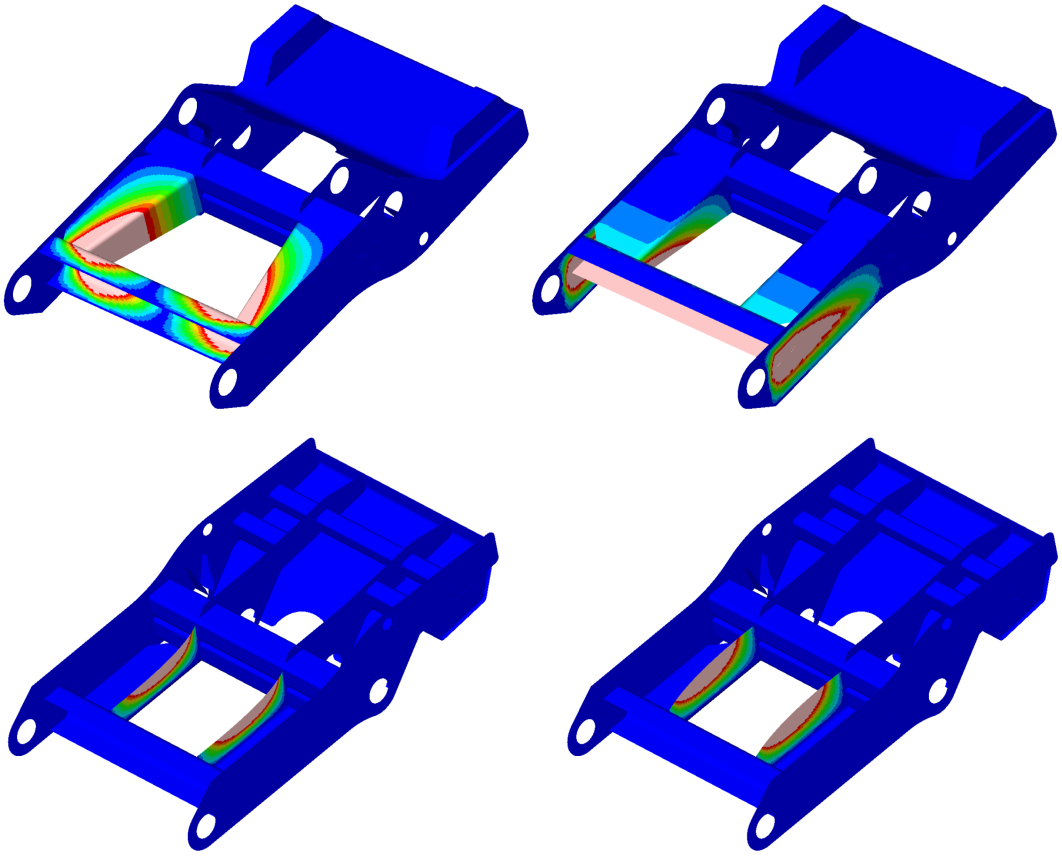

Figure E.1: Shape morphing sets 1 to 4 defined in Section 3.2.2, showing maximum and zero nodal displacement in red and dark blue, respectively

Stellenbosch University https://scholar.sun.ac.za

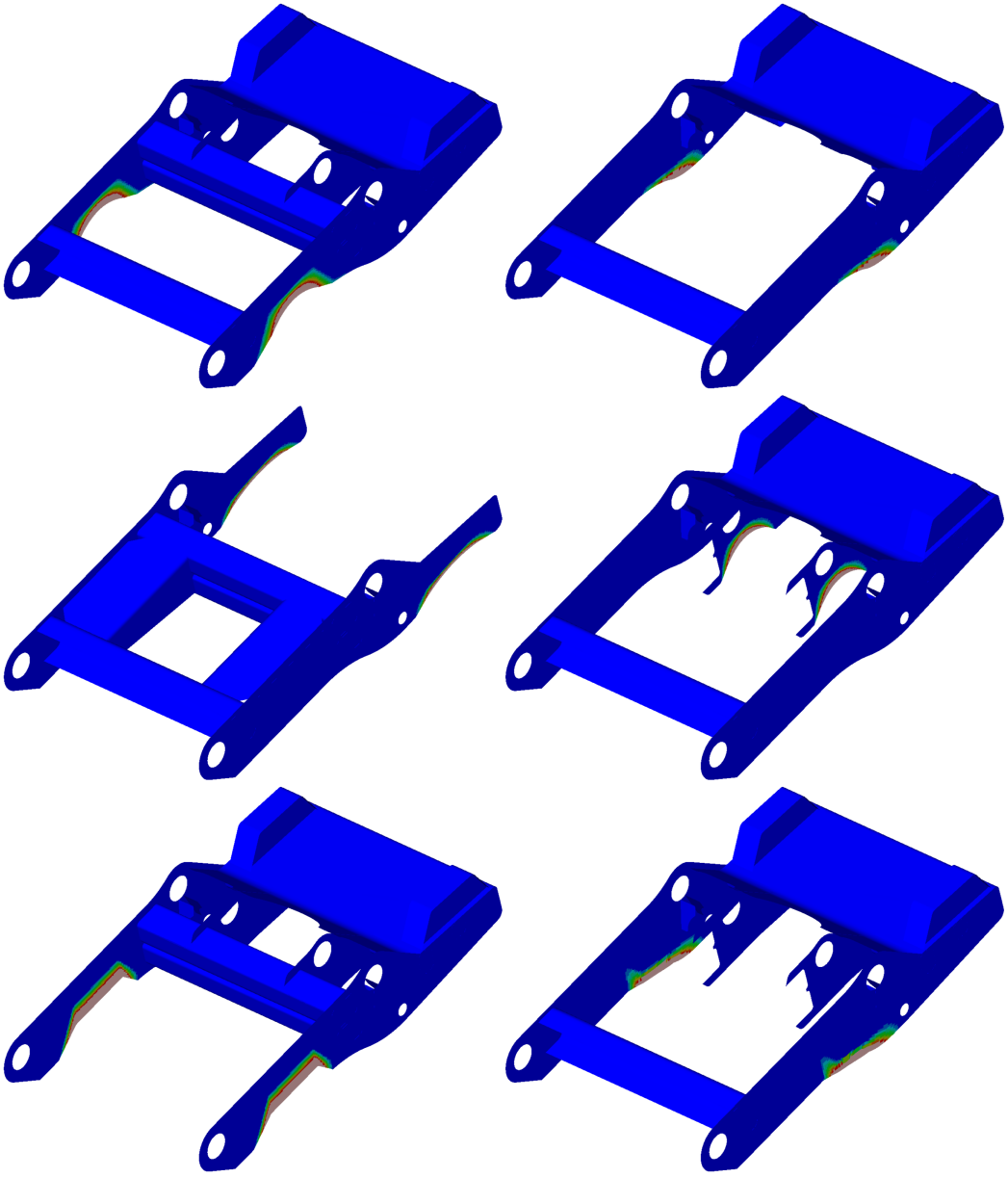

Figure E.2: Shape morphing sets 5 to 10 defined in Section 3.2.2, showing maximum and zero nodal displacement in red and dark blue, respectively

Stellenbosch University https://scholar.sun.ac.za

Appendix F

Boom Topometry Optimization Results

When defining a topometry optimization task, the number of size design variables should be controlled to prevent excessive numbers thereof. To do this, an important parameter allows for the clustering of elements and assigning those clusters size variables to avoid extreme numbers of design variables. This becomes very important when working with large models, as they typically contain a large number of elements. By using 4 element clusters in a plate that contains 100 elements, the size variables, for a topometry task, are reduced from 100 to 25. This is a large reduction in design variables, whilst still retaining a lot of mesh detail for the optimization process. Knowing that the boom contains 122 388 QUAD4 elements, the need for clustering elements becomes imperative. If elements clusters of 200 were to be used on the boom, a rough estimate of 612 design variables would be created. When compared to the amount of design variables used for the size optimization tasks, a substantial design variable increase of 51 times is found. Additionally, clumps of 200 elements are not going to give the necessary detail one would like. This caused a lot of concern, as topometry optimization tasks with such large clusters would not provide the required insight into a design problem. Further reduction in cluster size is possible, but this comes at the expense of computational costs. A topometry optimization task, Task 1, was set up with element clusters of 200. Unsatisfactory results were obtained, due to chaotic plate thickness adjustments, as well as, the resolution of the results. In an attempt to perform topometry optimization tasks with useful results, it was decided to create tasks that only allow the removal of material. The idea is to find places where holes are allowed to exist, within low stressed plate regions. The next task, Task 2, was created using 150 element clusters, with the hope of improving the resolution of the results. Symmetry constraints were added to ensure that the thickness changes are symmetrical. The resulting structures, shown in Figure F.1, were found.

The first design cycle, shown in Figure F.1a, showed a 10 kg reduction in

Stellenbosch University https://scholar.sun.ac.za

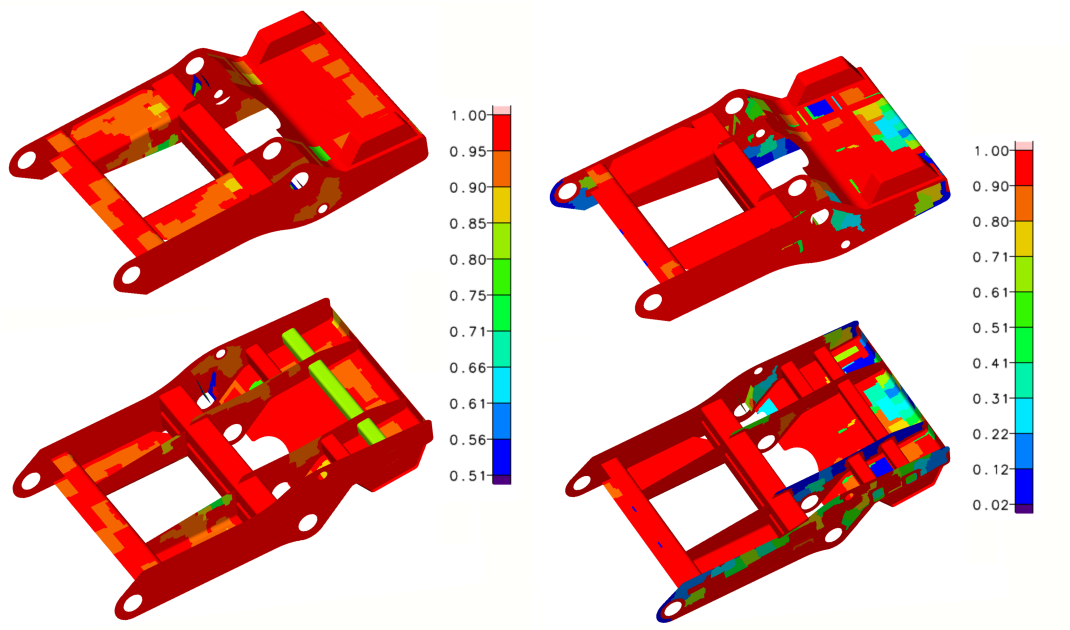

(a) Topometry design cycle 1, Task 2 **(b)** Topometry design cycle 25, Task 2

Figure F.1: Task 2 topometry results, displaying optimized plate thickness fractions

weight with no constraint violations. No holes have been cut, however, sections of material have been thinned, especially the gussets, which could be a future design change. The rear tube also saw a thickness reduction, similar to the size optimization tasks. As the optimization procedure progressed, constraint violations did occur, and a final result, shown in Figure F.1b, with a large stress constraint violation of 67.7 %, and weight of 418 kg was found. This could be due to the resolution of the cluster sizes, not being able to conform to the detailed geometries requirements. Furthermore, it was noted that the results were not at all symmetrical. This could be due to the combination of cluster sizes and the meshes not being symmetrical. Task 3 was created with topometry variable cluster sizes of 90. No real improvement was found. The results for Task 3 is shown in Figure F.2.

It was concluded that the decision, to only cut material out of the design domain, showed better results. Future design runs could consider limiting the plates to only have a thickness of 0 or the original plate thickness, directly cutting holes in low stressed areas, rather than adjusting plate sizes. Furthermore, the solving time became extreme towards the end of Task 3. Even though the solution time increased dramatically, much smaller cluster sizes should be used for future optimization tasks, if usable results are expected. This will require the use of high performance computers, to achieve reasonable solving times.

Stellenbosch University https://scholar.sun.ac.za

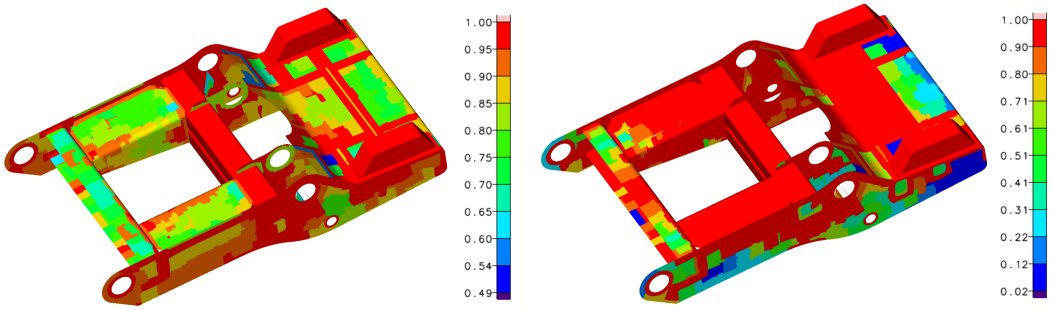

(a) Topometry design cycle 1, Task 3 **(b)** Topometry design cycle 30, Task 3

Figure F.2: Task 3 topometry results, displaying optimized plate thickness fractions

Stellenbosch University https://scholar.sun.ac.za

Appendix G

Combination of Size and Shape Optimization Results

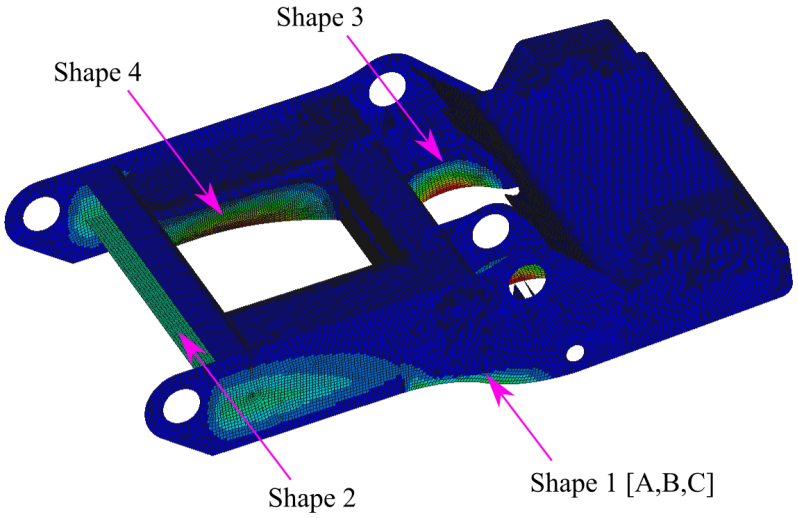

Figure G.1: Location and variants of shape changes to be shifted, with maximum- and no shape changes shown in red and dark blue, respectively

Table G.1: Shape variable shifts made for the input design

Task	Shape 1A	Shape 1B	Shape 1C	Shape 2	Shape 3	Shape 4
Task 1	0	0	0	0	0	0
Task 2	0.5	0	0	0.25	0.5	0.3
Task 3	0	0.5	0	0.5	0.5	0.3
Task 4	0	0	0.5	0.5	0.5	0.3
Task 5	0	0.5	0.5	0.5	0.5	0.3

Stellenbosch University https://scholar.sun.ac.za

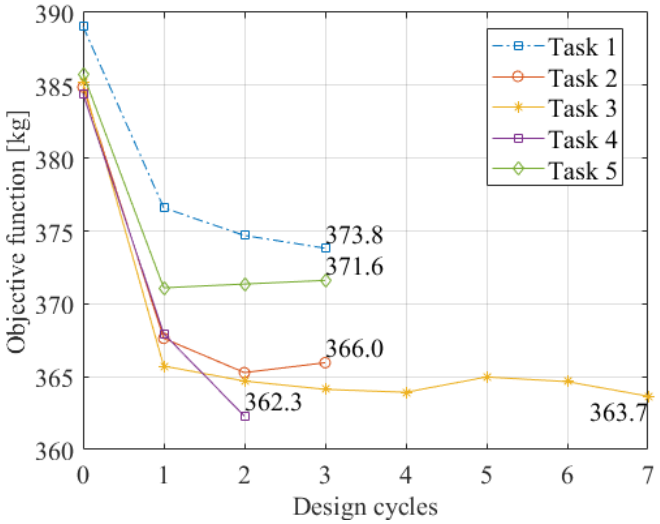

Figure G.2: Objective function summary for Tasks 1 to 5

Stellenbosch University https://scholar.sun.ac.za

Appendix H

Boom Topology Results

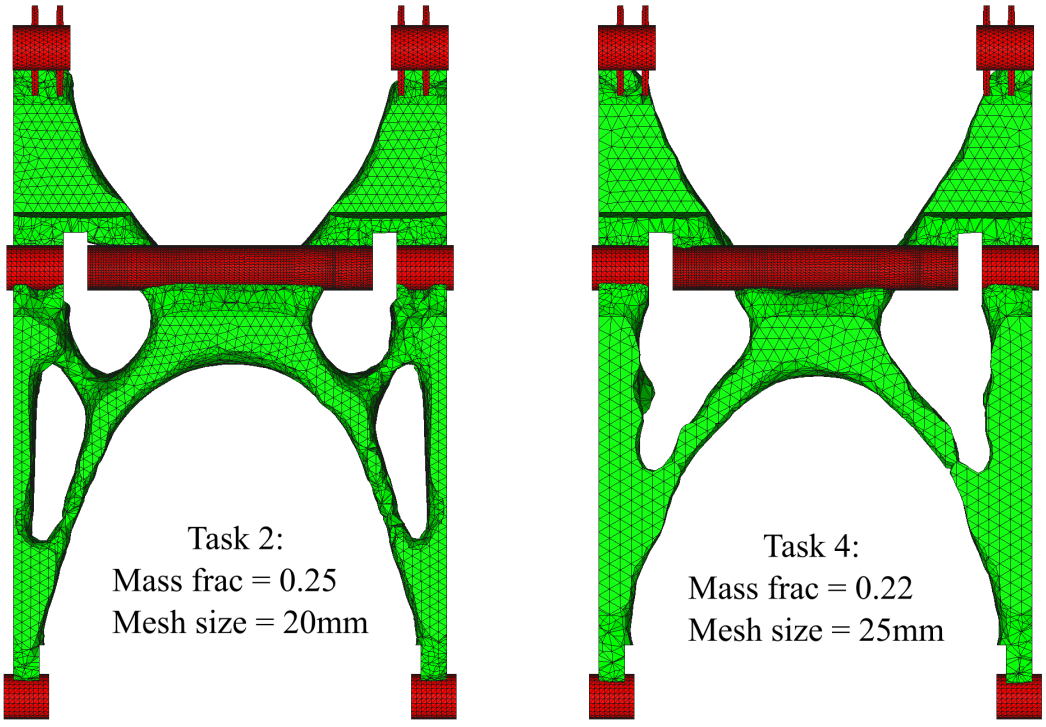

Figure H.1: Boom Tasks 2 and 4 topology results

Stellenbosch University https://scholar.sun.ac.za

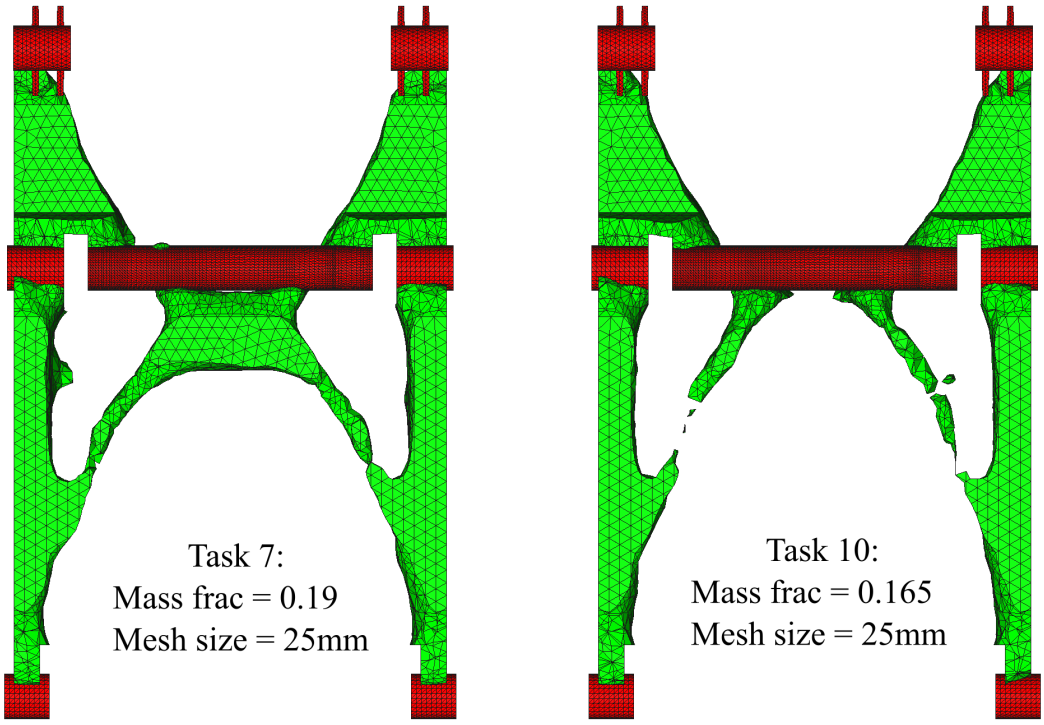

Figure H.2: Boom Tasks 7 and 10 topology results

Stellenbosch University https://scholar.sun.ac.za

Appendix I

Shape Morphing Sets used for the Boom Topology Task 5 Refinement

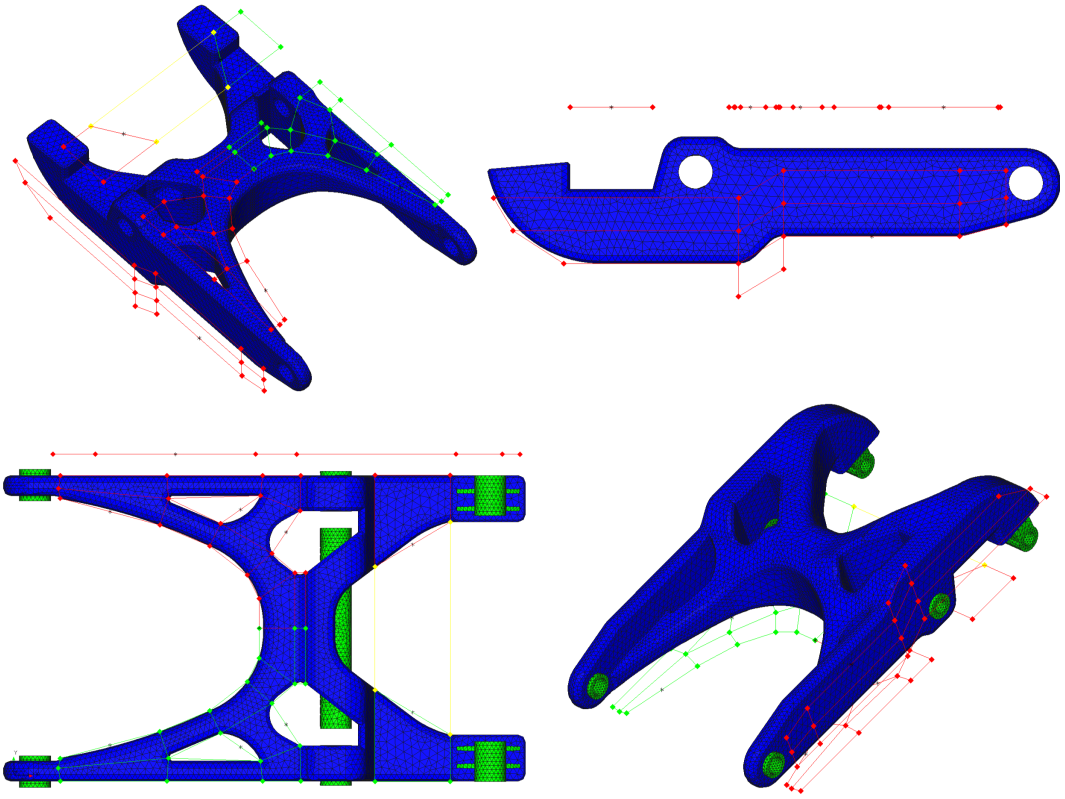

Figure I.1: Task 5 boom, with visible shape domains

Stellenbosch University https://scholar.sun.ac.za

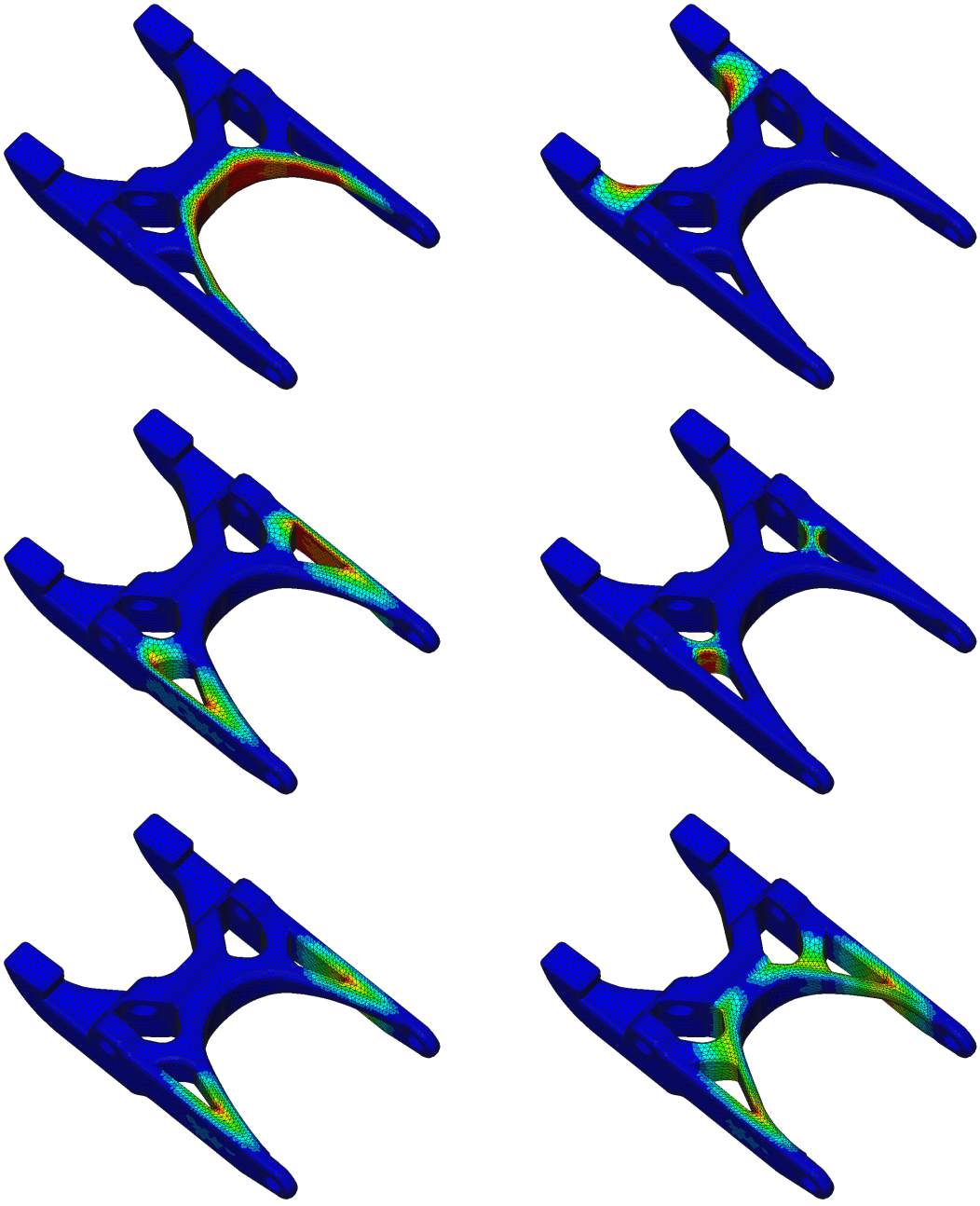

Figure I.2: Shape morphing sets 1 to 6 for Task 5 boom refinement, with maximum- and no shape changes shown in red and dark blue, respectively

Stellenbosch University https://scholar.sun.ac.za

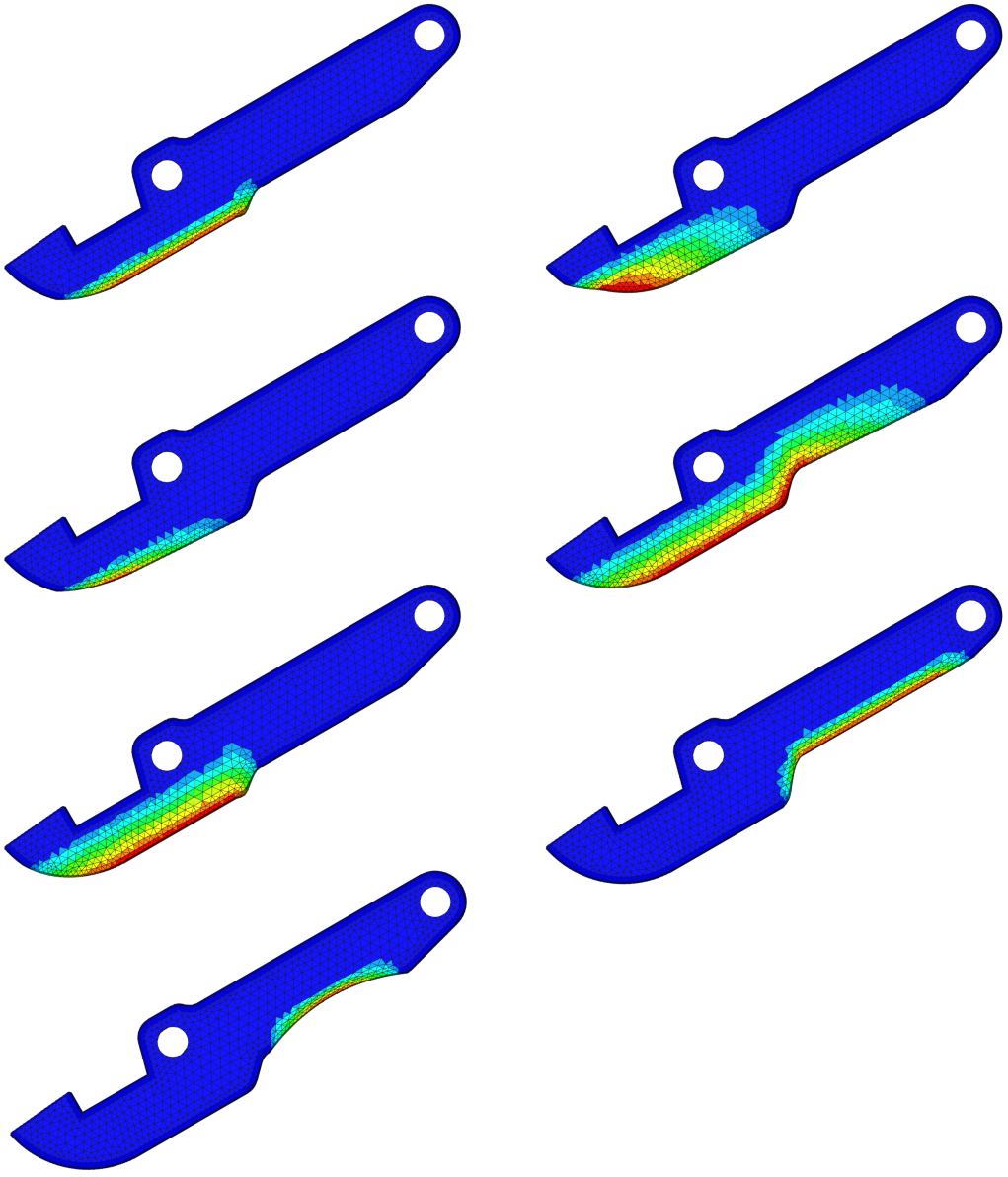

Figure I.3: Shape morphing sets 7 to 14 for Task 5 boom refinement, with maximum- and no shape changes shown in red and dark blue, respectively

Stellenbosch University https://scholar.sun.ac.za

Appendix J

Shape Morphing Sets used for the Boom Topology Task 11 Refinement

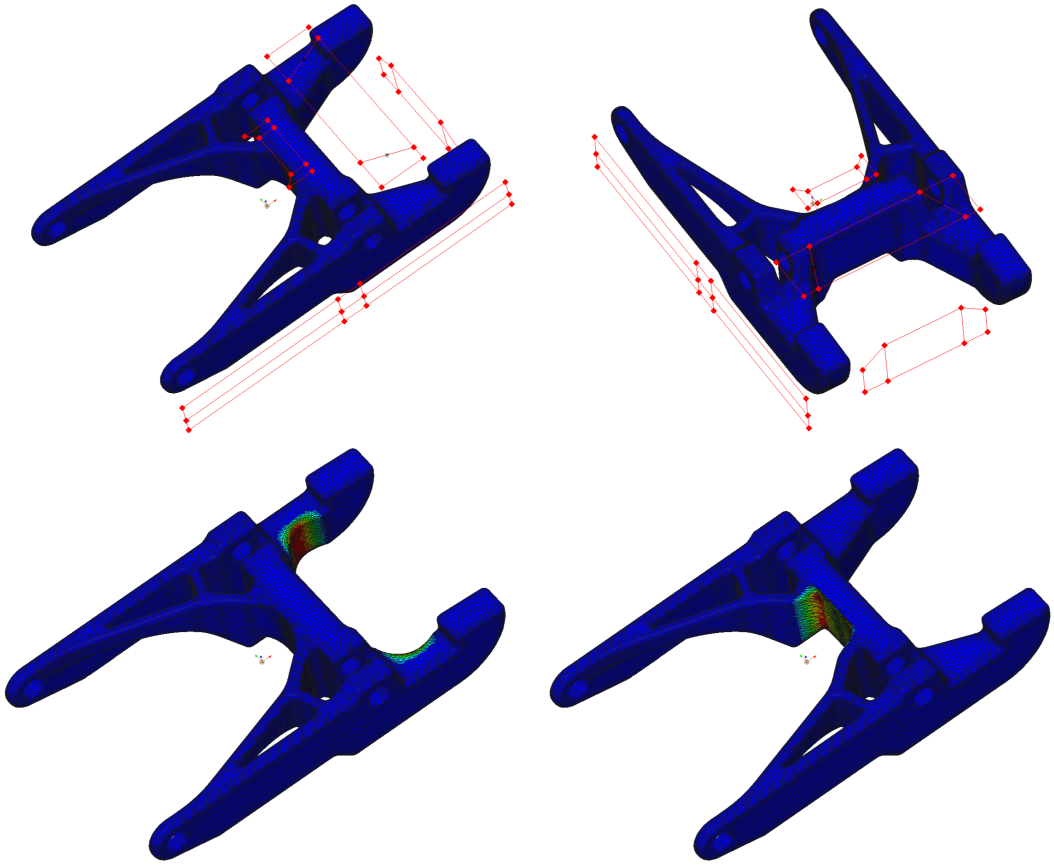

Figure J.1: Task 11 shape domains, with shape morphing sets 1 and 2 that displays maximum- and no shape changes in red and dark blue, respectively

Stellenbosch University https://scholar.sun.ac.za

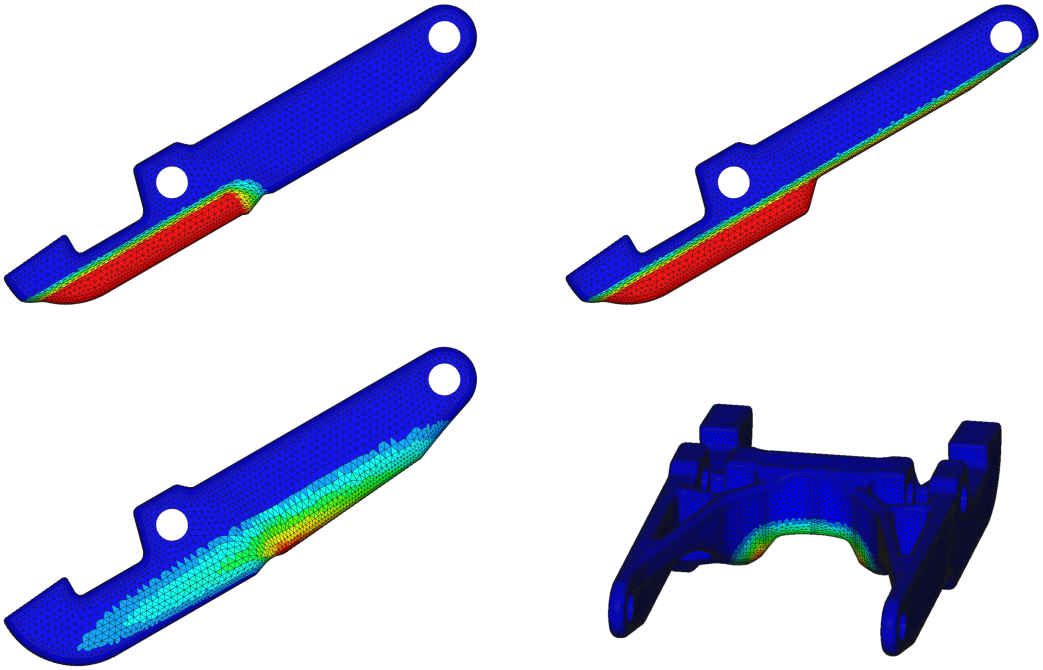

Figure J.2: Shape morphing sets 3 to 6 for Task 11's boom refinement, with maximum- and no shape changes shown in red and dark blue, respectively

Stellenbosch University https://scholar.sun.ac.za

Appendix K

Detailed Cross-member FE Model

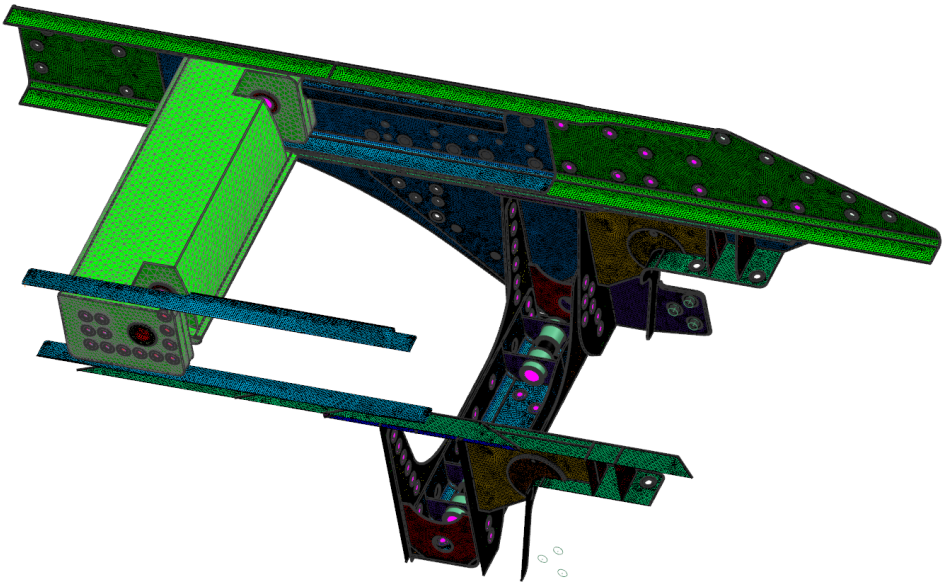

Figure K.1: Detailed cross-member FE model within a sectioned chassis model

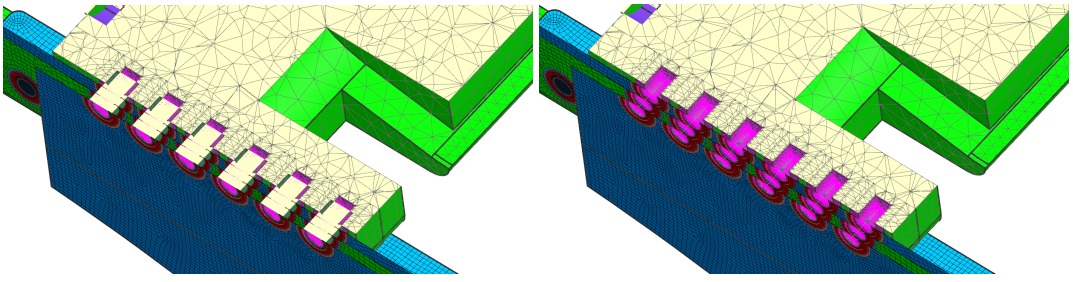

(a) Bolted detail displayed with solid beam element and RBE2 elements

(b) Bolted detail displayed with curve beam element and RBE2 elements

Figure K.2: Sectioned cross-member model to show bolted detail

Stellenbosch University https://scholar.sun.ac.za

Appendix L

Cross-member Topology Results

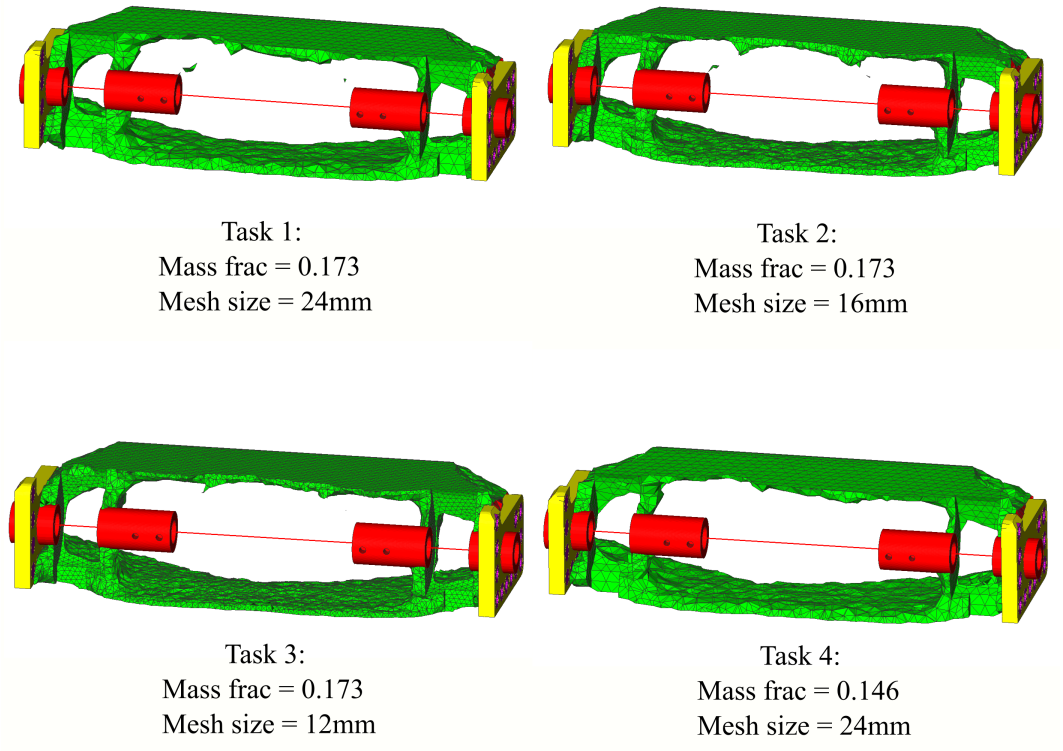

Figure L.1: Cross-member topology results for Tasks 1 to 4

Stellenbosch University https://scholar.sun.ac.za

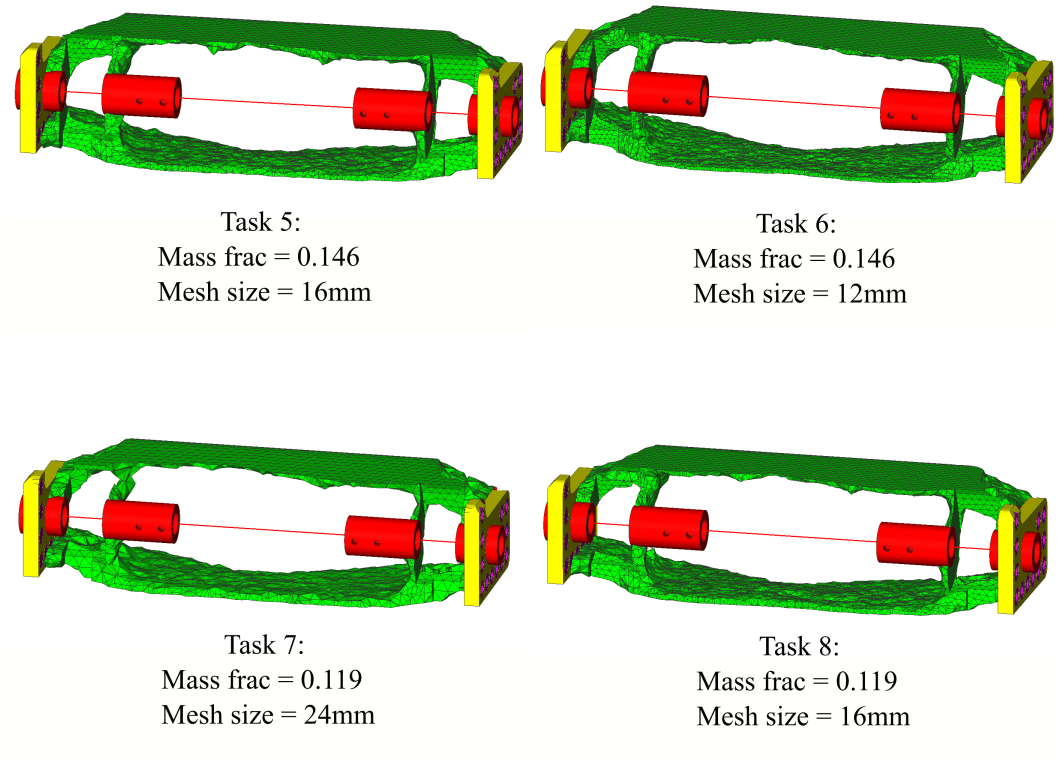

Figure L.2: Cross-member topology results for Tasks 5 to 8

Stellenbosch University https://scholar.sun.ac.za

Appendix M

Phase 4 FE Results and Shape Morphing Sets

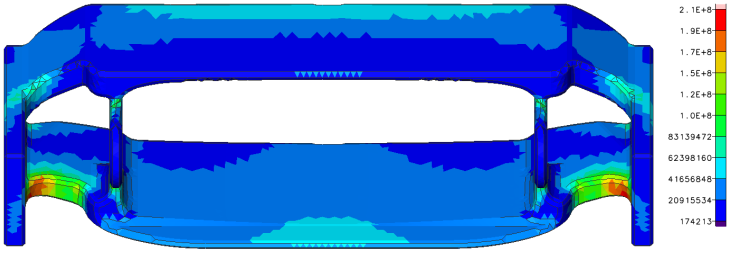

Figure M.1: Interpreted cross-member FE results for the 1st ultimate load case, with a maximum stress of roughly 210 MPa

Figure M.2: Interpreted cross-member FE results for the 2nd ultimate load case, with a maximum stress of roughly 250 MPa

Stellenbosch University https://scholar.sun.ac.za

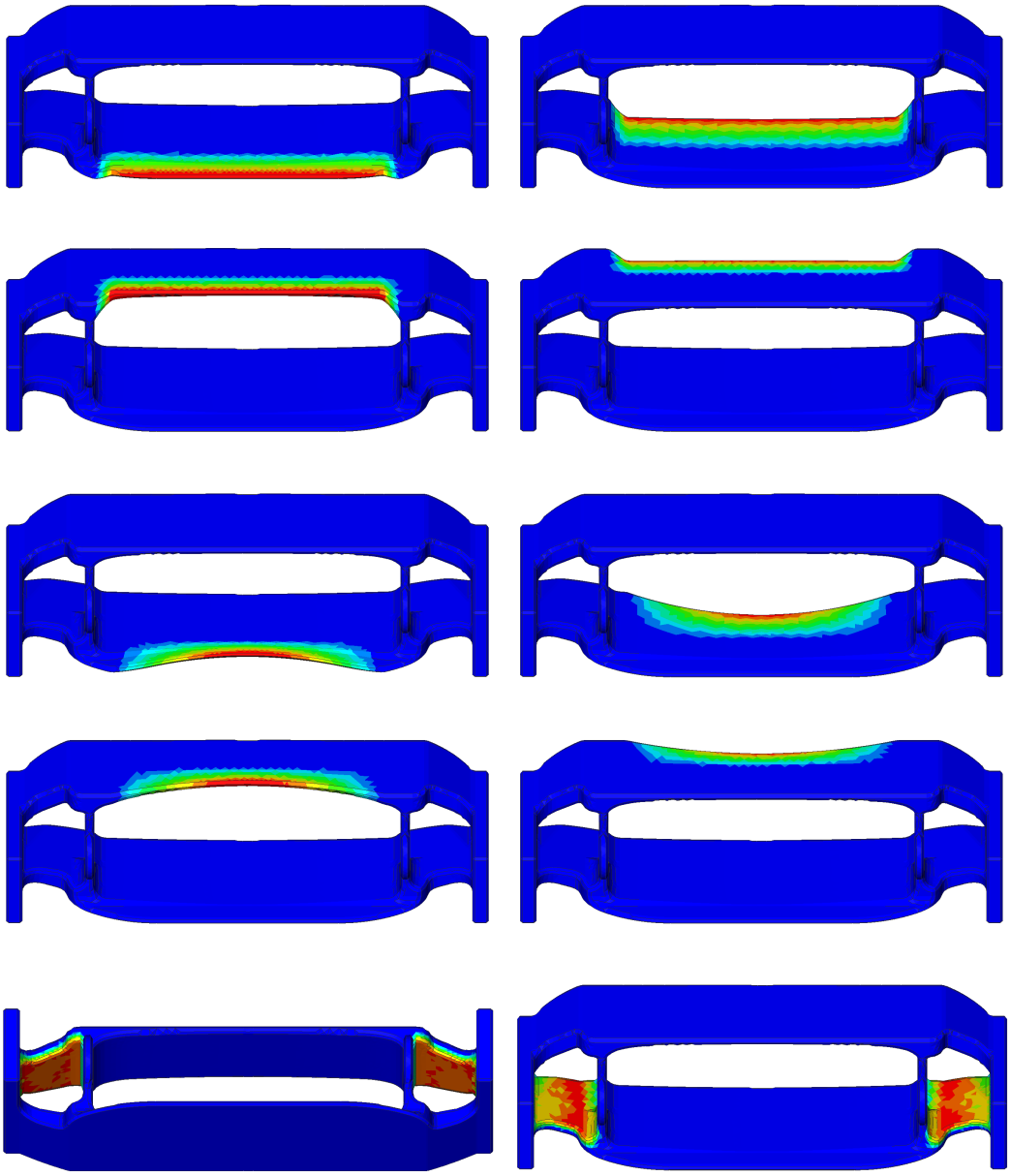

Figure M.3: Shape morphing sets used on interpreted cross-member model, that had a significant impact on the shape optimization results. Maximum shape changes are displayed in red, with no shape changes displayed in dark blue

Stellenbosch University https://scholar.sun.ac.za

Appendix N

Concept Design Finalization

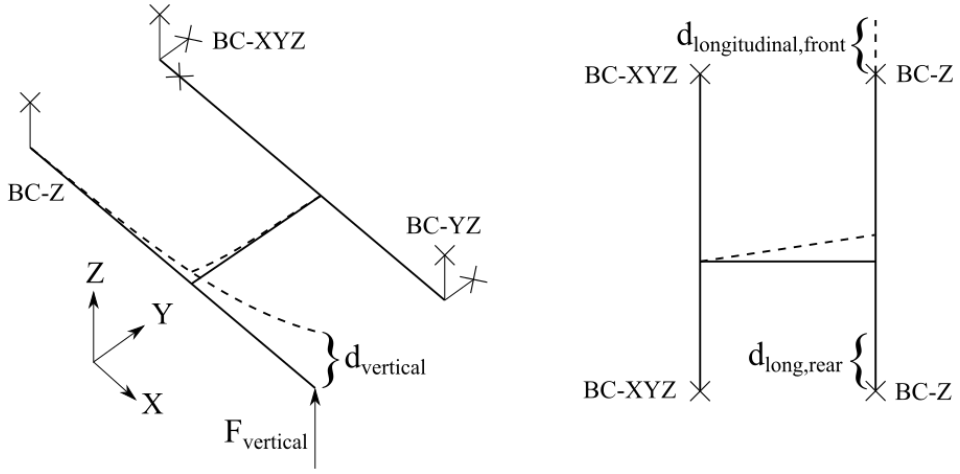

(a) Simplified chassis twist load case illustration

(b) Simplified split mu load case illustration

Figure N.1: Chassis twist and split mu load case illustrations

Stellenbosch University https://scholar.sun.ac.za

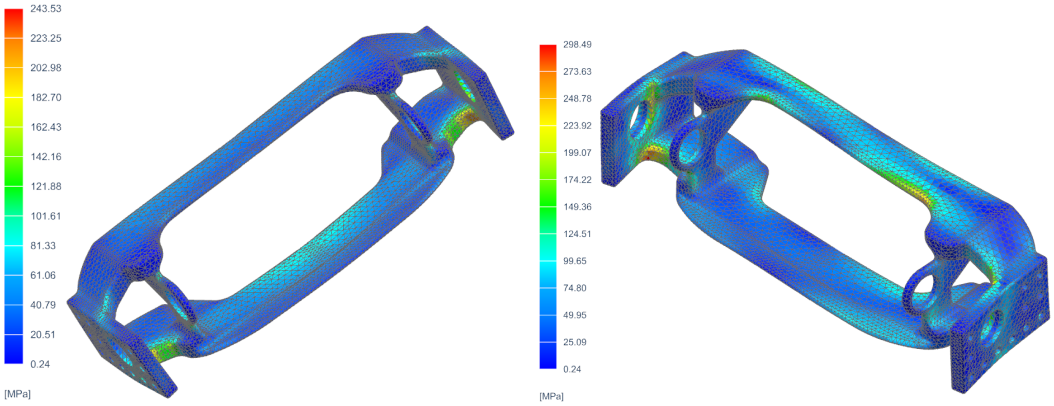

(a) 1st Ultimate load case FE results **(b)** 2nd Ultimate load case FE results

Figure N.2: Cross-member Concept 1 FE results

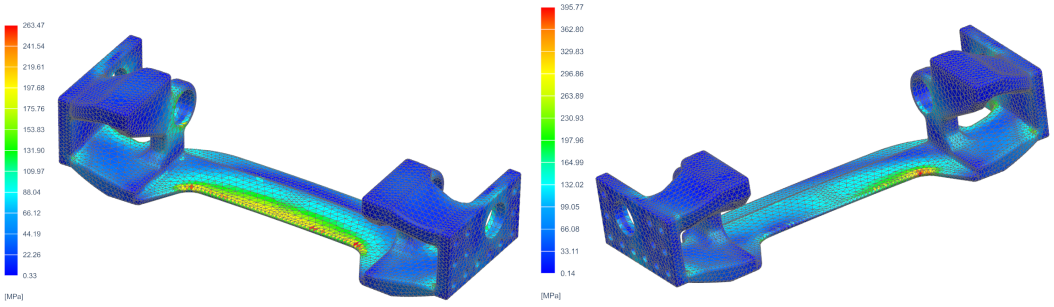

(a) 1st Ultimate load case FE results for Concept 2 **(b)** 2nd Ultimate load case FE results for Concept 2

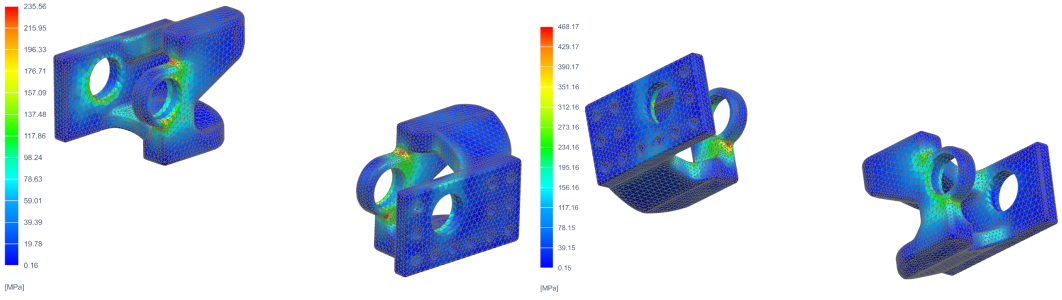

(c) 1st Ultimate load case FE results for Concept 3 **(d)** 2nd Ultimate load case FE results for Concept 3

Figure N.3: Cross-member Concepts 2 and 3 FE results

Stellenbosch University https://scholar.sun.ac.za

List of References

Alro Steel (2011). Metals Guide.
Available at: https://www.alro.com/Metals/

Autocar (2019). Autocar ACTT brosure.
Available at: https://www.autocartruck.com/actt/

Bajpai, P. and Kumar, D.R.M. (2010). Genetic Algorithm - an Approach to Solve Global Optimization Problems. *Indian Journal of Computer Science and Engineering*, vol. 1, no. 3, pp. 199–206.

British Standards Institution (2014). BSI Standards Publication Guide to fatigue design and assessment of steel products.

Femto Engineering (). Quick introduction to Topology Optimization.
Available at: https://www.femto.eu/stories/topology-optimization/

Leiva, J.P. (2008). Structural Optimization Methods and Techniques to Design Efficient Car Bodies. *12th European Conference on Research and Advanced Technology for Digital Libraries, ECDL 2008*, vol. 5173 LNCS. ISSN 03029743.
Available at: http://www.scopus.com/inward/record.url?eid=2-s2.0-55249116519{&}partnerID=40{&}md5=caefc92898ccaf378927f489b17038d7

Leiva, J.P. and Watson, B.C. (2016). Integrating Topology with Sizing and Shape Optimization Using the Approximation Concepts Approach. In: *International CAE Conference 2016*, pp. 1–9.

Liu, X., Yi, W.J., Li, Q.S. and Shen, P.S. (2008). Genetic evolutionary structural optimization. *Journal of Constructional Steel Research*, vol. 64, no. 3, pp. 305–311. ISSN 0143974X.

Metrology and Quality News (2016). Topology Optimization and DMP Combine to Meet GE Aircraft Engine Bracket Challenge.
Available at: https://cutt.ly/SkQLksY

Monarch Industries (2014). Foundary Offerings.
Available at: http://www.monarchindustries.com/pdf/140513-MonarchCastingOverview.pdf

Pagadala, B.P. (2008). Topography Optimization. vol. 0, p. 40.

Stellenbosch University https://scholar.sun.ac.za

Schmit, L. (1960). Structural design by systematic synthesis. In: *Proceedings of 2nd Conference on Electronic Computation*, pp. 105–122. New York.

Shimoda, M. and Liu, Y. (2014). A non-parametric free-form optimization method for shell structures. *Structural and Multidisciplinary Optimization*, vol. 50, no. 3, pp. 409–423. ISSN 16151488.

Siemens Product Lifecycle Management Software Inc. (2014). NX Nastran User's Guide.

Sigmund, O. and Petersson, J. (1998). Numerical instabilities in topology optimization: A survey on procedures dealing with checkerboards, mesh-dependencies and local minima. *Structural Optimization*, vol. 16, no. 1, pp. 68–75. ISSN 09344373.

Snyman, J.A. (2005). Practical Mathematical Optimization. vol. 97.

Stewart, J. (2012). *Calculus, 7th ed.* 7th edn. Brooks/Cole Publishing PUBLISH DATE: 2012. ISBN 978-0-538-49884-5.

Vanderplaats, G.N. (2005). *Numerical optimization techniques for engineering design.* 4th edn. Colorado Springs, CO : Vanderplaats Research & Development. ISBN 0944956033.

Vanderplaats, G.N., Thomas, H.L. and Shyy, Y.K. (1991). A review of approximation concepts for structural synthesis. *Computing Systems in Engineering*, vol. 2, no. 1, pp. 17–25. ISSN 09560521.

Vanderplaats Research & Development (2018). GENESIS v17.0. Design Manual.

Venter, G. (2010). Review of Optimization Techniques. *Encyclopedia of Aerospace Engineering*, pp. 1–12.

Zhang, Y., Wu, X., Guan, B., Zhao, Z. and Wan, M. (2020). Application and practical validation of topology optimization technology for the frame of biaxial tensile testing machine. *Structural and Multidisciplinary Optimization*, pp. 1519–1533. ISSN 16151488.